UNIVERSITY OF BELGRADE

FACULTY OF TECHNOLOGY AND METALLURGY

Amjed A. Karkad

LIPOSOMES AND BIO-POLYMERIC FILMS FOR EFFICIENT CONTROLLED RELEASE OF SILIBININ AND *Cotinus coggygria* Scop. EXTRACT

Doctoral Dissertation

Belgrade, 2026

UNIVERZITET U BEOGRADU

TEHNOLOŠKO-METALURŠKI FAKULTET

Amjed A. Karkad

LIPOZOMI I BIOPOLIMERNI FILMOVI ZA EFIKASNO KONTROLISANO OTPUŠTANJE SILIBININA I *Cotinus coggygria* Scop. EKSTRAKTA

Doktorska disertacija

Beograd, 2026

Supervisors:

_____

Prof. Dr. Aleksandar Marinković,
Full Professor, University of Belgrade,
Faculty of Technology and Metallurgy

_____

Dr. Tamara Erceg,
Senior Research Associate, University of Novi Sad,
Faculty of Technology Novi Sad

Members of the committee:

_____

Prof. Dr. Suzana Dimitrijević-Branković,
Full Professor, University of Belgrade,
Faculty of Technology and Metallurgy

_____

Prof. Dr. Antonije Onjia,
Full Professor, University of Belgrade,
Faculty of Technology and Metallurgy

_____

Dr. Aleksandra A. Jovanović,
Senior Research Associate, University of Belgrade,
Institute for the Application of Nuclear Energy INEP

Candidate:

_____

Amjed Abdullah Karkad

In Belgrade _____

Acknowledgments

I express my gratitude to my supervisors, Prof. Dr. Aleksandar Marinković, Full Professor at the University of Belgrade, Faculty of Technology and Metallurgy, and Dr. Tamara Erceg, Senior Research Associate at the University of Novi Sad, Faculty of Technology, for their continuous support, valuable guidance, and constructive suggestions.
I am also grateful to the members of the doctoral dissertation committee for their time, expertise, and insightful comments: Prof. Dr. Suzana Dimitrijević-Branković, Prof. Dr. Antonije Onjia (Faculty of Technology and Metallurgy), and Dr. Aleksandra Jovanović (Institute for the Application of Nuclear Energy - INEP).
Additionally, special thanks are extended to Dr. Aleksandra Jovanović for her significant contribution to this research, including her active involvement in the experimental work, as well as her valuable assistance in the preparation and writing of this dissertation and previous publications.
Special thanks to Dr. Andrea Pirković (Institute for the Application of Nuclear Energy - INEP), for her valuable assistance with all experiments on keratinocyte cells and for her continued assistance and commitment throughout this study.
I express my gratitude to Dr. Milena Milošević (Institute of Chemistry, Technology and Metallurgy) for her assistance in Fourier-transform infrared spectroscopy analysis, as well as performing antioxidant assays.
I am very grateful to Dr. Bojan Stojadinović (Institute of Physics) for his valuable contribution and for performing Raman measurements.
I express my gratitude to Katarina Simić and Stefan Ivanović (Institute of Chemistry, Technology and Metallurgy) for their invaluable assistance with the chemical characterization.
I sincerely thank Dr. Miroslav Novaković (Institute of Chemistry, Technology and Metallurgy) for his valuable assistance and for kindly providing the smoke tree plant used in this doctoral research.
Finally, I express my deepest gratitude to my family for support, understanding, and patience throughout my doctoral studies.

Liposomes and bio-polymeric films for efficient controlled release of silibinin and *Cotinus coggygria* Scop. extract

Summary

This doctoral research focused on the development and characterization of multifunctional liposomal and polymer-based delivery systems for silibinin and smoke tree extract, aiming to assess their physicochemical, structural, mechanical, and biological properties for potential pharmaceutical and biomedical applications. Silibinin encapsulated in liposomal vesicles was obtained *via* the proliposome procedure and subjected to ultraviolet irradiation, sonication, and freeze-drying. Developed formulations were analyzed *via* the efficiency of encapsulation, diameter, polydispersity index, surface charge, rheological properties, as well as storage stability over 60 days, Fourier-transform infrared (FT-IR), and Raman spectra. Biological potential (antioxidant, cytotoxic, and anti-inflammatory activity) was evaluated using HaCaT cells (keratinocytes). Smoke tree extract was analyzed for total phenolic and flavonoid content, and pullulan was chemically modified to obtain pullulan-isononanoate (Pull-Iso), confirmed by nuclear magnetic resonance (NMR) and FT-IR. Silibinin/smoke tree extract-loaded liposomes were incorporated into Pull-Iso films, and their microstructure, mechanical properties, surface wettability, moisture content, solubility, swelling behavior, and antioxidant performance were assessed. Liposome incorporation promoted controlled release of bioactives, suggesting Pull-Iso films as promising platforms for bioactive wound dressings. This study provides a robust base for multifunctional carriers and opens future experiments, including optimization of lyophilization, release kinetics, and skin-related therapeutic applications.

Keywords: biopolymer films, biological potential, *Cotinus coggygria*, extract, liposomes, physicochemical properties, polyphenols, pullulan, silibinin

Scientific field: Chemical Sciences
Scientific discipline:

Lipozomi i biopolimerni filmovi za efikasno kontrolisano otpuštanje silibinina i *Cotinus coggygria* Scop. ekstrakta

Rezime

Fokus doktorske disertacije je bio na razvoju i karakterizaciji multifunkcionalnih lipozomalnih i polimernih sistema za isporuku silibinina i ekstrakta ruja, sa ciljem procene njihovih fizičko-hemijskih, strukturnih, mehaničkih i bioloških svojstava za potencijalnu farmaceutsku i biomedicinsku primenu. Lipozomi sa silibininom su pripremljeni primenom prolipozomne metode i podvrgnuti ultraljubičastom zračenju, soniciranju i liofilizaciji. Razvijene formulacije su okarakterisane analizom efikasnosti inkapsulacije, dijametra čestica, polidsperznog indeksa, površinskog naelektrisanja, reoloških svojstava i stabilnosti tokom 60 dana, Furijeovih transformacionih infracrvenih (FT-IR) i Raman spektara. Biološki potencijal, uključujući antioksidativne, citotoksične i antiinflamatorne efekte, ispitan je na HaCaT ćelijama (keratinocitima). Ukupan sadržaj polifenola i flavonoida je ispitan u ekstraktu ruja, dok je pululan hemijski modifikovan u pullulan-izononanoat (Pull-Iso), što je potvrđeno primenom nuklearne magnetne resonance (NMR) i FT-IR spektroskopije. Lipozomi sa silibininom i ekstraktom ruja su inkorporirani u Pull-Iso filmove, čija su mikrostruktura, mehanička svojstva, vlažnost površine, sadržaj vlage, rastvorljivost, ponašanje pri bubrenju i antioksidativna aktivnost detaljno ispitani. Inkapsulacija lipozoma je omogućila kontrolisano oslobađanje bioaktivnih supstanci, što ukazuje na potencijal Pull-Iso filmova kao platformi za bioaktivne zavoje. Ovo istraživanje pruža osnovu za dizajn multifunkcionalnih nosača i otvara buduće eksperimente, poput optimizacije liofilizacije i ispitivanja kinetike oslobađanja i dermalnih terapijskih formulacija.

Ključne reči: biopolimerni filmovi, biološki potencijal, *Cotinus coggygria*, ekstrakt, lipozomi, fizičko-hemijska svojstva, polifenoli, pullulan, silibinin

Naučna oblast: Hemijske nauke

Uža naučna oblast:

CONTENT

1. INTRODUCTION

1.1. Polyphenols and their biological effects: silibinin as a representative

Polyphenols are compounds that contain hydroxyl-substituted aromatic rings and exist as free forms, glycosides bound to sugars, or complexes with organic acids, amines, and lipids (Manach et al., 2004). Their distribution in plant tissues is uneven; water-soluble polyphenols are mostly stored in vacuoles, while flavonoids and hydrophobic polyphenols are often associated with cell walls. In plants, polyphenols serve diverse functions, acting as antioxidants, antimicrobial agents, herbivore repellents, light receptors, and protective compounds against excessive ultraviolet (UV) radiation. Phenolic acids, including hydroxybenzoic and hydroxycinnamic derivatives, contribute to cell wall stability, regulate growth, and help plants respond to stress factors like high temperature, pathogens, or pollutants (Buer et al., 2007; Cheynier et al., 2013). Flavonoids, named after the Latin word *flavus*, meaning yellow, include compounds that can be colorless, blue, purple, or red, all sharing two benzene rings connected by a three-carbon bridge. Major dietary sources of polyphenol molecules include fruits, vegetables, legumes, cereals, nuts, and herbs, possessing numerous benefits in human health (Manach et al., 2004). Polyphenol compounds could be observed to enhance the function of the cardiovascular system *via* scavenging free radicals (*i.e.*, preventing oxidative stress), enhancing nitric oxide production, and preventing platelet aggregation (Jovanović et al., 2017). They also demonstrate protective effects on the liver, reduce inflammation, act against ulcers, and exhibit antibacterial, antifungal, and antiviral effects. Certain polyphenols could stop the growth of tumor cells and initiate the process of apoptosis, as well as stimulate deoxyribonucleic acid (DNA) repair mechanisms, highlighting their potential in disease prevention. In addition to health benefits, polyphenols are responsible for sensorial characteristics of foods and their stability toward oxidation, and can act as natural antioxidants and preservatives (Manach et al., 2004; Scalbert et al., 2005; Shahidi and Ambigaipalan, 2015). As shown in Figure 1, the structures of selected polyphenols demonstrate key functional groups responsible for their bioactivity.

Oxidation is a crucial biological process that generates free radicals, which can change lipids, proteins, and DNA, causing aging and various diseases. The body relies on enzymatic defenses, yet during stress or disease, these systems may be overwhelmed, leading to stress caused by free radicals. Natural polyphenol components act as antioxidant agents by neutralizing radicals, chelating metals, and preserving the integrity of cellular structures, including membranes, nucleic acids, and lipid components, as well as proteins. Through these mechanisms, polyphenols can reduce oxidative damage, support cardiovascular and neurological health, and potentially prevent chronic disorders - cancer, diabetes, and neurological illnesses (Bravo, 1998; Crozier et al., 2009; Scalbert et al., 2005; Shahidi and Ambigaipalan, 2015).

Polyphenol molecules show significant anti-inflammatory properties and the ability to modulate signaling pathways within inflammation (Pan et al., 2010). They can inhibit the generation of cytokines and enzymes (cyclooxygenase and lipoxygenase), which are responsible for inflammation and tissue damage. By reducing oxidative stress, polyphenols also indirectly decrease inflammatory reactions in cells and tissues. These compounds can protect organs and tissues from chronic inflammation, preventing conditions like diseases of the cardiovascular system and diabetes, as well as neurological illnesses. Additionally, their interaction with cellular pathways helps regulate immune responses, supporting overall health (García-Lafuente et al., 2009; Shakibaei et al., 2009).

Polyphenols play an important role in skin health, reducing damage caused by stressors, particularly ultraviolet exposure (Pandey and Rizvi, 2009). Their antioxidant properties allow them to neutralize UV-produced free radicals and prevent cellular damage, as well as premature skin aging. Additionally, polyphenol components can reduce inflammation in skin cells and support the repair of damaged tissues. By enhancing the skin's natural defense mechanisms, these compounds help maintain skin health, elasticity, and overall appearance. Some polyphenols also inhibit enzymes that degrade collagen and elastin, further contributing to skin protection and resilience (Afaq and Katiyar, 2011; Radan et al., 2024; Nichols and Katiyar, 2010).

Namely, polyphenols are natural compounds that provide multiple protective effects on the organisms, combining antioxidant, skin-protective, and anti-inflammatory effects. Their antioxidant action allows them to neutralize free radicals and reduce lipid, nucleic acid, and protein lesions, which are linked to aging and chronic diseases. Polyphenols also modify inflammation by preventing the generation of cytokines and enzymes, helping in the prevention of tissue lesions, as well as chronic inflammation. In addition to these systemic benefits, polyphenols protect the skin by shielding cells from UV exposure, preventing stress caused by radicals, while supporting the damaged tissues' repair. They enhance the skin's natural defenses, maintain elasticity, and inhibit enzymes that break down collagen and elastin, slowing the signs of aging. Through their combined effects, polyphenols contribute to cardiovascular and neurological health while also acting as a natural barrier against environmental and cellular stressors. Overall, these compounds are valuable for promoting general wellness and preserving the integrity of skin and other organs.

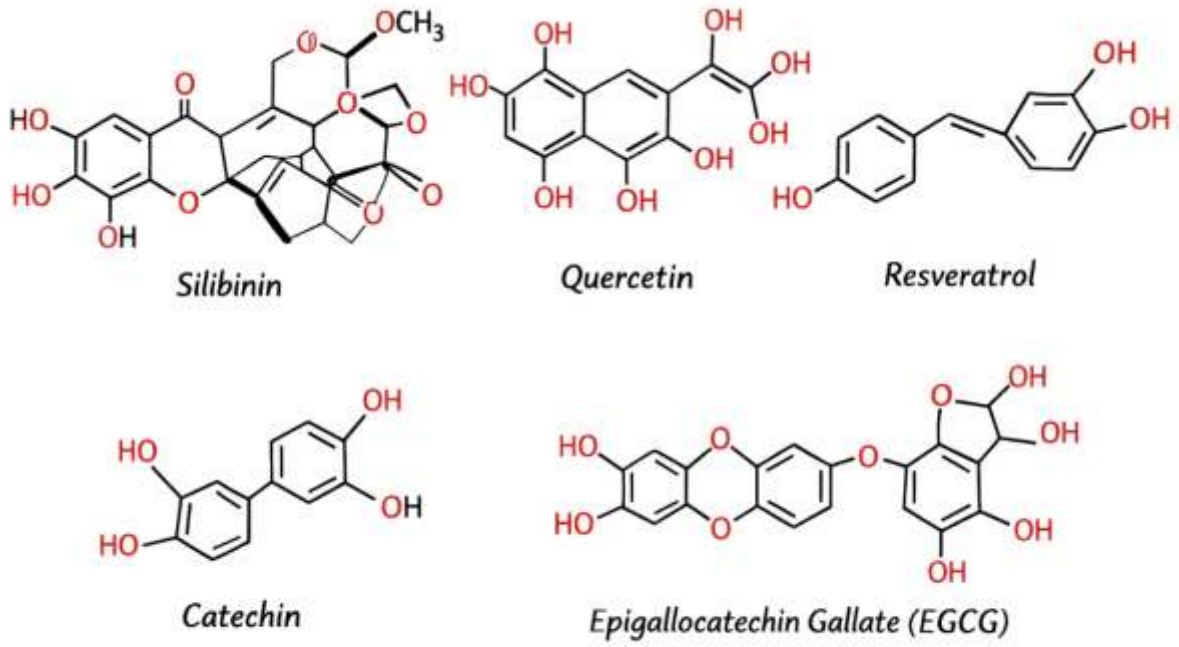

Figure 1. Chemical structures of selected polyphenols

Silibinin, a flavonolignan, is a bioactive molecule of silymarin. Sylimarin is a mixture of polyphenols contained in milk thistle that also includes isosilybin, silydianin, and silychristin (Zhang et al., 2022). These polyphenols display antioxidant, antimicrobial (Liu et al., 2019), and anti-inflammatory properties (Singh and Agarwal, 2009; Zhang et al., 2022). They also show immunomodulatory (Zhao et al., 2015), antitumor (Ahmad et al., 2018), and other effects, contributing to potential health benefits. In addition, silibinin can be found in artichoke (*Cynara scolymus*) (Singh and Agarwal, 2002). Silibinin (flavonolignan composed of 2 main diastereomers) features a 15-carbon skeleton formed by a hybrid structure composed of a flavonoid unit and a phenylpropanoid moiety (Figure 2), which contributes to its strong antioxidant activity (Singh and Agarwal, 2002). The dual diastereomers of silibinin, silybin A and B, may exhibit differential bioactivities, which could be leveraged to optimize therapeutic outcomes

(Singh and Agarwal, 2002). Silibinin's antioxidant activity is largely connected to its capacity to neutralize radicals, alter antioxidant enzymes, thereby reducing oxidative stress in various tissues (Singh and Agarwal, 2002; Zhang et al., 2022). Apart from hepatoprotective effects, silibinin has been shown to modulate inflammatory signaling pathways, crucial in chronic diseases (Singh and Agarwal, 2009; Zhang et al., 2022). Silibinin also modulates multiple intracellular signaling pathways named STAT3 and PI3K/Akt, thereby regulating cell proliferation, apoptosis, and inflammatory responses. Additionally, silibinin interferes with the TGF-β signaling pathway, thereby inhibiting epithelial-mesenchymal transition and reducing cell migration and invasion. Studies suggest that silibinin can sensitize cancer cells to chemotherapy *via* causing apoptosis, enhancing its role in adjunctive therapy (Ahmad et al., 2018; Verdura et al., 2021). Silibinin's antiviral properties have been explored in the context of hepatitis C virus infection, highlighting its ability to inhibit viral replication (Liu et al., 2019). In Verdura et al.'s study (2021), silibinin was investigated in lung cancer cells and acted as a chemopreventive and drug, and experimental studies have shown its significant chemopreventive properties in prostate cancer, as well as cancer of the skin (animals) (Singh and Agarwal, 2002; Singh et al., 2002). Song et al.'s study (2022) shows that the aforementioned compound offers hepatoprotective effects in the presence of toxic agents, whereas another study reports the inhibition of the aggregation of amyloid-beta by interacting with polypeptides (García-Viñuales et al., 2022). Emerging evidence indicates that silibinin's neuroprotective effects may involve inhibition of protein aggregation and modulation of neuroinflammatory pathways, which could have implications for neurodegenerative diseases (García-Viñuales et al., 2022). Matsumura and Ananthaswamy (2004) demonstrated that silibinin protects skin from ultraviolet B-induced damage, preventing photo-carcinogenesis, sunburn, UV-B-triggered epidermal hyperplasia, and DNA lesions, while also modulating the cell cycle to maintain genomic integrity (Singh and Agarwal, 2002; Singh and Agarwal, 2009). According to Mohammadi et al. (2022), despite these benefits, its clinical usage is reduced by low solubility and restricted absorption, as well as poor bioavailability, which necessitates encapsulation strategies. Encapsulation approaches, such as nanoparticles and liposomes, have been proposed to overcome silibinin's low solubility and bioavailability, improving its pharmacological performance (Mohammadi et al., 2022).

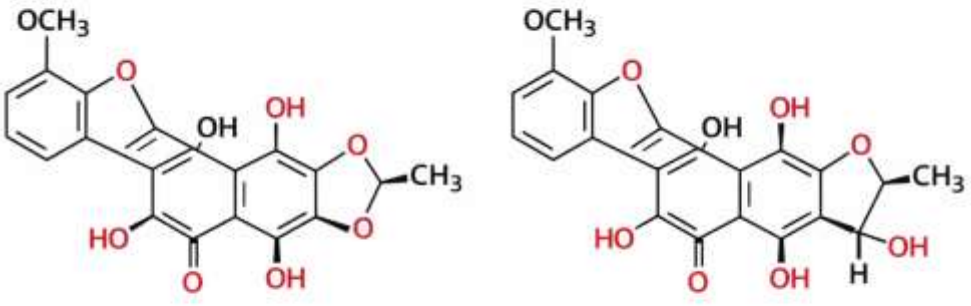

Figure 2. Structural formula of silibinin A and B

1.2. *Cotinus coggygria* Scop. (smoke tree)

Cotinus coggygria Scop., the "smoke tree," is a member of a small genus within the Anacardiaceae family. It is a multi-stemmed, deciduous shrub (small tree), typically growing up to about 5-7 m tall with simple, oval leaves that often turn vibrant shades in autumn (Figure 3). Its name comes from the large, airy inflorescences whose long, hairy stalks give a cloud-like, "smoky" appearance when viewed from a distance. Smoke trees are native to warm temperate regions of Europe, Asia, and North America, found on hillsides, where they tolerate poor soil and full sun exposure (Encyclopaedia Britannica; Matić et al., 2016). It is recognized as a valuable natural reservoir of oil and bioactive compounds, exhibiting a variety of benefits (Novaković et al., 2007). Various parts of *C. coggygria* demonstrate antioxidant, antigenotoxic, antimicrobial, hepatoprotective, anti-inflammatory, and antihemorrhagic effects. The antioxidant properties of plant-derived compounds are particularly noteworthy because of their overall potential to safeguard products from oxidation (Jovanović et al., 2017).

Figure 3. *Cotinus coggygria* Scop. (smoke tree)

Phytochemical analyses of *C. coggygria* revealed a valuable profile of phenolics (flavonoid molecules and phenolic carboxylic acid components, as well as tannin compounds, including sulfuretin, gallic acid, rutin, hyperoside, fisetin, quercetin, luteolin, apigenin, butin, eriodictyol, and isoquercitrin, with significant differences observed between leaf and bark extracts. High-performance liquid chromatography (HPLC) analyses identified myricetin and rosmarinic acid as major constituents in methanolic extracts, along with several hydroxycinnamic acids (Matić et al., 2016; Stojković et al., 2025). Essential oils are characterized mainly by monoterpenes, particularly limonene and α-pinene, with composition varying according to plant part and geographical origin (Matić et al., 2016). Essential oils extracted by hydrodistillation from *C. coggygria* leaf and branch collected at 2 Serbian locations were subjected to gas chromatography. Thirty-one components were detected, with monoterpene hydrocarbons representing the predominant chemical group (87.4% and 93.1%, respectively). Limonene was identified as the major constituent in both oils, accounting for 47.0% and 39.2% of the total composition (Novaković et al., 2007). The literature also reported that the ethanol extract of smoke tree collected in Armenia contained 0.94% flavonoids. Additionally, twenty-two constituents were found in the leaf volatile oil. Chemical profiling indicated that germacrene D and thunbergol, as well as linalool

formate and α-terpineol, were the main compounds in *C. coggygria* oils (Shaboyan et al., 2021), which contribute to the strong antioxidant capacity of the plant. According to the Fraternale and Ricci study (2014), GC-MS characterization of smoke tree essential oils in Italy showed that they were primarily composed of limonene and α-pinene, as well as (E)-β-ocimene and (Z)-β-ocimene. Due to various polyphenols (including sulfuretin, rutin, isoquercitrin, and phenolic acid - gallic acid), the extracts from smoke tree showed strong antimicrobial activity in the case of *Micrococcus luteus*, *Streptococcus parasanguinis*, and *Candida tropicalis*, as well as significant cytotoxic effects on gastrointestinal carcinoma cell lines, with the methanolic leaf extract being the most active, possibly due to inhibition of proinflammatory cytokine release in $CD4^+$ cells, *i.e.*, CD4-positive T lymphocytes (Stojković et al., 2025). In Pašić et al.'s (2025) study, several flavonoids were identified in smoke tree, and plant extract formulations and isolated molecules exhibited strong and specific cytotoxic activity toward multiple cancer cell lines, particularly leukemia and HeLa cells (Henrietta Lacks cells). They start apoptosis and inhibit the migration of the cancer cells while showing cytoprotective effects in normal fibroblasts.

Traditionally, ethanol-based infusions prepared from the woody sections of the plant have been used to alleviate gastric ulcers and diarrhea. Moreover, smoke tree extracts have historically been applied in the healing of cancer, ocular disorders, gastrointestinal disorders, etc. (Matić et al., 2011; Matić et al., 2016; Stojković et al., 2025). Its extracts have been shown to induce apoptotic processes in the HeLa cell line, inhibit cell migration, while providing safeguarding effects on non-cancer fibroblast cells (Pašić et al., 2025). The extract of *C. coggygria* showed hepatoprotective activities in Wistar rats exposed to oxidative stress, reducing lipid peroxidation, DNA damage, and liver enzyme levels while enhancing antioxidant defense mechanisms and modulating Akt/NF-κB signal (Matić et al., 2011). Leaves of the smoke tree have traditionally been employed for wound healing in folk medicine across the Balkans and Anatolia. Previous research demonstrated that ethanol extracts from *C. coggygria* leaves, in rats, markedly enhance the healing of cutaneous wounds (Aksoy et al., 2016a). The literature data also demonstrate the potential of ethanol *C. coggygria* extract to enhance the regeneration of diabetic cutaneous wounds in models in Wistar albino rats, supporting its traditional medicinal applications (Aksoy et al., 2016b). Smoke tree extract exerts its biological effects primarily through the alteration of the stress caused by radicals and inhibition of mediators involved in inflammation.

1.3. Encapsulation of plant bioactives

The growing interest in plant-derived secondary metabolites, particularly polyphenols, for food, pharmaceutical, and cosmetic applications underscores their health-promoting properties and drives research into phenolic compounds. Nevertheless, polyphenols, including anthocyanins, hydroxybenzoic and hydroxycinnamic acids, flavanones, and flavonols, are vulnerable to light, heat, enzymes, and low/high pH values, making them prone to degradation (Jovanović et al., 2023a; Kalita et al., 2025). Their low water solubility further limits bioavailability, and only a small fraction of polyphenols applied topically is effectively absorbed due to poor permeability and instability under physiological and environmental conditions (Karkad et al., 2024; Liu et al., 2023). Although various research have shown dietary polyphenols' benefits to human health, their broader application is limited by low stability, poor bioavailability, and the bitter taste of polyphenol-containing products (Baljak et al., 2025).

To maintain their stability, activity, and delivery efficiency, polyphenols are frequently encapsulated in a variety of carriers (delivery vehicles, delivery systems). Encapsulation protects bioactive compounds from oxidative damage, light exposure, moisture, temperature fluctuations, enzymatic degradation, and pH changes, while also enabling controlled release and extending product shelf life. Common encapsulation techniques include spray drying, nanoencapsulation, liposomes, lyophilization, emulsification, coacervation, extrusion, and inclusion complexation (Baljak et al., 2025; Jovanović et al., 2019; Munin and Edwards-Lévy, 2011; Zhou et al., 2021. Methods such as liposome formation and freeze-drying not only preserve sensitive compounds but also improve their bioavailability, making them highly effective for delivering polyphenols, vitamins, and other bioactive molecules (Jovanović et al., 2019; Jovanović et al., 2023a; Munin and Edwards-Lévy, 2011; Zhou et al., 2021).

Figure 4. Encapsulation techniques for plant extracts and polyphenols

Several studies have demonstrated the successful encapsulation of plant bioactives for enhanced stability and functionality. For instance, flavonoid-rich extracts from *S. marianum* (milk thistle) and *Camellia sinensis* (green tea) were incorporated into liposomes, resulting in improved antioxidant activity and controlled release profiles (Erdoğan and Uğur, 2025; Jara-Quijada et al., 2023). Similarly, anthocyanin-rich berry extracts were encapsulated *via* nanoemulsion and spray-drying, protecting them from thermal and oxidative degradation, while enabling sustained delivery in cosmetics and nutraceuticals (Chen et al., 2019; Gomes et al., 2021). Polyphenols from *Vitis vinifera* (grape) seed and *Punica granatum* (pomegranate) were also effectively entrapped in polymeric nanoparticles, preserving their anti-inflammatory and antimicrobial properties for topical and oral applications (Rahul et al., 2025; Salem et al., 2024). Zhou et al. (2021) examined the encapsulation of lipophilic polyphenols, such as curcumin, resveratrol, and quercetin, in plant-based nanoemulsions and demonstrated that both the type of carrier oil (coconut, sunflower, and flaxseed oils) and the polyphenol significantly influenced their gastrointestinal stability and bioaccessibility. Păvăloiu et al.'s (2021) study investigated the entrapment of *Lycium barbarum* (Goji berry) polyphenol molecules from leaf within lipid particles and showed that the resulting nanocarriers exhibited high entrapment efficiency, good stability, controlled release, and a cytoprotective effect *in vitro*. All the above-mentioned studies collectively highlight the versatility of encapsulation strategies in protecting sensitive plant-derived bioactives and enhancing their therapeutic and functional potential. Due to its high polyphenol content and chemical instability, smoke tree extract is a suitable candidate for encapsulation to improve its stability, bioavailability, and controlled release.

Figure 4 illustrates the common process of encapsulating plant bioactive compounds into carrier particles, a widely adopted approach in nutraceutical and drug delivery systems. By selecting appropriate carriers and encapsulation methods, it is possible to tailor release kinetics, enhance bioavailability, and improve the overall efficacy of plant-derived bioactive formulations.

1.3.1. Liposomes as carriers for plant bioactives and their post-preparation treatment

Lipid-based vesicular systems, including liposomes, have gained considerable attention as advanced carriers for therapeutic agents in modern wound care formulations. Liposomes boost the solubility and stability, as well as bioavailability of encapsulated bioactives by preventing enzymatic deterioration and enabling effective transport into cells. Liposome architecture, composed of concentric phospholipid layers, allows interaction with biological membranes, which supports efficient penetration and localization of active substances within the skin. Owing to these characteristics, such a carrier has been widely adopted to boost the effectiveness and availability of molecules at the target site (Rizkita et al., 2024; Sun et al., 2024a). The internal organization of these vesicles enables simultaneous incorporation of compounds with differing physicochemical properties. Water-soluble substances can be retained within the internal aqueous compartment, while non-polar molecules are accommodated within the lipid domains of the membrane (Sengupta et al., 2021). These vesicular systems are typically fluid, nearly transparent, and exhibit favorable rheological properties, allowing easy handling, uniform application, and further incorporation of bioactive compounds without compromising their stability or functional performance. This versatility is particularly important for achieving optimal therapeutic performance of chemically diverse agents, including poorly water-soluble compounds such as silibinin and polar phytochemical preparations like smoke tree extracts (Figure 5).

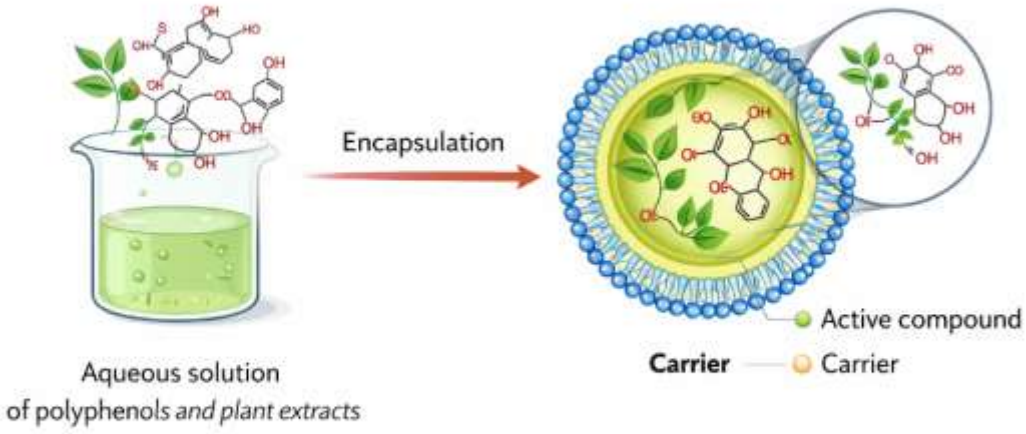

Figure 5. Schematic representation of polyphenol and plant extract encapsulation in liposomes/nanoparticles

Liposomes are capable of providing controlled release of biologically active substances, while simultaneously preventing degradation or modification caused in the presence of the light, oxygen, ultraviolet exposure, free radicals, enzymes, pH fluctuations, etc. (Zhang et al., 2022). Numerous papers demonstrated that liposomal encapsulation enhances the bioavailability of pharmaceuticals, proteins, nutraceuticals, and polyphenolics, due to the similar structure of lipids in liposomes to the membrane of the epithelial cells (Baljak et al., 2025; Isailović et al., 2013; Lee, 2020; Srinivasan et al., 2019).

Liposomal vesicles can be prepared using various techniques, including the hydration of the thin lipid film, extrusion, injection, proliposome formation, etc. (Akbarzadeh et al., 2013; Isailović et al., 2013; Jash et al., 2021; Jovanović et al., 2019; Shade et al., 2016). Among these, proliposome technology appears particularly suitable for large-scale manufacturing (Isailović et al., 2013).

Additionally, sonication together with cavitation could provide the dispersion of lipid molecules and reduce droplet size, which is widely applied to generate small unilamellar vesicles (Huang et al., 2010; Jovanović et al., 2018). Vesicle size has a critical role in the penetration of bioactives and the overall efficiency (Castañeda-Reyes et al., 2020), making it an important factor when selecting liposome preparation methods.

Ultraviolet sterilization can also affect liposome stability and influence the release of encapsulated compounds (Yao et al., 2021). Therefore, its impact should be assessed, particularly in applications involving dermal and transdermal delivery of bioactives-loaded liposomes, which may be exposed to sunlight.

Lyophilization is a widely employed procedure for stabilizing thermosensitive components. By freezing the sample under low pressure and applying minimal heat to sublimate ice, lyophilization produces liposomal powders with long-term stability, preventing hydrolytic and oxidative degradation that occurs in aqueous environments (Akbarzadeh et al., 2013; Munin and Edwards-Lévy, 2011). Given that liposomal formulations often contain 70-95% water, hydrolysis, oxidation, and microbial contamination can significantly shorten shelf life. Freeze-drying is therefore frequently applied to enhance storage stability and extend product longevity (Fang and Bhandari, 2010). However, this process may also alter vesicle structure and bioactivity, necessitating careful evaluation. Considering these factors, lyophilization was selected as a method with the potential to positively or negatively affect liposome properties and the stability of encapsulated bioactives.

1.3.2. Biopolymeric films as carriers for plant bioactives

Chronic and hard-to-heal wounds represent a significant clinical challenge due to their prolonged inflammation, impaired tissue regeneration, and high susceptibility to infection. Current treatment options are often insufficiently effective, particularly for ulcers, which are among the most common types of wounds that exhibit delayed healing. The expanding application of biopolymers in wound care has emerged to develop advanced, environmentally responsible therapeutic materials. Biopolymeric films serve as versatile matrices for the incorporation of plant-derived bioactive compounds, enabling their stabilization and protection from environmental degradation. These films can also provide controlled recovery of the encapsulated compounds, boosting their bioavailability, as well as therapeutic efficacy.

Biopolymers from biological reservoirs exhibit favorable compatibility with human tissue, thereby showing a low risk for inflammation, as well as removing the potential necessity for traumatic dressing removal procedures. As a result, their use contributes simultaneously to improved patient outcomes and a reduction in medical waste generation. In addition to their inherent safety, biopolymeric materials actively support the healing process by promoting cellular proliferation, facilitating faster wound contraction, and minimizing fibrotic tissue formation. Moreover, these materials can be engineered to function as delivery matrices for bioactive substances, enabling localized and sustained therapeutic action. In contrast, conventional dressings for wounds are primarily physical barriers; they frequently fail to maintain the moist wound environment essential for optimal healing. Their limited antimicrobial properties, poor adaptability to fluctuating exudate levels, and insufficient tissue compatibility significantly restrict their clinical effectiveness (Karkad et al., 2026; Su et al., 2023).

Furthermore, traditional dressings lack the capability to regulate the release of therapeutic agents or to actively stimulate tissue regeneration. Inadequate mechanical adaptability and restricted gas permeability also compromise patient comfort and may hinder healing (Karkad et al., 2026; Zhang et al., 2024). These limitations have driven intensive research efforts toward the formation of next-generation dressings for wounds, which contain functional biomaterials (Su et al., 2023; Zhang et al., 2024). Effective wound dressing should not only exhibit excellent biocompatibility but also enable the controlled transport of active compounds across the skin barrier.

Figure 6. Biopolymeric films for the incorporation and release of plant bioactives

Advanced biopolymer-based films (Figure 6), particularly those incorporating liposome-encapsulated bioactive agents, have demonstrated significant potential in fulfilling the aforementioned requirements. Incorporating phenolic bioactive compounds into liposomal carriers prior to embedding them within biopolymer films provides enhanced molecular stability, optimizes the interface with the skin by expanding the effective contact area, and allows for gradual, controlled release. This strategy minimizes compound degradation while ensuring prolonged exposure at the therapeutic site (Cevc, 2004; Yoon et al., 2013). Additionally, encapsulation within phospholipid vesicles significantly improves dermal absorption and bioavailability than in the case of unencapsulated agents. Namely, these particles improve interaction with cellular membranes and promote diffusion, resulting in more efficient delivery once released from the polymeric matrix (Cevc, 2004; Puri et al., 2009).

1.3.3. Pullulan as a carrier for bioactives

Designing biopolymer-based matrices that incorporate bioactive agents, including liposome-encapsulated therapeutic molecules, presents a considerable challenge in advanced wound care. This task requires maintaining the liposome integrity during lipid vesicle integration within the network of biopolymers, while also reaching controlled recovery of the encapsulated compounds. Furthermore, the selection of an adequate carrier (delivery system), optimizing the ratio between the biopolymer and liposomes, as well as managing interactions, is critical to reduce the presence of the aggregates and ensure uniform distribution. Such systems offer more promising skin contact, facilitate higher delivery of entrapped bioactives in lipid particles, as well as provide sufficient adaptability in wound dressing applications.

Among film-forming, biocompatible polymers, pullulan is a candidate for wound dressings, as well as plant bioactives' release (Figure 7). Pullulan, as a polysaccharide formed by *Aureobasidium pullulans* (water-soluble and non-toxic), is widely used as a biopolymeric carrier for bioactive compounds. Its excellent film-forming ability, biocompatibility, and oxygen-impermeable nature make it suitable for stabilizing and delivering sensitive plant-derived compounds. Pullulan-based matrices can also provide controlled release, enhancing the bioavailability and potential of encapsulated bioactive molecules in pharmaceutical and biomedical products.

Nevertheless, despite its advantageous features, its broader use in medical and pharmaceutical contexts is constrained by limited strength, as well as relatively elevated production costs. Thus, it is often combined with various materials or chemically modified to enhance its functional performance (Li et al., 2023). Several modification strategies have been explored in the literature. Oxidative treatments, for example, enhance the mechanical characteristics (Agrawal et al., 2022). Duceac et al. (2021) successfully synthesized 6-carboxypullulan using 2,2,6,6-tetramethylpiperidine-1-oxyl and mediated oxidation, whereas Bruneel and Schacht (1993) were among the first to describe pullulan periodate oxidation. The resulting aldehyde functionalities facilitate reactions with amine-containing polymers or biopolymers (Emam and Mohamed, 2021). Additionally, Emam and Mohamed (2021) showed pullulan carboxymethylation under alkaline water-organic conditions using monochloroacetic acid. Glutaraldehyde was a crosslinker to achieve controlled release of povidone-iodine in dressings for wounds (Li et al., 2020). Further, Enomoto-Rogers et al. (2015) examined how acyl chain length affects the thermotropic, mechanical, and morphological characteristics of esterified films based on pullulan. Esterification strategies for pullulan in food packaging have functional films that are designed by incorporating various carboxylic acids and octenyl succinic anhydride, frequently in combination with chitosan (Carvalho et al., 2020).

Despite the extensive range of chemical modifications reported, achieving a balance between improved mechanical performance and preservation of biocompatibility remains a key objective in pullulan-based material design. Structural tailoring through esterification, in particular, offers a versatile approach to modulating hydrophobicity, thermal behavior, and intermolecular interactions within the polymer network. Such modifications can enhance compatibility with lipid-based carriers, including liposomes, thereby promoting more stable incorporation and homogeneous dispersion within the film matrix. Consequently, rational selection of the modifying agent and degree of substitution is essential for optimizing the characteristics of pullulan-derived systems intended for advanced uses.

Moreover, the integration of pullulan with other biopolymers or nanocarriers can further improve its functional versatility. By combining pullulan with materials such as chitosan, alginate, or gelatin, it is possible to enhance mechanical strength, water resistance, and film elasticity, while maintaining biocompatibility. These hybrid systems also allow fine-tuning of the release profiles for encapsulated bioactive molecules, including lipophilic or hydrophilic compounds. In addition, controlling the microstructure and porosity of the film can facilitate sustained diffusion and prevent rapid aggregation of the active agents. Optimizing processing conditions, such as casting techniques, drying temperature, and crosslinking density, plays a critical role in achieving uniform films with reproducible properties. Thus, pullulan-based composite matrices present a promising platform for advanced wound care applications, combining safe skin interaction with efficient delivery of therapeutic agents.

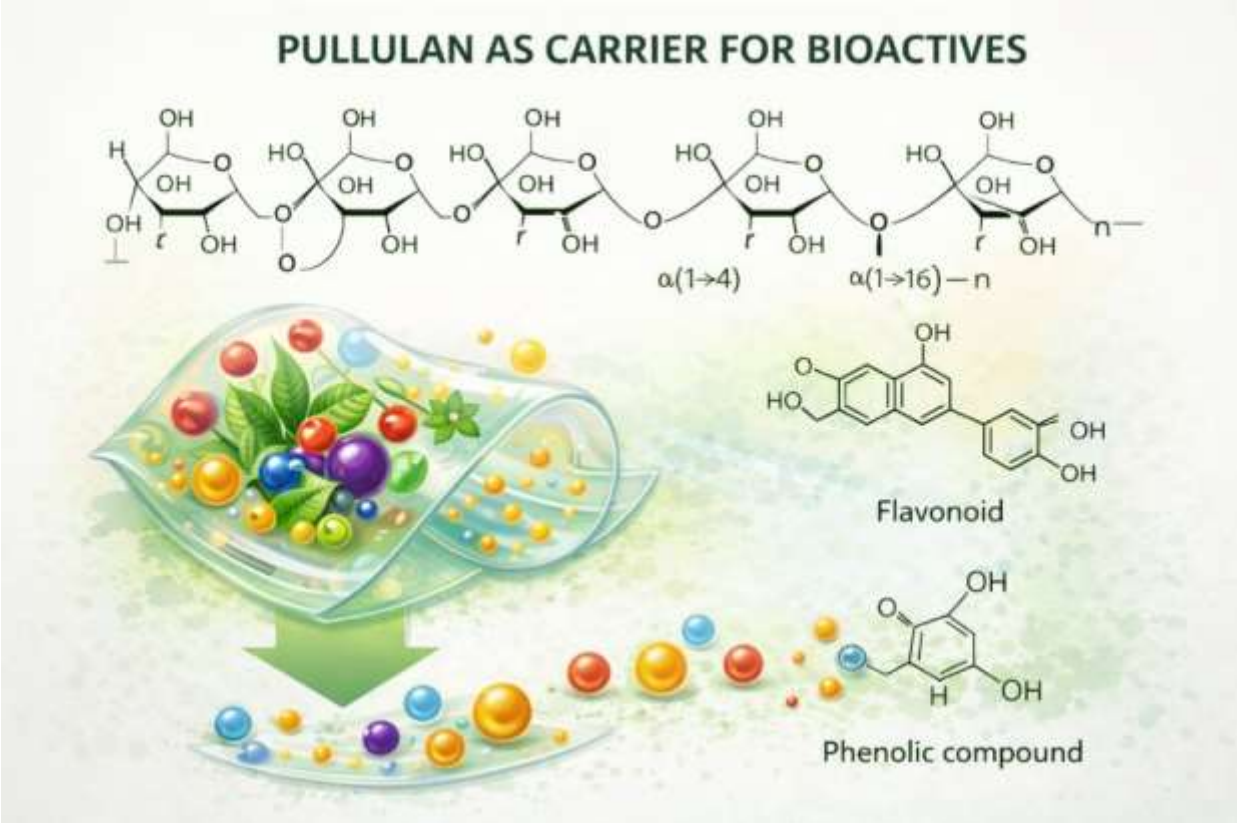

Figure 7. Pullulan as a natural polymer carrier for plant bioactives

Due to its highly hydrophilic nature, pullulan can present limitations in certain delivery applications. To address these challenges, a novel strategy for biopolymer modification can be achieved through direct ester formation using isononanoyl chloride, producing a branched polymer architecture. This method permits fine-tuning of solubility, molecular flexibility, and interfacial properties, facilitating the creation of a hydrophobic biopolymer that maintains water-processability, a combination that is both uncommon and highly valuable for biomedical and related technological applications.

This esterification strategy adjusts the pullulan lipophilic-hydrophobic balance and influences pullulan thermal and mechanical properties, allowing the design of films with tailored stability and flexibility. The introduction of branched isononanoate groups creates additional free volume along the polymer backbone, enhancing chain mobility and facilitating more efficient interaction with encapsulated lipophilic compounds. Moreover, the modified polymer exhibits improved compatibility with lipid-based carriers, such as liposomes, promoting uniform dispersion and controlled release within the film matrix. Ultimately, such modifications expand the functional versatility of pullulan, making it suitable for advanced biomedical, pharmaceutical, and nutraceutical delivery systems.

2. AIMS OF INVESTIGATION

The overall goal of the doctoral thesis was to obtain and examine multifunctional liposomal and polymer-based delivery systems for silibinin and smoke tree extract, and to evaluate their physicochemical, structural, mechanical, and biological properties with potential applications in pharmaceutical and biomedical fields.

The specific aims of this research were:

- To prepare silibinin-loaded liposomal particles in the proliposome procedure and systematically investigate the effects of different post-processing treatments, including ultrasonic irradiation, UV exposure, and lyophilization, on their characteristics and biological potential (antioxidant, cytotoxic, and anti-inflammatory effects).

- To perform comprehensive physicochemical characterization of the liposomal formulations by determining encapsulation efficiency (EE) using UV–Vis spectrophotometry, size of vesicles, size distribution (PDI), surface charge, and conductivity, as well as electrophoretic mobility using dynamic light scattering (DLS).

- To evaluate additional rheological parameters of liquid liposomal formulations (non-treated liposomes, UV-irradated liposomes, and sonicated liposomes), including density (using a silicon crystal), surface tension (using the Wilhelmy plate method), and viscosity (rotational viscometry), to assess their colloidal behavior and formulation stability.

- To investigate the storage stability of liposomes with encapsulated silibinin (non-treated, UV-irradated, sonicated liposomes, and freeze-dried liposomes) under controlled environmental conditions (kept in the refrigerator at 4°C) *via* measuring diameter, PDI, surface charge, and electrophoretic mobility, as well as conductivity over a period of 60 days.

- To elucidate the molecular interactions between silibinin and lipid bilayers using FT-IR spectroscopy and Raman spectroscopy, and to notice characteristic functional group shifts associated with drug encapsulation and post-processing treatments (UV treatment, sonication by using an ultrasound probe, and lyophilization).

- To assess the biological activities of silibinin-loaded liposomes through antioxidant tests in the *in vitro* conditions (ABTS - 2,2'-azino-bis(3-ethylbenzothiazoline-6-sulfonic acid) and DPPH, *i.e.*, 2,2-diphenyl-1-picrylhydrazyl, cytotoxicity test on immortalized human keratinocyte cell lines, *i.e.*, HaCaT cells (3-(4,5-dimethylthiazol-2-yl)-2,5-diphenyltetrazolium bromide test), investigaion of an antioxidant capacity in the H_2O_2-induced oxidative strees in the HaCaT cells of the liposomes with encapsulated silibinin and unloaded liposomes, and evaluation of anti-inflammatory potential by measuring the reduction in the generation of cytokines (induced by the *Escherichia coli*-produced lipopolysaccharide) in the presence of liposomes with encapsulated silibinin, as well as plain liposomes.

- To prepare and characterize smoke tree (*Cotinus coggygria* Scop.) extract, including determination of extraction yield, total polyphenols (*via* Folin-Ciocalteu assay), and total flavonoids (aluminum chloride colorimetric test).

- To synthesize pullulan-isononanoate (Pull-Iso) *via* isononanoic acid chloride-induced pullulan esterification, and to confirm the chemical modification *via* nuclear magnetic resonance spectroscopy, as well as FT-IR spectroscopy.

- To prepare silibinin/smoke tree extract-loaded liposomes and perform comprehensive physicochemical characterization of the liposomal formulations by determining EE using UV–Vis spectrophotometry, liposome size, distribution of particles, and surface charge (DLS measurements), and monitoring their stability (60-day storage in the refrigerator at 4°C).
- The incorporation of silibinin/smoke tree extract-loaded liposomes into Pull-Iso polymer matrices to obtain composite films with different liposome loadings.
- To investigate the microstructure and dispersion of liposomes within Pull-Iso films using optical microscopy.
- The universal testing machine was used to assess the mechanical behavior of the composite biobased film samples, including tensile strength and Young's modulus, as well as elongation at break, according to standardized tensile testing protocols.
- To characterize surface wettability and hydrophobicity of the films, the sessile drop method was employed to determine the static water contact angle.
- To test the physical properties of the developed biobased film samples by measuring moisture content (gravimetric method), total soluble matter (water solubility test), and swelling behavior in aqueous media.
- To investigate the antioxidant activity of liposomal vesicles with silibinin/smoke tree extract, Pull-Iso composite films (in the presence and the absence of the liposomal particles with bioactives) under simulated skin conditions using ABTS and DPPH assays, thereby evaluating their potential for topical biomedical applications.
- To explore the potential of the developed liposomal and polymer-based systems as advanced multifunctional platforms for controlled delivery of natural bioactives (antioxidants, anti-inflammatory agents, and compounds with cytotoxic or cytoprotective effects).

3. EXPERIMENTAL PART

3.1. Herbal material, cells, compounds, and reagents

C. coggygria or smoke tree wooden sections, which were utilized to prepare ethanol smoke tree extract, were gathered in Belgrade, Serbia. After the removal of the bark, the wooden portion of the smoke tree was finely pulverized into homogeneous powder.

Used chemicals included 96% ethanol, Na_2CO_3, Folin-Ciocalteu reagent, $NaNO_2$, $AlCl_3$, ABTS, ascorbic acid, DPPH, phosphate-buffered saline - PBS, and sodium dodecyl sulfate - SDS, NaOH, gallic acid, catechin, and $K_2S_2O_8$. Mueller-Hinton and Sabouraud Dextrose agar plates were used for antimicrobial testing. Pullulan, isononanoic acid, 2-pyrrolidone, thionyl chloride, triethylamine, dimethyl sulfoxide (DMSO), dimethylformamide (DMF), glycerol, KOH, and HCl are also used. Phospholipon 90G and silibinin were used for liposome preparation. HaCaT keratinocyte line was obtained courtesy of the Institute for Biological Research "Siniša Stanković". Lipopolysaccharide - bacterial origin (LPS from *Escherichia coli*), MTT assay reagent, DMEM/F12, Tween 20, RPMI 1640, fetal bovine serum - FBS, antimycotic-antibiotic solution, H2DCFDA (2′,7′-dichlorofluorescin diacetate), fetal calf serum - FCS, trypsin-EDTA, bovine serum albumin (BSA), and secondary antibodies (anti-rabbit immunoglobulin, horseradish peroxidase-linked and anti-mouse immunoglobulin, horseradish peroxidase-linked) were employed for cell analyses. Simplicity UV® (Merck Millipore, Germany) was employed as the water purification system to obtain ultrapure water.

HaCaT was cultured in the flasks under conditions including 37°C and 5% of carbon dioxide. The cells were maintained in a growth solution composed of DMEM/F12 supplemented with FCS and antimicrobial medium. Upon achieving approximately the confluence of 70%, HaCaT was detached using medium with trypsin and EDTA and subsequently transferred to the plates with 96 wells (1.5×10^4). Prior to experimental treatment, the HaCaT cells adhered for one day in the same incubation conditions. Ethical approval for the use of HaCaT cells was obtained from the Institute for the Application of Nuclear Energy (No. 0203-07-013/007/2025, from 14th February 2025).

3.2. The extraction from the smoke tree's wooden part

C. coggygria extract sample was obtained by combining 5 g of finely ground wood with 200 mL of 80% (*v*/*v*) ethanol in water, followed by extraction *via* ultrasound waves (Sonorex ultrasound bath, Bandelin, Germany). The extraction time was 0.5 h (Jovanović et al., 2025), as shown in Figure 8. The sample was then filtered before being employed in liposome preparation. The liquid extract was stored at 4°C in a refrigerator befor the further analyses.

Following the initial extraction, the obtained liquid was carefully handled to preserve its bioactive components, minimizing exposure to light and oxygen, which could degrade sensitive phenolic compounds. The extract was kept under controlled conditions to achieve a consistent concentration for subsequent encapsulation into liposomes. Prior to incorporation, preliminary characterization, such as determination of total phenolic/flavonoid content and antioxidant activity, was performed to ensure reproducibility and efficacy. The use of ultrasound-assisted extraction not only accelerated the process but also enhanced the release of active molecules from the lignocellulosic matrix of the wood. This extract, with its rich composition of bioactive compounds, provided a suitable payload for the design of stable, uniform liposomal systems intended for biomedical applications. Finally, all handling and storage steps were standardized to maintain the integrity and functionality of the extract until further use in formulation studies.

Figure 8. Ultrasound-assisted extraction of the smoke tree wooden part using ethanol in water (80%)

3.2.1. Measurement of the extraction yield

The mentioned parameter was evaluated for a liquid extract from the smoke tree's wooden part. The extraction yield was calculated according to the next formula:

$$\text{Extraction yield} = (100 - \frac{m}{x-y}) \times 100 \qquad \text{(Eq. 1)}$$

In this equation, sign *x* denotes the mass of the glass container with the liquid extract prior to drying (expressed in g), while sign *y* represents the same container mass following heating, expressed in grams. Drying was carried out for approximately 2 h under 105°C using a Memmert 30-1060 drying oven (Memmert, Germany). The variable *m* corresponds to the extract mass (expressed in g). The data was reported as dry matter content, expressed as a percentage (%).

3.2.2. Total polyphenols in smoke tree extract

The determination of the polyphenol yield provides an essential measure of the extract's antioxidant potential and overall phytochemical richness. Accurate quantification using the modified Folin-Ciocalteu method allows comparison between different extracts and supports the assessment of their suitability for incorporation into bioactive delivery systems.

The total polyphenols - TPC was analyzed by spectrophotometric analysis (modified Folin-Ciocalteu procedure) according to Jovanović et al. (2017) (Figure 9). Briefly, the extract (0.020 mL) (previously diluted) was combined with aqua (1.20 mL) and Folin-Ciocalteu reagent (0.10 mL, water/reagent ratio was 2:1). After mixing, 300 μL of NaOH (20%) was transferred. The final mixture was adjusted using aqua (up to 2.0 mL), mixed, and incubated for 2 h (dark, 25°). The reading of absorbance was performed using a blind probe sample for reference at the wavelength of 765 nm in the

UV-1900 spectrophotometer (Shimadzu, Japan). The standard compound, gallic acid, was used for constructing the curve, and the results were presented in mg GAE/g of herbal matrix.

3.2.3. Total flavonoids in smoke tree extract

The quantification of the flavonoid yield gives valuable insight in the chemical profile and potential plant extract bioactivity. Precise measurement using the described colorimetric method enables comparison of flavonoid levels across different samples and supports evaluation of their functional properties in bioactive formulations.

The total flavonoids - TFC was quantified in the colorimetric procedure according to Xi and Yan (2022) (Figure 9). In this assay, extract (0.25 mL, previously diluted), 75 μL of $NaNO_2$ solution (5%), and aqua (1.25 mL) were mixed. Following a 5 min incubation period, 150 μL of $AlCl_3$ solution (8.8%) was transferred. At the sixth minute, NaOH solution (1M, 0.50 mL) was introduced, and the volume was adjusted using aqua (up to 3.0 mL). The absorbance readings (at a wavelength of 510 nm) were performed immediately. The reference standard was catechin, and the results were presented as mg CE/g of herbal matrix.

Figure 9. Total polyphenols and total flavonoids of the smoke tree extract

3.3. Development of liposomal particles

3.3.1. Development of liposomal particles with silibinin

Silibinin-loaded liposomes (MLVs, multilamellar) were produced by the proliposome technique with minimal adjustments (Jovanović et al., 2023a) (Figure 10). Briefly, phospholipids (10 g) were combined with silibinin (1 g) in 96% (*v*/*v*) ethanol (40 mL). The sample was warmed (60°C) at continuous stirring (800 rpm) during 15 min using a laboratory magnetic stirrer. Following cooling (approximately 23°C), aqua (80 mL) was gradually transferred in small aliquots. The resulting solution was further mixed (800 rpm, 60 min) to promote liposome formation. Empty multilamellar particles, used as a control, were prepared using phospholipids (2.5 g), 96% (*v*/*v*) ethanol (10 mL), and ultrapure water (20 mL) under identical conditions. Following complete ethanol evaporation in both loaded and unloaded formulations, the final phospholipid concentration - 0.125 g/mL.

3.3.2. Development of liposomal particles containing *Cotinus coggygria* extract/silibinin

Multilamellar liposomal vesicles encapsulating silibinin/*C. coggygria* extract were produced *via* the proliposome approach as well (Isailović et al., 2013) (Figure 10). In short, phospholipids (6 g) were combined with 60 mL of the ethanol smoke tree extract and silibinin (1.5 g). The sample was maintained under stirring (50-60°C, 15 min, at 800 rpm. At approximately 23°C, aqua (120 mL) was transferred gradually to induce vesicle formation. The mixture was then stirred during an additional 60 min (800 rpm). As ethanol was completely removed during processing, the phospholipid content in the formulation - 0.050 g/mL.

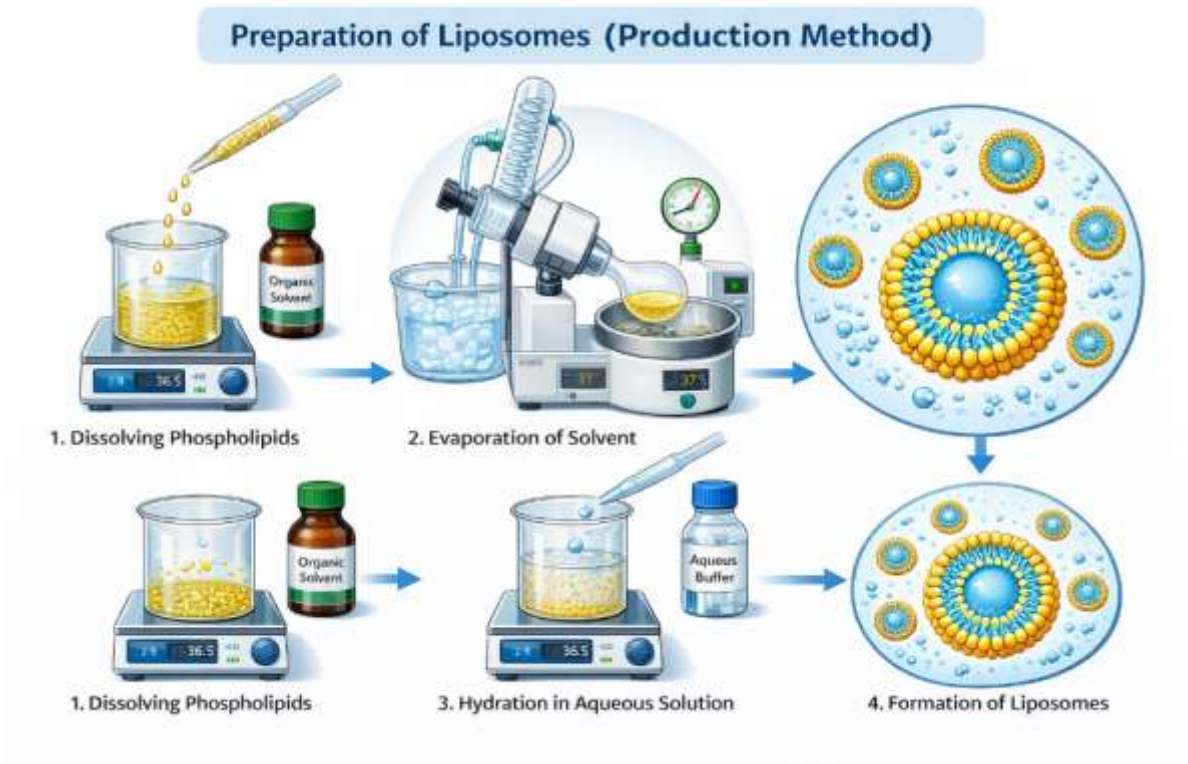

Figure 10. Liposome preparation

3.4. Modification of silibinin-loaded liposomes by ultrasound probe

To decrease vesicle size and obtain small unilamellar vesicles (SUVs) with encapsulated silibinin, multilamellar liposome dispersions containing silibinin (20 mL) were subjected to probe sonication for 15 min using a pulsed regime (30 s *on*/10 s *off*) (Figure 11). Sonication was performed with a Sonopuls ultrasonic probe (Bandelin, Germany) operating at 40% amplitude, while maintaining a controlled temperature (approximately 25-28°C). Namely, the flask and sample were continuously cooled with ice. The temperature was monitored to prevent overheating (Jovanović et al., 2018).

Figure 11. Sonication of liposomes with silibinin by an ultrasound probe using a pulsed regime

3.5. Modification of silibinin-loaded liposomes by UV irradiation

The UV-C exposure was designed to evaluate the photostability of silibinin encapsulated within multilamellar liposomes, providing insight into the protective effect of the lipid bilayer. Controlled irradiation allows assessment of degradation kinetics and identification of potential structural changes induced by high-energy UV photons. Such studies are essential to understand the shelf-life of liposome formulation samples, as well as their performance under environmental stress conditions. Moreover, this approach enables optimization of formulation parameters to strengthen the efficacy, as well as stability of bioactive compounds-loaded liposomal particles in pharmaceutical and cosmetic applications.

For UV treatment, multilamellar liposome samples with silibinin (20 mL) were spread as a thin layer and UV-C irradiated at a wavelength of 253.7 nm (Figure 12) (Yao et al., 2021). Irradiation was carried out for periods ranging from 15 min to 90 min in the laminar, following previously reported procedures (Petrović et al., 2017).

The effect of UV-C exposure on silibinin-loaded liposomes was further monitored to determine any subtle alterations in particle size and surface charge, which could influence stability. Observations of potential changes in encapsulation efficiency helped to clarify the protective capacity of the lipid bilayer against photodegradation. Additionally, UV irradiation provided valuable information on how formulation parameters, such as lipid composition and lamellarity, can be adjusted to enhance photostability. These insights contribute to the rational design of liposomal carriers capable of maintaining bioactive compound efficacy under prolonged light exposure.

Figure 12. Ultraviolet irradiation of plain liposomes and liposomes with silibinin in a laminar flow cabinet (15-90 min)

3.6. Modification of silibinin-loaded liposomes by lyophilization

Lyophilization is a widely performed strategy to boost the prolonged stability of liposomal formulations by minimizing hydrolytic degradation and preventing aggregation. The process preserves the integrity of bilayers while maintaining the encapsulated bioactive compound, allowing reliable post-rehydration recovery of physicochemical properties. Evaluating lyophilized liposomes ensures that key functional parameters, such as particle size, encapsulation efficiency, and antioxidant activity, are retained after drying. Additionally, preparing UV-treated and differently loaded samples under identical lyophilization conditions facilitates consistent comparative analysis using spectroscopic and cell-based assays, supporting a comprehensive assessment of formulation stability and performance.

The effect of freeze-drying on liposomal formulation with silibinin was also evaluated. Freshly prepared liposomes with bioactive compound silibinin (silibinin in MLVs) and plain lipid spheres (10 mL) were centrifuged, after which the supernatants were removed. The remaining precipitates were left in a deep freezer during 60 min (-80°C). Lyophilization was conducted using Alpha 2-4 LSCplus laboratory freeze dryer (Christ, Germany) under the following conditions: -75°C during one day in vacuum (Figure 13). The dried liposomes were rehydrated to restore the initial volume prior to future analyses, including entrapment efficiency determination and DLS, as well as antioxidant assays, followed by experiments on the cells. For Fourier transform infrared (FT-IR) and Raman spectroscopic measurements, UV-treated liposomes with silibinin and silibinin-loaded SUVs were lyophilized under identical conditions, together with both plain and entrapped MLVs.

Figure 13. Lyophilization of plain liposomal spheres and liposomes entrapped with silibinin (non-treated, ultraviolet-irradated samples, and sonicated samples)

3.7. Measurement of encapsulation efficiency

Encapsulation efficiency (EE) in silibinin and silibinin/smoke tree extract liposomes was detremined by quantifying amounts of non-entrapped silibinin and polyphenols from smoke tree extract present within supernatants:

$$\text{Encapsulation efficiency (\%)} = \frac{C_i - C_{sup}}{C_i} \times 100 \quad \text{(Eq. 2)},$$

where C_i represents the initial amount of silibinin or silibinin/smoke tree polyphenols used during liposome preparation, and C_{sup} denotes the silibinin or silibinin/smoke tree polyphenols concentration measured in the supernatant.

Unencapsulated silibinin or silibinin and smoke tree polyphenols were separated from liposomal mixtures (multilamellar, ultraviolet-treated, and freeze-dried) *via* ultracentrifugation during 1 h (17,500 rpm, 4°C) using a Thermo Fisher Scientific ultracentrifuge (USA) (Figure 14). In the case of SUVs, separation was achieved by ultracentrifugation during 6 h (10,000 rpm, 4°C) with a Beckman Coulter ultracentrifuge (USA). The silibinin or silibinin/smoke tree polyphenols contents in the collected supernatants were measured spectrophotometrically at 765 nm (modified Folin-Ciocalteu assay) (Jovanović et al., 2017) (UV-1800 spectrophotometer, Shimadzu, Japan) (Figure 14).

Figure 14. Centrifugation and UV–Vis spectrometry

3.8. Dynamic light scattering and storage stability evaluation

DLS is widely used for the precise determination of particle size, distribution of particles, and zeta potential of colloidal systems, including liposomal formulations. It provides critical insight into the homogeneity and stability of lipid-based carriers, which are essential for predictable bioactive delivery. Evaluating zeta potential, electrophoretic mobility, and conductivity further allows assessment of colloidal stability and potential aggregation tendencies over time. In this study, DLS was employed to characterize silibinin-loaded and silibinin/smoke tree extract-entrapped liposomal spheres, and to monitor liposome storage stability during storage (in a refrigerator, 4°C, during 60 days).

The diameter, PDI, surface charge, electrophoretic mobility, as well as conductivity of dispersions (multilamellar, small unilamellar, ultraviolet-treated, and freeze-dried formulations containing silibinin, as well as plain liposomes) and the diameter, size distribution, and zeta potential of silibinin/smoke tree extract were characterized using the aforementioned technique (Zetasizer, Malvern Instruments Ltd., UK), covering a particle size range from 0.6 nm to 6000 μm (Figure 15). The determination was conducted at approximately 23°C following a 200-fold dilution. Conductivity, electrophoretic mobility, and surface charge determination was performed in a DTS 1070 capillary cell at 25°C. Measurements were in triplicate, and the data is reported as a mean value. The liposome sizes were expressed in nanometers (nm), while the PDI is reported as a dimensionless parameter. The measured value of surface charge was reported in millivolts (mV), while the data for electrophoretic mobility were expressed as micrometers centimeter per volt second (μmcm/Vs). Conductivity data are expressed as conductivity factors (CF), where 1 CF corresponds to 10 μS/cm (micro siemens per centimeter).

The physical stability of silibinin-loaded liposomal particles (multilamellar, small unilamellar, ultraviolet-exposed, and freeze-dried) and silibinin/smoke tree extract-loaded liposomes was evaluated for 60 days (4°). DLS measurements were performed on days 1, 7, 14, 21, 28, and 60 (for silibinin-entrapped liposomal spheres) and on days 1, 7, 14, 30, and 60 (for silibinin/smoke tree extract-loaded liposomes). Throughout the monitoring of liposome stability, the freeze-dried liposome with silibinin was kept in the dry state. Namely, it was rehydrated with ultrapure water immediately prior to each measurement.

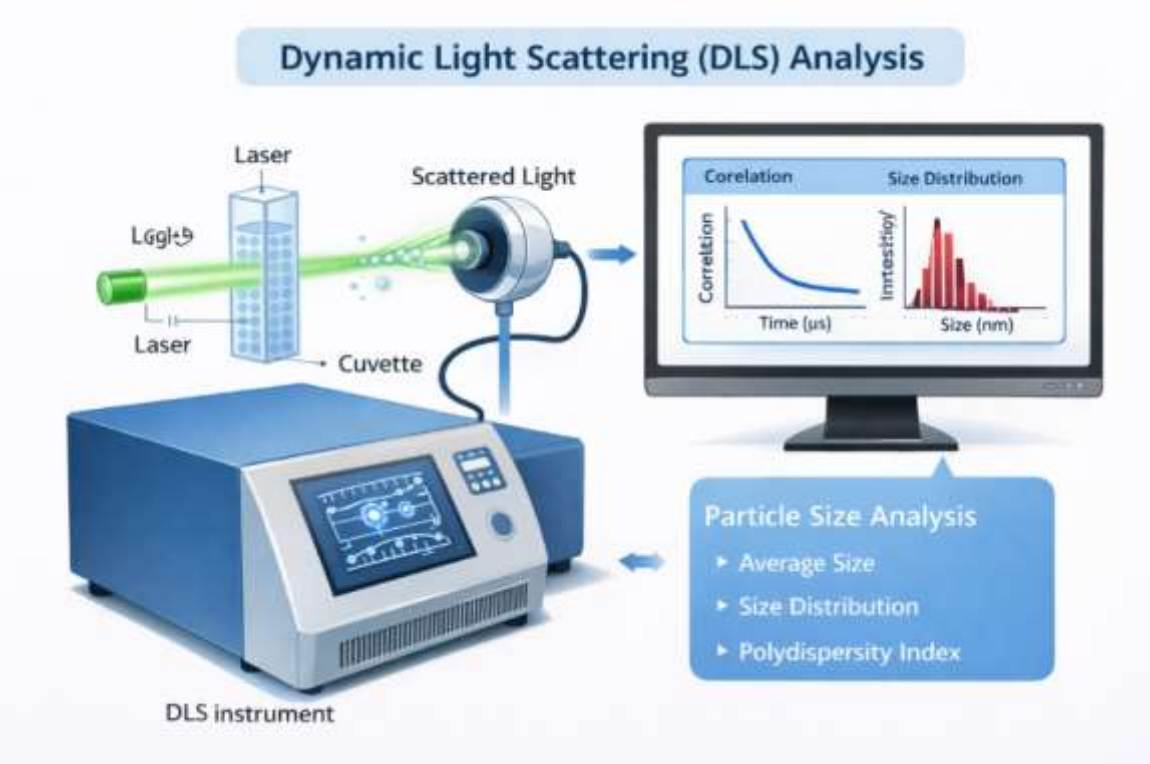

Figure 15. Dynamic light scattering analysis of developed liposomes

3.9. Density and surface tension measurement and viscosity determination

The rheological properties of liquid silibinin-entrapped liposomal formulations, specifically density and surface tension of multilamellar, small unilamelar and ultraviolet-treated, were analyzed in the Force Tensiometer K20 (KRÜSS, Germany). The silicon crystal was the probe for density measurements, while tension was assessed in the Wilhelmy plate method. Formulations were analyzed in triplicate at a controlled ambient temperature. The viscosity values of the identical samples were further assessed in the Rotavisc instrument (VOL-C-RTD chamber and spindle, as well as VOLS-1 adapter, IKA, Germany). Formulations (6.7 mL) were measured in triplicate at a controlled ambient temperature.

3.10. Pullulan modification

To prepare esterified pullulan (pullulan-isononanoate, *i.e.*, Pull-Iso) at its solubility limit, achieving sufficient esterification to increase lipophilicity with maintained solubility in water, the next method was employed: isononanoic acid chloride was synthesized in the reaction between isononanoic acid and thionyl chloride (a molar ratio of 1:3) at 70°C during 8 h. Thionyl chloride (excess amount) was eliminated using the process of distillation, and the product was further purified *via* vacuum distillation (107°C, 22 mmHg), yielding 3,5,5-trimethylhexanoyl chloride (purity of 95%). After that, 19.6 g of pullulan was mixed with 2-pyrrolidone/DMF (ratio 3:1, 0.20 L, ambient temperature). Subsequently, 15.2 mL of triethylamine was transferred. The flask was immersed in ice, and 19.2 g of isononanoyl chloride was introduced dropwise (period of 2 h). It was stirred continuously during 12 h at ambient temperature, followed by 2 h at 40°C. Upon completion, it was added to a beaker (2 L, mechanical stirrer, Teflon propeller). While stirring at a speed of 1100 rpm. Subsequently, methyl alcohol (1000 mL) was introduced dropwise (period of 2 h). It results in white fibrous components. The product was purified three times by dissolving it in aqua (0.20 L, 30°C, 3 h) under mixing, followed by precipitation with methyl alcohol

(1000 mL) over a 2-hour period (~1000 rpm). The designated pullulan-isononanoate was transferred to the oven and dried during one day (52°C). Pull-Iso was then exposed to a vacuum during 16 h (52°C and 2000 Pa). FT-IR spectroscopy, as well as ^{1}H and ^{13}C NMR analyses, collectively provide clear evidence confirming the successful synthesis of 3,5,5-trimethylhexanoic acid, *i.e.*, isononanoic acid (Supplementary Materials).

3.11. Nuclear magnetic resonance spectroscopy

^{1}H and ^{13}C spectra of nuclear magnetic resonance spectroscopy was obtained using the 400-MR spectrometer (Agilent Technologies, USA) equipped with a 400-MR console and a 1H/19F/X 5 mm probe; 399.74 MHz - ^{1}H and 100.53 MHz - ^{13}C. Measurement was carried out using dimethyl sulfoxide-d6 (298 K). Further, chemical shifts - δ (referenced to the residual medium signals) were δH of 2.50 ppm, while δC was 39.52 ppm. The spectral interpretation was carried out in the MestReNova software.

3.12. Determination of the esterification degree (potentiometric titration)

The esterification degree (EV) was determined using potentiometric titration, providing quantitative insight into the extent of chemical modification of the pullulan backbone. Accurate assessment of esterification is essential for correlating structural changes with the resulting physicochemical, thermal, and mechanical properties of the modified polymer.

The pullulan EV was evaluated through potentiometric titration. Initially, free carboxylic group amounts were detremined. Subsequently, following complete hydrolysis of the ester groups, the total amount of carboxylic acids was quantified. The acid value, presented as AV, was measured following the method given in ASTM D3644 standard (2022). Pullulan-isononanoate was dissolved using water/DMSO. It was titrated potentiometrically with potassium hydroxide (0.1 N). The acid value was detremined:

$$AV = \frac{56.1 \times cKOH \times VKOH}{mPull-Iso} \quad \text{(Eq. 3)},$$

where c_{KOH} - concentration of potassium hydroxide, V_{KOH} - standard potassium hydroxide solution volume, $m_{Pull\text{-}Iso}$ - pullulan-isononanoate sample mass.

Following the quantification of free carboxylic groups, the SV (*i.e.*, saponification value) was determined (ISO 3657:2023, 2023). The procedure involves complete base-catalyzed hydrolysis of the ester groups, followed by neutralization of the liberated acidic moieties with a potassium hydroxide solution. The resulting mixture was then titrated using HCl (0.1 mol/L):

$$SV = \frac{56.1 \times cHCl \times (VHCl0 - VHCl)}{mPull-Iso} \quad \text{(Eq. 4)}$$

In this equation, c_{HCl} - concentration of HCl, V_{HCl0} - volume of HCl employed for the KOH neutralization, *i.e.*, blank titration, while V_{HCl} is the HCl volume employed for the Pull-Iso solution neutralization after KOH treatment.

The esterification value (EV) was determined as SV - AV, providing a quantitative measure of the number of hydroxyl groups that were successfully esterified. A higher EV indicates a greater degree of substitution, reflecting more extensive chemical modification of the polysaccharide backbone. This parameter is crucial for correlating structural changes with resulting physicochemical characteristics (hydrophobicity, thermal behavior, solubility of the modified polymer, etc.).

3.13. Differential scanning calorimetry method

The thermotropic behavior of pullulan-isononanoate was investigated by the DSC Q20 system (TA Instruments, USA). Experiments were conducted in a nitrogen atmosphere with 50 mL/min as a flow rate. The device is calibrated by indium. Pullulan-isononanoate warmed from ambient temperature to 250°C (10°C/min). T_g (glass transition temperature) was calculated as the midpoint of the heat capacity (ΔC_p) transition. The temperature measurements were associated with a standard uncertainty of u(T) = 0.5°C, while all data acquisition, processing, and visualization were carried out in the TA Analyzer software.

3.14. Development of bio-based films

A plain biobased film sample was obtained by mixing pullulan-isononanoate (1000 mg) and water (12.5 mL). Glycerol (200 mg) was transferred to the solution. The mixture was placed in the Petri dishes. The samples were dried (50°C) until they reached a constant weight, confirming complete solvent removal. Biobased film samples incorporating liposomes and silibinin/smoke tree extract were formed using the same procedure, with 250 mg, 500 mg, or 750 mg of liposome dispersions containing encapsulated silibinin and smoke tree extract. The liposomes were homogenized into the polymer solution at room temperature prior to casting.

3.15. Infrared spectral characterization *via* Fourier transform

FT-IR spectroscopy can characterize molecular structures and detect potential chemical changes in both pure compounds and complex liposomal or polymeric formulations. This technique provides detailed information on functional groups, intermolecular interactions, and the effects of UV exposure, sonification, formulation, and/or post-formulation processes on the chemical integrity of bioactive-loaded systems.

FT-IR spectra were recorded for silibinin, Phospholipon 90G, and its ultraviolet-exposed form, as well as freeze-dried liposomal formulations with encapsulated silibinin (multilamellar, small unilamellar, and ultraviolet-treated). The lyophilized sample was used for all measurements. Analysis was acquired in the Thermo Fisher Scientific spectrometer (USA) with ATR (400-4000 cm^{-1}) (Figure 16). Measurement was performed using 20 scans per sample; the spectral resolution was 4 cm^{-1}. Liposomal formulations (in the presence or the absence of the encapsulated silibinin) were irradiated with UV for 15, 30, 45, and 90 min to examine the effect of exposure time on chemical changes. In addition, spectral deconvolution was applied to the FT-IR data to enhance the detection of bond alterations.

FT-IR spectra were also recorded for smoke tree extract, silibinin/smoke tree extract-loaded liposomes, empty liposomes, pullulan, pullulan-isononanoate, plain film, and films with silibinin/smoke tree extract in liposomes using the same device.

The FT-IR analysis allowed for a comparative evaluation of structural integrity across different liposomal types and polymeric matrices. Changes in characteristic absorption bands provided insight into possible interactions between silibinin, smoke tree extract, and the lipid or polymer components. Time-dependent ultraviolet exposure revealed subtle shifts in functional group vibrations, indicating partial chemical modifications or stabilization effects within the formulations. The use of spectral deconvolution enhanced the resolution of overlapping peaks, facilitating more precise identification of bond alterations. Therefore, FT-IR spectroscopy proved to be a valuable tool for monitoring the chemical stability and compatibility of bioactive-loaded systems under various processing and environmental conditions.

Figure 16. Fourier transform infrared spectroscopy

3.16. Spectroscopic analysis *via* Raman scattering

Raman spectroscopy of silibinin, Phospholipon 90G, as well as freeze-dried multilamellar, small unilamellar, and ultraviolet-treated lipid formulations with silibinin was performed in the T64000 triple spectrometer (HORIBA Jobin-Yvon, Japan) containing the liquid-nitrogen-cooled detector, CCD (150-3400 cm^{-1}, spectral resolution was 2 cm^{-1}). The wavenumber accuracy was ±3 cm^{-1}. Excitation was performed using an argon/krypton ion laser at 514.5 nm, with the laser power maintained below 1 mW to prevent sample heating or degradation.

3.17. Optical microscopy

Developed films with silibinin/smoke tree extract-entrapped liposomal spheres (containing various amounts of the incorporated lipid particles with bioactives) were also analyzed by the optical microscope (Delta Optical, Poland). All images were acquired and processed using HiView software.

3.18. Determination of the water contact angle

The wettability of the film surfaces was evaluated *via* the sessile drop method. At ambient temperature, droplets of water were deposited on the biobased film samples, and the resulting contact angles were determined using Ossila Contact Angle software (Ossila Ltd, UK). Five independent determinations were carried out. The mean value was calculated to ensure accuracy and reproducibility.

3.19. Assessment of the films' content of moisture, swelling capacity, and total soluble solids

The characteristics of the prepared biobased film samples were evaluated by assessing their content of moisture, swelling capacity, and total soluble solids. The contents of moisture were calculated after oven-drying of films (~103°C), with the observed weight loss related to water evaporation.

Total soluble solids were evaluated as the proportion of the dry mass of developed film samples (dissolved into buffer solution - 25 mL, over a 24-hour period), adapting the method described by Erceg et al. (2025). For each film type, three 10 × 10 mm specimens were weighed (m_1) prior to immersion in a pH 5.5 buffer (simulation of the skin conditions), at ambient temperature. Following 24 h incubation, the remaining undissolved material was separated by filtration, heated using the oven (~103°C) until a stable weight was reached, and then reweighed (m_2) to calculate the dissolved fraction:

$$TSM = \frac{m1-m2}{m1} \times 100\% \qquad \text{(Eq. 5)}$$

The capacity of swelling of the films was determined by immersing pre-weighed 10 × 10 mm samples in a pH 5.5 buffer (25 mL) during 30 min (ambient temperature). Following immersion, the films were gently removed, surface water was carefully blotted with filter paper, and the film was immediately weighed. This technique was adapted from the method presented in the literature (Apriliyani et al., 2020). All experiments were conducted in triplicate, and the swelling ratio was determined:

$$SD = \frac{m2-m1}{m1} \times 100\% \qquad \text{(Eq. 6)}$$

Here, m_1 - weight of the dried film, and m_2 - the swollen film weight.

3.20. Determination of mechanical features

The mechanical behavior of plain films and film samples containing various concentrations of silibinin/smoke tree extract-entrapped liposomal particles was evaluated by the Shimadzu Universal Testing Machine (Japan) (23 ± 2°C). A specimen with the following dimensions, 50 × 10 mm and 1 mm of thickness, was analyzed using 1 mm/min of a crosshead speed. The analysis was carried out three times in order to provide accuracy and reproducibility.

3.21. Antioxidant potential of developed liposomal spheres and films

The antioxidant activity of all liposomes with silibinin and silibinin/smoke tree extract and bio-based films was assessed in 2 complementary tests, specifically ABTS and DPPH. Additionally, the intracellular antioxidant effects of silibinin-entrapped liposomes (MLVs, UV-treated, and SUVs) were evaluated in cells generating free radicals. Evaluation of the antioxidant activity of liposomes/biobased films incorporating bioactive compounds is essential, as the encapsulation process may significantly affect their chemical stability, structural integrity, and bioavailability. Determining the antioxidant capacity of such formulations provides insight into whether the liposomal delivery system preserves or enhances the functional efficacy of the incorporated active components.

3.21.1. ABTS

The activity of silibinin-entrappted liposomal vesicles (MLVs, UV-treated, and SUVs) against $ABTS^{\bullet+}$ was determined according to Zuhair et al. (2013) (Figure 17). The $ABTS^{\bullet+}$ working mixture containing ethanol had the absorbance of 0.717 (wavelength of 734 nm). $ABTS^{\bullet+}$ mixture (2 mL) was combined with 20 μL of liposomal formulation. After incubation for 6 min, the absorbance values were read:

$$\Delta A = A_c - A_s \qquad \text{(Eq. 7)}$$

In this equation, A_c denotes the $ABTS^{\bullet+}$ mixture absorbance value without any sample, A_s - absorbance value measured in the presence of liposomes and silibinin. The activity was presented as IC_{50}, representing the amount needed to quench 50% of radicals. Vitamin C served as a control.

Figure 17. ABTS test

The anti-$ABTS^{\bullet+}$ ability of the silibinin/smoke tree extract-entrapped liposomal vesicles, plain biobased film sample, as well as film samples incorporating silibinin/smoke tree extract-loaded liposomes (containing various concentrations of the mentioned liposomes) was also evaluated following the method of Zuhair et al. (2013) $ABTS^{\bullet+}$ mixture (2.8 mL) was combined with either dissolved film (200 μL) or liposomal fomrulations (200 μL). The anti-radical ability was determined:

$$\%\ inhibition\ = \frac{A0ABTS - AxABTS}{A0ABTS} \times 100 \qquad \text{(Eq. 8)}$$

In this equation, A_{0ABTS} - $ABTS^{\bullet+}$ mixture absorbance without any sample, A_{xABTS} - absorbance values measured in presence of bio-based film or liposomes with silibinin/smoke tree extract. Vitamin C served as a control.

3.21.2. DPPH

The antioxidant activities of silibinin-entrapped lipid spheres (multilamellar, ultraviolet-exposed, as well as SUVs) were analyzed in the presence of free DPPH• radicals, which measures hydrogen-donating ability (Zuhair et al., 2013) (Figure 18). Liposomes in the amount of 0.2 mL at various concentrations were combined with DPPH• solution (2 mL, absorbance of 0.811, wavelength of 517 nm).

After incubation (20-min period), the absorbance values were read, and the inhibition was detremined:

$$\%\ inhibition\ = \frac{Ac - As}{Ac} \times 100 \qquad \text{(Eq. 9)}$$

Here, A_c - absorbance of the control, while A_x - absorbance of the sample containing liposomal formulations. The results were presented as IC_{50}. Vitamin C was a reference standard.

Figure 18. DPPH assay

The anti-DPPH• ability, reflecting hydrogen-donating capacity, was determined for both plain films and film samples containing silibinin/smoke tree extract-loaded liposomes (containing various liposome amounts), as well as for silibinin/smoke tree extract-loaded liposomes (Zuhair et al., 2013). The sample (dissolved film - 0.2 mL or liposomes with silibinin and smoke tree extract - 0.2 mL) was combined with the DPPH• mixture (2.8 mL). The inhibition was determined:

$$\%\ inhibition\ = \frac{A0DPPH - AxDPPH}{A0DPPH} \times 100 \qquad \text{(Eq. 10)}$$

In this equation, A_{0DPPH} - DPPH• mixture absorbance, while A_{xDPPH} - absorbance measured in presence of bio-based film or liposomes with silibinin/smoke tree extract. Vitamin C was a positive control.

3.22. Cell culture tests

3.22.1. Preparation of treatments

Stock solutions of silibinin-containing liposomes were diluted to 10 mg/mL and stored in a refrigerator. For experimental use, the required treatment concentration was obtained by diluting the previous sample using culture medium to achieve 0.1, 1, 10, 25, 50, and 100 μg/mL. Those concentrations were then applied to the cells.

3.22.2. Cytotoxicity assessment

MTT test represents a colorimetric technique to investigate cell metabolic activity and viability, providing a reliable measure of cytotoxic effects of tested formulations. This assay allows the quantification of mitochondrial dehydrogenase activity in living cells, thereby enabling assessment of the biocompatibility of liposomal and control samples. HaCaT was transferred to the plates (1.5×10^4 in the PMI medium). The medium was replaced after one day, while treatments (silibinin-entrapped lipid vesicles - multilamellar, small unilamellar, and ultraviolet-exposed, as well as freeze-dried and plain particles) or solvent control were transferred. Following 24 h (37°C), cell viabilities were evaluated (Pirković et al., 2023) (Figure 19).

Figure 19. Cytotoxicity assessment using the keratinocyte cells

Ten microliters of MTT reagent were transferred (2 h, dark, 37°C). The resulting purple formazan crystal was dissolved with SDS. The absorbance readings were performed at a wavelength of 570 nm using Epoch (BioTek, USA). Data was presented as a percentage of viable cells relative to the 100% of control. The mean value was plotted based on 3 independent experiments, each carried out 3 times.

3.22.3. H2DCFDA test

The H2DCFDA test is employed for assessing intracellular reactive oxygen species generation, providing insight into the oxidative stress induced by tested formulations. This fluorescent probe enables sensitive detection of changes in cellular redox status, allowing examination of the pro-oxidant or antioxidant effects of bioactive-loaded liposomes, as well as control treatments.

Namely, the H2DCFDA assay is widely utilized in cell biology to monitor intracellular oxidative stress, providing a reliable indicator of reactive oxygen species levels under various experimental conditions. The test was performed as described below.

HaCaT was kept in the incubator (37°C, 5% of carbon dioxide). The following day, the cell culture solvent was replaced. HaCaT was exposed to silibinin-entrapped lipid spheres or plain liposomes (0.1-100 μg/mL). The next day, liposomes were eliminated, and HaCaT was washed by using phosphate-

buffered saline (Bruić et al., 2024). Cells were mixed with H2DCFDA (5 μM) and incubated during 45 min, washed, and then exposed either to a negative control (PBS) or a positive control (200 μM ofH_2O_2) for a 2-hour period. Intracellular ROS generation was measured *via* fluorescence in the Wallac 1420 multilabel counter Victor 3V (PerkinElmer, USA). The excitation/emission wavelengths were 485/535 nm. Results were presented as fluorescence intensity, with mean values from 3 experiments in triplicate.

3.22.4. Protein expression analysis *via* cell-based ELISA

The anti-inflammatory activity of liposomal samples containing silibinin (MLVs, UV-treated, lyophilized, and SUVs) was evaluated using a cell-based ELISA, *i.e.*, enzyme-linked immunosorbent assay (c-ELISA) (Bojić-Trbojević et al., 2008). Cell-based ELISA (c-ELISA) is the sensitive and quantitative technique for evaluating anti-inflammatory potential of bioactive formulations by measuring specific cytokine and enzyme expression levels. This approach allows assessment of how silibinin-loaded liposomes, including UV-treated and lyophilized variants, modulate key inflammatory mediators in human keratinocyte (HaCaT) cells. Protein expression analyses using cell-based ELISA were carried out to quantitatively examine specific inflammatory mediators' levels in treated HaCaT.

Detailed procedures, including sample preparation, antibody incubation, and detection steps, are presented in the next section to ensure reproducibility and clarity of the analytical approach.

HaCaT was transferred to the plates (2×10^5) and incubated during one day (37°C, 5% of carbon dioxide). Later, cells were treated with liposomes with silibinin or plain liposomes (10 μg/mL) for 24 h. Subsequently, HaCaT was treated with LPS (2.5 μg/mL) during 4 h. After washing with PBS and drying, HaCaT was treated using acetone and methanol. The peroxidase was blocked with H_2O_2 (0.3%, 30 min) and later blocked by BSA (1%, 0.5 h, 37°C). The antibody (primary) targeting IL-1β, MIF, or COX-2 (diluted 1:500 in 1% BSA/PBS) was transferred. After the 2-hour period of incubation at ambient temperature and washing, secondary HRP-conjugated antibodies (1:2000) were applied for 2 h. Color development was performed by adding substrate, stopping with a stop reagent, and the absorbance readings were performed at a wavelength of 450 nm in the ELx800 (BioTek, USA). Results were presented as mean values from 3 experiments performed in 3 replicates.

3.23. Data evaluation

Statistical analysis is crucial for providing the reliability of experimental findings. It enables objective evaluation of variability within datasets and determines whether observed differences are statistically significant rather than the result of random variation. Moreover, appropriate statistical treatment strengthens the validity of conclusions and enhances the overall scientific rigor of the study.

All experiments related to the liposome characterisation (except cell testing) were performed 3 times. Statistical analysis of data was performed in STATISTICA 7.0 software (Figure 20). Differences among groups were evaluated by one-way analysis of variance and Duncan test. Additionally, the value presented within tables/figures is expressed as mean value±standard deviation (SD), with a p-value lower than 0.05 considered significant.

The repeated measurements ensured consistency and allowed for reliable estimation of experimental variability. By applying one-way ANOVA and Duncan's test, significant differences between sample groups could be clearly identified. Presenting results as mean ± standard deviation provided a transparent view of data dispersion and reproducibility. Thus, this statistical approach reinforced the credibility of the findings and supported a confident interpretation of liposome characterization results.

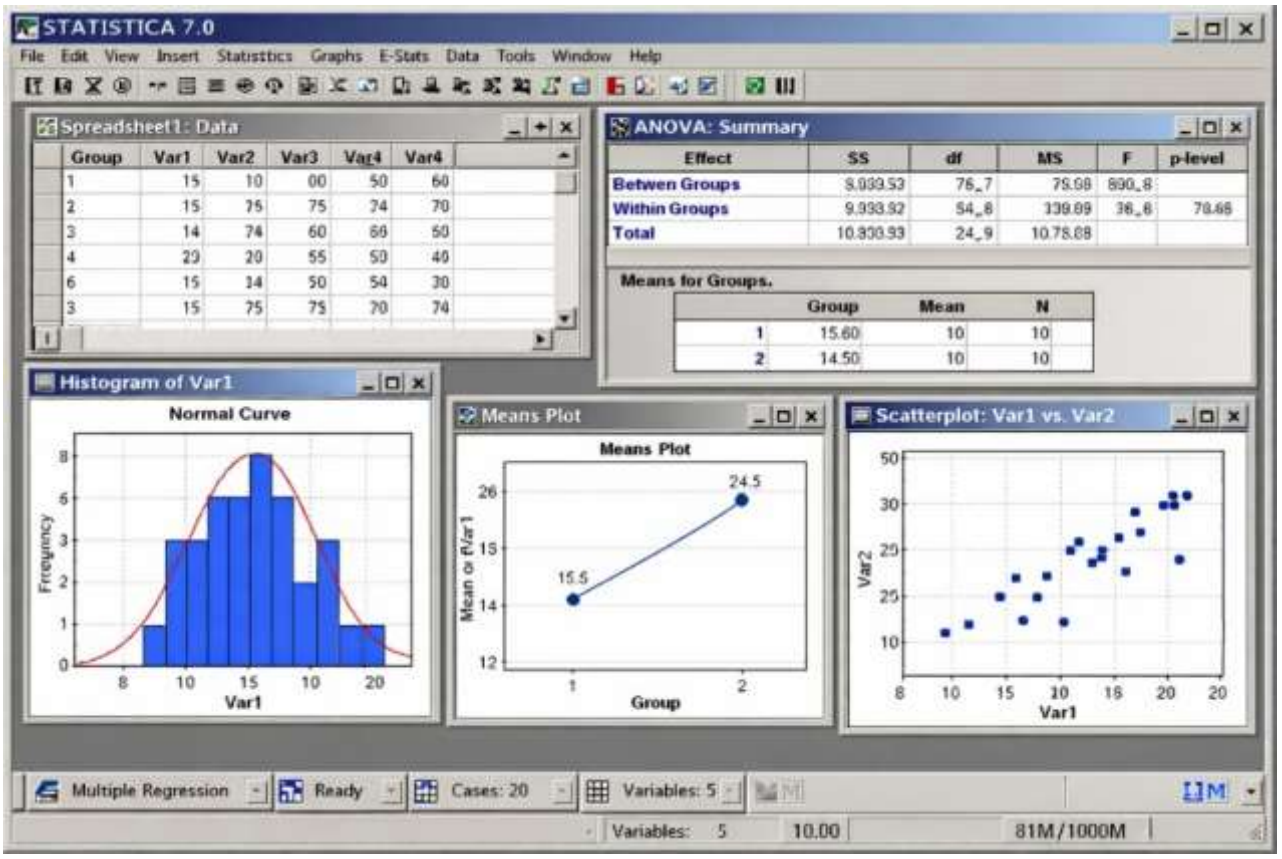

Figure 20. Statistical analysis using STATISTICA 7.0 software

For cell-based assays, one-way analysis of variance and Tukey test were applied to examine variations between treated samples and the control group after confirming data normality. Data is reported as mean value±standard error of the mean (SEM). GraphPad Software (USA) was used for analysis, and significance was set at a p-value lower than 0.05. Data were obtained from 3 independent experiments in triplicate.

4. RESULTS AND DISCUSSION

The initial step of this doctoral thesis involved preparation of silibinin-entrapped liposomal spheres, as well as the evaluation of ultrasound waves, ultraviolet exposure, and freeze-drying impact on their characteristics, such as encapsulating efficiency, diameter, distribution of particle size, electrophoretic mobility, surface charge, conductivity, and stability. For liquid formulations (non-treated, UV-exposed, and sonicated liposomes containing silibinin), additional measurements included density measurement, determination of the surface tension, and examination of the viscosity values. The next phase focused on chemical characterization of the liposomes using FT-IR/Raman spectroscopy. The third phase assessed biological activities of the formulated silibinin-entrapped liposomal samples (antioxidant potential, anti-inflammatory properties, as well as cytotoxic ability).

The next phases encompassed: the development and examination of pullulan-isononanoate and the formulation of pullulan-isononanoate film samples containing lipid spheres with smoke tree extract/silibinin (at various concentrations), with the aim of investigating their physicochemical and functional properties. Smoke tree extract was characterized *via* extraction yield, total polyphenol content, and flavonoid content. Ester derivatives of pullulan were synthesized using isononanoic acid chloride, and the modification was confirmed using ^{1}H and ^{13}C NMR and FT-IR spectroscopy. Liposomes embedding smoke tree extract/silibinin were prepared and examined by EE, size, PDI, surface charge, and stability, and subsequently, incorporated into Pull-Iso films at different loadings. The films were characterized using optical microscopy to evaluate liposome dispersion and microstructure, and mechanical testing to assess tensile properties. The films were also characterized for surface wettability using the determination of the water contact angle (sessile drop method), while the content of moisture, swelling behavior, and total soluble solids were tested to assess their physicochemical properties as well. Additionally, antioxidant ability of developed film samples and silibinin/smoke tree extract-entrapped liposomal vesicles within simulated conditions of the human skin was examined in the ABTS and DPPH methods.

4.1. Encapsulation capacity for liposomes with silibinin

Since EE, defined as the proportion of the target compound successfully incorporated into the carrier, is a key parameter (Jovanović et al., 2019), silibinin EE in the 4 liposome formulations (multilamellar, ultraviolet-exposed, freeze-dried, as well as sonicated) is presented in Table 1. The mentioned parameter directly affects the recovery profile, stability, performance, as well as the level of bioavailability of the loaded bioactives, making it a critical parameter for formulation optimization.

As presented in Table 1, silibinin EE in multilamellar vesicles was ~89.7%, and exposure to ultraviolet light did not produce a significant change in this value (~88.1%). Sonicated liposomes exhibited a notably reduced silibinin EE (~74.9%) compared to the bigger MLVs, yet their EE of silibinin remained significantly higher than that of lyophilized liposomes, which displayed a silibinin EE of 62.5 ± 1.9% (Table 1).

Silibinin EE of the various liposomal formulations followed a trend: multilamellar and ultraviolet-exposed > sonicated > freeze-dried. The markedly reduced EE observed in the freeze-dried samples was anticipated, as freeze-drying can destabilize the lipid bilayer structure and integrity.

A higher EE observed in MLVs is likely due to their multilamellar structure, which provides additional lipid bilayer volume for silibinin incorporation. In contrast, the lower EE in SUVs may be due to the reduced diameter and reduced internal compartmentalization, limiting the capacity to accommodate the hydrophobic compound. Because of that, it is important to select an appropriate liposomal architecture, as well as processing conditions, to improve/boost encapsulation while maintaining functional stability, particularly when subjecting vesicles to stressors such as UV irradiation or lyophilization.

Table 1. Efficiency of encapuslation (EE, expressed as %), vesicle diameter (expressed as nm), index of polydispersity (PDI, dimensionless parameter), surface charge (ζ, expressed as mV), conductivity factor (CF, dimensionless parameter), electrophoretic mobility (μ, expressed as μm·cm/V·s) of multilamellar vesicles (MLVs), ultravioled-exposed vesicles, freeze-dried vesicles, and sonicated vesicles (SUVs) containing silibinin, as well as plain liposomes (except value of encapsulation efficiency).

Samples	EE [%]	Size [nm]	PDI	ζ [mV]	CF	μ [μmcm/Vs]
MLVs with silibinin	89.7±1.4^{a,*}	1675.0±44.3^{a}	0.310±0.019^{b}	−35.5±0.7^{a}	0.38±0.01^{d}	−2.78±0.02^{a}
UV-irradiated with silibinin	88.1±1.2^{a}	1701.5±58.7^{a}	0.272±0.034^{b}	−36.5±0.7^{a}	1.15±0.02^{b}	−2.89±0.07^{a}
Lyophilized with silibinin	62.5±1.9^{c}	724.9±27.5^{c}	0.334±0.031^{b}	−14.9±0.5^{c}	2.64±0.30^{a}	−0.70±0.06^{c}
SUVs with silibinin	74.9±1.0^{b}	277.8±2.7^{d}	0.520±0.059^{a}	−21.6±0.1^{b}	1.24±0.08 ^{c}	−1.58±0.04^{b}
Unloaded MLVs	n.a.	1435.8±22.1^{b}	0.287±0.022^{b}	−10.3±0.4^{d}	0.32±0.02^{e}	−0.51±0.03^{d}

*Data sharing the same superscript letter = no significant difference among various liposomes.

Literature reports indicate that lyophilized liposomal formulations often show reduced EE, especially in the case without cryoprotectants (Chotphruethipong et al., 2021; Ghanbarzadeh et al., 2013), which was the case for the silibinin-entrapped liposomal spheres prepared in this research. Freeze drying can lead to liposome degradation due to ice crystal formation, phospholipid bilayer disruption, and subsequent entrapped molecules' release (Chotphruethipong et al., 2021; Ghanbarzadeh et al., 2013). Extended sonication may also affect a further drop in EE, as can be noticed in silibinin-loaded liposomes, because enhanced cavitation can rupture vesicles and cause excessive release of the encapsulated drug (Schroeder et al., 2009). However, sonication can improve EE and the stability of liposomes when protein hydrolysates are present, which adhere to the membrane from the inside (Sharma et al., 2023). In contrast, exposure to ultraviolet light did not impact silibinin EE, as UV light does not damage the liposomal bilayer. This observation aligns with literature reports showing that UV irradiation does not induce leakage of encapsulated plant bioactives (Jovanović et al, 2023a).

4.2. Dynamic light scattering data of silibinin-loaded liposomal samples

According to Mozafari et al. (2008), the average liposome diameter is an essential parameter influencing the biodistribution and recovery profile of entrapped molecules. Therefore, size of all silibinin-loaded liposomal formulations (multilamellar, ultraviolet-treated, freeze-dried, and sonicated liposomes containing silibinin) was measured (Table 1). The MLVs containing silibinin were ~1675 nm, and exposure to UV light did not significantly alter their size (1701.5 ± 58.7 nm). In contrast, sonication markedly reduced the vesicle size to ~277 nm. Freeze-dried lipid particles with silibinin showed an intermediate size of ~724 nm, indicating freeze-drying influence on the reduction in particle diameter. Index of polydispersity for multilamellar, ultraviolet-irradiated, and freeze-dried samples containing silibinin was from ~0.272, over ~0.310 to ~0.334. A PDI with the highest level was observed for SUVs with silibinin (~0.520), suggesting a wide distribution of particle sizes, possibly because of the MLVs' coexistence alongside SUVs. A size of unloaded MLVs amounts to 1435.8 ± 22.1 nm, while the size distribution was 0.287 ± 0.022 (Table 1).

The liposome diameter is strongly influenced by the lipids' type and method of development, as well as properties of the entrapped molecules (Jovanović et al., 2019). Proper vesicle diameter is critical for effective transdermal delivery, as larger liposomes cannot efficiently penetrate the *stratum corneum* and deeper layers. to reach the target site. For instance, 50 nm liposomes exhibit faster diffusion than 200 nm vesicles, while smaller vesicles (around 120 nm) promote a high level of the accumulation of entrapped molecules in various skin layers compared to larger spheres (Castañeda-Reyes et al., 2020).

For silibinin-loaded liposomes, the particle size followed the order: multilamellar and ultraviolet-treated > freeze-dried > sonicated (Table 1). Ultraviolet exposure did not significantly alter vesicle size, whereas sonication resulted in a notable reduction. Lyophilization induced MLV size drop, while in smaller vesicles (50-300 nm), freeze-drying may promote membrane fusion and the generation of bigger aggregates because of enhanced vesicle concentration, followed by the absence of hydration barriers (Chen et al., 2010a). In contrast, for larger vesicles like those in this study, according to Chen et al. (2010b), lyophilization can lead to fragmentation, reducing diameter. The measured SUVs' diameter aligns with literature reports (250-280 nm), reflecting the successful change of multilamellar liposomes to unilamellar vesicles *via* ultrasound wave exposure (Sharma et al., 2023). Vesicle size is closely linked to the content of lipid bilayers, with significantly varied thickness (Morais et al., 2004). Short sonication (15 min in this case) is sufficient to achieve nano-vesicles. But long exposure to ultrasound waves may alter the membrane and result in rupture of the membrane, leakage of encapsulated compounds, and re-aggregation, increasing vesicle size (Sharma et al., 2023; Sun et al., 2024b). Silva et al. (2010) showed similar findings and obtained vesicles of 200 nm following the exposure to ultrasound waves during 15 min. Ultraviolet light can modify features of liposome membranes, increasing membrane fluidity and permeability. Specifically, UV exposure may alter the physicochemical behavior of liposomal membranes by disrupting phospholipid organization, leading to looser molecular packing and enhanced membrane fluidity (Toopkanloo et al., 2020; Wong-ekkabut et al., 2007). However, no significant changes were observed following ultraviolet exposure of liposomal particles with entrapped silibinin. Silibinin etreption further stabilizes the bilayer by inserting hydrophobic molecules between lipid layers, protecting against additional damage (Toopkanloo et al., 2020).

Indexes of polidisersity in multilamellar, ultraviolet-treated, and freeze-dried lipid formulations containing silibinin were approximately 0.3 (Table 1), indicating monodispersity (Chadorshabi et al., 2022). Liofilization of rutin-loaded liposomes also did not alter PDI (Lopez Polo et al., 2020), consistent with our observations for silibinin liposomes. PDI with the highest value was observed in the sonicated formulation, suggesting the coexistence of larger multilamellar and smaller unilamellar vesicles. Sonication, while commonly used to produce SUVs, has limitations including reduced efficiency of the entrapment capacity, potential degradation of lipids and payloads, contamination from the probe, and presence of residual MLVs (Akbarzadeh et al., 2013).

Surface charge, reflecting the liposome zeta potential, had negative values in all formulations, confirming that vesicle surfaces carried a negative charge. Silibinin-loaded MLVs and their UV-irradiated counterparts (containing silibinin) had similar zeta potentials (~-35.5 and ~36.5 mV), while lyophilization and sonication significantly altered this parameter (~-14.9 and ~-21.6 mV). The electrical conductivity was measured by DLS. Immediately after preparation, the conductivity factor (as a non-dimensional parameter) was 0.38 ± 0.01 for silibinin-loaded MLVs, 1.15 ± 0.02 for silibinin-loaded UV-irradiated liposomes, 2.64 ± 0.30 for lyophilized silibinin-loaded liposomes, and 1.24 ± 0.08 for silibinin-loaded SUVs. Electrophoretic mobility was also determined for all formulations, yielding values of -2.78 ± 0.05, -2.89 ± 0.07, -0.70 ± 0.06, and -1.58 ± 0.04 μm·cm/V·s in multilamellar, ultraviolet-treated, freeze-dried, and sonicated formulations containing silibinin, respectively (Table 1). As presented in Table 1, the aforementioned parameters of unloaded liposomes were ~-10.3 mV, ~0.32, and ~0.51 μm·cm/V·s, respectively.

Zeta potential measurements showed all silibinin-loaded liposomes were negatively charged, with the highest absolute values observed for MLVs and UV-irradiated vesicles (Table 1), indicating strong electrostatic repulsion and stability against aggregation, flocculation, or sedimentation (Lopez-Polo et al., 2020). Sonication and lyophilization reduced the absolute zeta potential, likely due to partial release of surface-associated molecules or changes in lipid structure (Sharma et al., 2023; Sun et al., 2024b). Hydrophobic compounds in the bilayer can mask negative charges, further contributing to reduced zeta potential (Bouarab et al., 2014; Hosseini et al., 2017). The liposomal suspension conductivity in formulations with encapsulated silibinin was as follows: freeze-dried > sonicated > ultraviolet-treated > multilamellar (Table 1). Increased conductivity in UV-exposed samples with silibinin may be due to water evaporation, while higher conductivity in lyophilized and SUV formulations containing silibinin correlates with lower EE and partial recovery of compounds (Froude and Zhu, 2009). Liposome mobility depends on the diameter of the particle, potential, phospholipid chemical profile, as well as the properties of encapsulated substances (Duffy et al., 2001). Reduced mobility in sonicated and freeze-dried silibinin-loaded liposomal vesicles than in MLVs and ultraviolet-treated vesicles with encapsulated silibinin may result from surface adsorption of flavonoids, consistent with lower efficiency of the entraptment capacity (Table 1) (Yang et al., 2015).

4.3. Data on stability of liposomal particles containing silibinin monitored for a storage period

A key difficulty when applying liposome-based systems in foods, functional products, dietary supplements, pharmaceuticals, and cosmetics is their poor physical and chemical stability when dispersed in water and exposed to environmental factors. This instability is largely due to their lipid composition and the presence of water (a favorable medium for the development of microorganisms) and can result in undesirable outcomes, such as lipid oxidation, hydrolysis, and decreased level of the EE (Tian et al., 2019). Literature reports (Rahdar et al., 2019) indicate that such physicochemical instability can lead to vesicle fusion, aggregation, alterations in size, fluidity of bilayers, phospholipid content, and reductions in encapsulated compound retention. In order to assess storage stability in the liposomal particles with loaded silibinin developed in this study (mulitilamellar, ultraviolet-treated, freeze-dried, and sonicated liposomes containing silibinin), samples were stored at 4°C during a 60-day period, with data shown in Figure 21 (Figure 21A - particle size/PDI, Figure 21B - surface charge, electrophoretic mobility, conductivity factor).

The observed liposome instability may be due to vesicle collisions, membrane fusion, and chemical processes such as lipid oxidation and aldehyde formation. The enhanced stability at 4°C is likely due to reduced membrane permeability and decreased phospholipid mobility, which slows down the reactions toward unsaturated fatty acids (such as oxidation) and overall liposome degradation (Chadorshabi et al., 2022; Hamadou et al., 2020). Despite this, a significant increase of particle size was observed for all silibinin-loaded liposomes over the storage period in a refrigerator (Figure 21A). Initially, the vesicle sizes were ~1675.0 nm, ~1701.5 nm, ~724.9 nm, and ~277.8 nm for multilamellar, ultraviolet-treated, freeze-dried, and sonicated vesicles containing silibinin, respectively (Figure 21A). Following 60 days, these values increased to ~2466.0 nm (+32%), ~2601.0 nm (+34%), ~2104.0 nm (+65%), and ~538.7 nm (+48%), respectively (Figure 21A).

Values of the size distribution, indicated above the bars in Figure 21A, exhibited two distinct trends. Lyophilized liposomal particles with encapsulated silibinin had a modest increase of heterogeneity, with PDI ranging from ~0.334 to ~0.468 (Figure 21A, values above bars). In contrast, MLVs with silibinin (~0.310 → ~0.600), UV-irradiated liposomes (~0.272 → ~0.649), and SUVs (~0.520 → ~0.832) (Figure 21A, values above bars) demonstrated substantial increases in PDI over time, reflecting reduced homogeneity and enhanced aggregation.

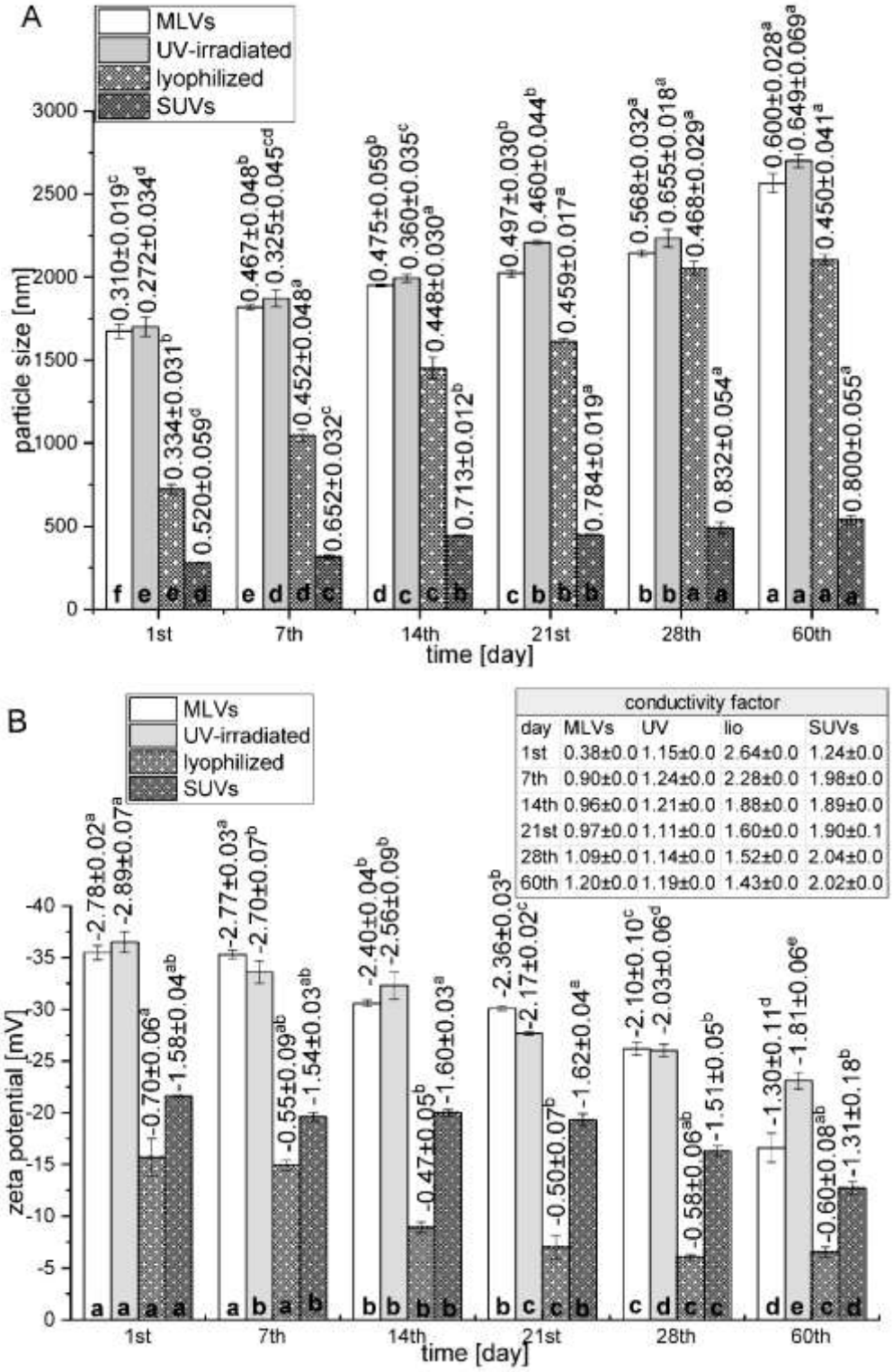

Figure 21. Particle size (with polydispersity index values indicated above the bars) and zeta potential (with mobility values - μm·cm/V·s shown above the bars), as well as conductivity data (table in figure B, shown as the conductivity factor), MLVs (mulitlamelar), ultraviolet-treated, freeze-dried, and SUVs (sonicated) formulations containing silibinin, tracked over a 60-day period of keeping in a refrigaretor. Data sharing the same letter indicates no significant differences.

Zeta potential measurements (Figure 21B) revealed a marked reduction in absolute values for all formulations over the 60-day period. Initial zeta potentials were approximately -35.5 mV, -36.5 mV, -14.9 mV, and -21.6 mV for multilamellar, ultraviolet-treated, freeze-dried, and small unilamellar vesicles containing silibinin, which decreased to approximately -16.6 mV (-53%), -23.1 mV (-36%), -6.0 mV (-60%), and -12.7 mV (-41%) after storage (Figure 21B).

Conductivity changes were formulation dependent (Figure 21B, values in the table). MLVs and SUVs with encapsulated silibinin exhibited substantial increases (conductivity factors of approximately 0.38 → 1.20 and 1.24 → 2.02, respectively), while UV-irradiated liposomes with silibinin remained largely unchanged. Lyophilized liposomes containing silibinin, however, showed a pronounced decrease in conductivity factor from ~2.64 to ~1.43 (Table in Figure 21B).

Multilamellar and ultraviolet-treated vesicles containing silibinin had important reductions in mobility over 60 days, from approximately -2.78 to -1.30 μm·cm/V·s and from approximately -2.89 to -1.81 μm·cm/V·s, respectively (Figure 21B). SUVs and lyophilized liposomes containing silibinin exhibited slower reductions in mobility, with silibinin-loaded SUVs dropping from approximately -1.58 to -1.31 μm·cm/V·s and lyophilized liposomes decreasing from approximately -0.70 to -0.47 μm·cm/V·s, as shown in Figure 21B.

A pronounced enhancement in particle diameter was observed within silibinin-loaded liposomal vesicles over the 60-day period in a refrigerator (Figure 21A). Literature data reported that aggregation resulting from vesicle accumulation can substantially influence both liposome size and size distribution (Hamadou et al., 2020). Among the formulations studied, lyophilized silibinin-loaded liposomes exhibited the largest increase in size, which correlates with their lowest absolute zeta potential (Table 1) and, consequently, the weakest ability to prevent particle aggregation. For SUVs containing silibinin, the absolute zeta potential below 30 mV likely contributed to significant size growth due to reduced electrostatic and steric repulsion, creating conditions favorable for vesicle accumulation (Chadorshabi et al., 2022).

UV-irradiated silibinin-loaded liposomes also showed considerable size changes, with particle diameter significantly increasing after 21 days compared to untreated controls. This effect may be attributed to photochemical reactions induced by photon absorption, which alter bilayer conformation and compromise membrane integrity (Toopkanloo et al., 2020; Wong-ekkabut et al., 2007). UV light can cause photodegradation of very irregular polyunsaturated fatty acids within phospholipid molecules, exposing hydrophobic regions, as well as promoting vesicle aggregation over time (Toopkanloo et al., 2020).

Physical factors (aggregation, coalescence, fusion, flocculation, and diameter alterations also influence liposome shelf-life and may lead to drug leakage, highlighting a limitation of liposomal delivery systems. While freeze drying is adequate in the protection of vulnerable components, the physical features and stability of freeze-dried liposomal particles depend on freezing rate, formulation technique, membrane content, and the amount of non-eliminated water. The selection of the optimized factors, as well as the use of adequate cryoprotectants, can improve vesicle stability, efficiency of the encapsulation technique, and biological activity (Yu et al., 2021). Potential strategies include the incorporation of carbohydrates (mono-, di-, and polysaccharides, as well as synthesized analogues), alcohols, amino acids, or secondary carriers such as cyclodextrins (double-loading systems), which can reduce aggregation, prevent payload leakage, and protect membranes from ice-crystal-induced damage (Sebaaly et al., 2016; Yu et al., 2021).

PDI analysis indicated a slight increase in heterogeneity for lyophilized lipid vesicles with entrapped silibinin, whereas multilamellar, ultraviolet-treated liposomes, as well as SUVs containing silibinin, showed a marked PDI increase, reflecting decreased homogeneity and enhanced aggregation. Since PDI is closely associated with the physical stability of liposomal suspensions, maintaining low values is critical for long-term stability of vesicle size distributions (Chadorshabi et al., 2022).

A notable decline in absolute zeta potential was observed in all formulations over 60 days, consistent with previous studies on liquid and lyophilized liposomes stored at 4°C (Lopez-Polo et al., 2020). Despite this decrease, all liposomes retained negative surface charge, indicating that phospholipid

reorganization within the membrane cannot be noticed during storage, as the negative charge arises from phosphate functional groups and heads (polar part) of lipids such as phospholipids (Hosseini et al., 2017). The reduction of surface charge can also be connected to increasing vesicle size, since smaller particles have a larger surface area, exposing more phosphate groups, resulting in a higher negative charge. As vesicles grew during storage, the corresponding decrease in surface area led to a lower zeta potential. Partial neutralization of surface charge may occur *via* interactions between released compounds and negatively charged phospholipids, promoting aggregation (Chotphruethipong et al., 2021). This is in agreement with the noticed simultaneous increase of vesicle diameter, as well as a decrease in surface charge for silibinin-loaded liposomes.

Conductivity measurements showed a significant rise in silibinin-entrapped multilamellar and small unilamellar vesicles, while ultraviolet-treated liposomes remained unchanged. The decrease in conductivity observed in freeze-dried silibinin-entrapped lipid vesicles is likely due to initially smaller vesicle size on day 1, which exposed more phospholipid headgroups and elevated conductivity; as vesicles enlarged during storage, the conductivity decreased correspondingly (Lidgate et al., 1993).

Electrophoretic mobility of multilamellar and ultraviolet-exposed lipid vesicles containing silibinin lowered markedly over time, whereas sonicated and freeze-dried formulations containing encapsulated silibinin exhibited a more gradual decline. The observed reduction in mobility across all formulations (Figure 21B) may be connected to the enlargement of vesicle diameter during storage (Figure 21A). Prior studies have demonstrated that liposome size significantly impacts vesicle mobility through circulation, as well as tissues and cells (Yanagihara et al., 2023).

4.4. Data on rheological analysis of liposomes containing silibinin

The rheological characteristics of developed liposomal formulations with silibinin in their liquid forms were evaluated prior to and following ultraviolet radiation, as well as exposure to the ultrasound waves. The densities of multilamellar, ultraviolet-exposed, and sonicated lipid particles containing silibinin were approximately 0.939, 0.917, and 0.916 g/cm³. Silibinin-loaded multilamellar spheres exhibited a higher level of surface tension (approximately 28.7 mN/m), while ultraviolet-exposed and sonicated samples with silibinin had values of approximately 27.1 and 26.5 mN/m (Table 2). The viscosities were similar in all formulations, ranging from approximately 3.28 mPa·s (silibinin-loaded UV-irradiated sample), over ~3.43 mPa·s (silibinin-loaded SUVs) to around 3.45 mPa·s (silibinin-loaded MLVs) (Table 2).

Table 2. Rheological characteristics of MLVs (multilamellar liposomes), UV-treated liposomes, and SUVs (small unilamellar vesicles) containing silibinin, including density (ϱ, expressed as g/mL), surface tension (γ, expressed as mN/m), and viscosity (η, expressed as mPa·s).

Samples	ϱ [g/mL]	γ [mN/m]	η [mPa·s]
MLVs with silibinin	0.939±0.005 [a,*]	28.7±0.1 [a]	3.45±0.02 [a]
UV-irradiated with silibinin	0.917±0.004 [b]	27.1±0.2 [b]	3.28±0.03 [b]
SUVs with silibinin	0.916±0.006 [b]	26.5±0.2 [c]	3.43±0.02 [a]

*Data marked with the same letter do not differ significantly.

A noticeably lower density in liposomal suspensions containing silibinin following ultraviolet treatment and exposure to ultrasound waves (Table 2) can likely be associated with hydrolytic reactions occurring in the aqueous environment. Reduced density is generally linked to increased fluidity and decreased stability, which is a critical consideration for formulations intended for prolonged use and storage (Zheng et al., 2013).

The measured values related to the surface tension of liquid silibinin-loaded liposomes (Table 2) were higher than those reported in the literature data for various liposomes (Čutović et al., 2023; Jovanović et al., 2023a). This difference may arise from the specific lipid composition of the bilayer, particularly the presence of lecithin, which can act as a surfactant, as well as from variations in the

entrapped bioactives' features. Flavonoids are known to stabilize emulsions through adsorption at interfaces (Luo et al., 2011). Since SUVs contained a greater proportion of silibinin in the aqueous phase, as indicated by their lower encapsulation efficiency (Table 1), this likely accounts for the significantly reduced surface tension observed for this formulation.

All silibinin-loaded liposomes exhibited very low viscosity values (Table 2). Earlier papers have reported that liposomal suspensions with low values of the viscosity are more susceptible to changes in vesicle size over time (Jovanović et al., 2023a; Narenji et al., 2016), which is in agreement with stability data presented here (Figure 21A). According to Stokes' law, viscosity is inversely related to sedimentation rate; therefore, higher viscosity slows vesicle settling and helps maintain a stable size distribution during long time (Narenji et al., 2016). Consequently, incorporation of suitable viscosity-modifying agents may be beneficial for silibinin-loaded liposomal formulations to minimize size heterogeneity, prevent sedimentation, and enhance overall stability.

4.5. Data on Fourier transform infrared spectroscopy of liposomes containing silibinin

FT-IR spectroscopy is a simple and versatile technique commonly applied to investigate molecular interactions within liposomal formulations. Here, FT-IR analyses were employed to evaluate effects of ultraviolet treatment on phospholipids, plain liposomal particles, as well as silibinin-entrapped liposomal vesicles. The phospholipid and unloaded lipid vesicle spectra, recorded prior to and following ultraviolet exposure, is presented in Supplementary Materials – Fig. S1, while chemical structures of phospholipids and silibinin were shown in Supplementary Materials – Fig. S2. Structural changes were assessed by examining variations in characteristic absorption bands and by applying spectral deconvolution to resolve overlapping signals corresponding to individual functional groups affected by post-preparation treatments.

The broad absorption band (3000-3600 cm^{-1} region) was attributed to the O–H stretching vibrations originating from the residues of glycerol and phosphate groups in the spectrum of phospholipids (Supplementary Materials - Fig. S1). A narrow band at 3010 cm^{-1} was connected to the C–H stretching vibrations of the residues from oleic acid (Lewis and McElhaney, 1992). The modes at 2853 and 2923 cm^{-1} were assigned to stretching vibrations (asymmetric and symmetric) of methyl and methylene functional groups within the chains of fatty acids. A band observed at 1735 cm^{-1} in all phosphatidylcholine-containing spectra is characteristic of C=O stretching (ester carbonyl stretching). A weaker band (1652 cm^{-1}) was connected to the O–H deformation vibrations and minor contributions from C=C stretching in oleic acid moiety. A spectral region between 1466 cm^{-1} and 1375 cm^{-1} corresponds to deformation vibrations in the methyl and methylene functional groups. Vibrations related to C–O and C–O–C, as well as P=O stretching in phospholipids, were detected at approximately 1250, 116, 1090, and 1059 cm^{-1}. The peak at approximately 1062 cm^{-1} is connected to combined stretching vibrations of C–O and P–O–C within phospholipids, while absorption at 869 cm^{-1} was connected to asymmetric stretching of P–O. Stretching vibrations of γ(=C–H) were at 770-370 cm^{-1} range and overlapped by vibrations originating from phospholipids (O–CO–C bending), typically noticed around 734 cm^{-1} (Batinić et al., 2020).

Comparison of phospholipid, unloaded liposome particles, and silibinin-entrapped liposomes revealed no detectable differences in band positions or intensities (Fig. S1 - Supplementary Materials and Figure 22, respectively). This suggests that the intra- and intermolecular interactions established within the packed phosphatidylcholine structure do not result in observable spectral shifts. Furthermore, the absence of additional absorption bands in silibinin-loaded liposomes relative to unloaded systems indicates that no chemical reactions occur between phospholipid molecules and bioactive compound silibinin, confirming the absence of incompatibility.

Fig. S3 (Supplementary Materials) presents the spectrum of free silibinin, plain lipid spheres, multilamellar vesicles with silibinin, as well as ultraviolet-irradiated silibinin-containing liposome spheres recorded over irradiation times ranging from 15 min to 90 min (spectral region of 1550-1800 cm^{-1}).

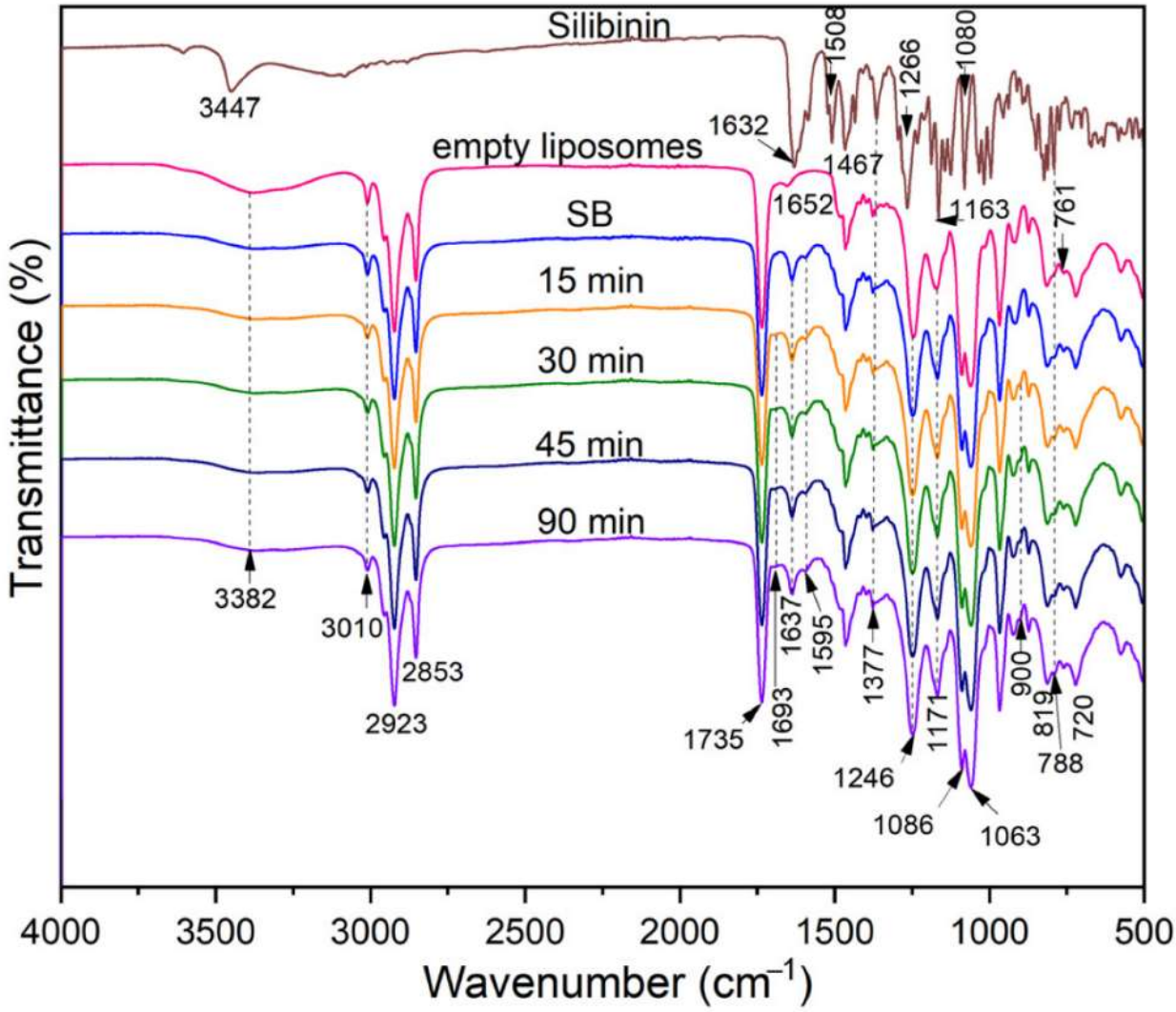

Figure 22. Fourier transform infrared spectrum of pure silibinin, unloaded liposome spheres, silibinin-entrapped multilamellar vesicles (MLVs), and silibinin-containing liposome spheres exposed to UV irradiation for varying durations (15-90 min)

The incorporation of silibinin into liposomes, specifically the impact of its aromatic moieties prior to and in the ultraviolet exposure, did not result in pronounced changes in absorption intensity within the 1550-1675 cm^{-1} region. However, a subtle intensity enhancement in absorption minimum around 1693 cm^{-1} was detected. It can be associated with oxidation and peroxidation processes, leading to the formation of oxygen-containing functional groups.

In this context, allylic hydrogen atoms may be activated through reactions with reactive oxygen species, particularly hydroxyl radicals (Murru et al., 2021). Subsequent formation of hydroperoxides and cyclic intermediates can promote C–C bond cleavage, yielding aldehydes that may further oxidize to carboxylic acids (Lazzari and Chiantore, 1999). To enhance the visibility and quantitative evaluation of these spectral features, peak deconvolution was applied. The corresponding data is shown in Supplementary Materials - Fig. S4.

Comparable spectral behavior was observed for both phosphatidylcholine and liposomal systems, indicating that similar oxidative pathways occur in these matrices, albeit with different intensities. A well-established relationship exists between the gradual loss of double bonds (Fig. S1, Supplementary Materials) and changes in band structure and intensity near 1652 cm^{-1} and 1702 cm^{-1}, which arise from

oxidation and hydroperoxidation of ethylenic bonds, producing oxygen-rich, low-stability intermediates. These intermediates ultimately undergo structural rearrangement, predominantly forming aldehyde groups that can further oxidize into carboxylic functionalities. Consistent conclusions were derived due to the deconvolution of the FT-IR spectrum related to the silibinin-loaded multilamellar vesicles and ultraviolet-treated counterparts (Supplementary Materials - Fig. S5).

The conclusions indicate silibinin's function in stabilizing or crosslinking within the phosphatidylcholine bilayer through intramolecular interactions while being embedded within the bilayer (hydrophobic part). Concurrently, a lipid matrix provides protection to silibinin against external influences, as evidenced by the observation that UV-induced structural changes were primarily associated with phosphatidylcholine rather than the encapsulated compound.

An analogous approach was employed to evaluate UV-induced structural modifications in phospholipids, plain liposomal spheres (Supplementary Materials, Fig. S6), as well as liposome particles with silibinin (Figure 23). In these cases, spectral overlap and signal complexity prevented the application of reliable deconvolution procedures.

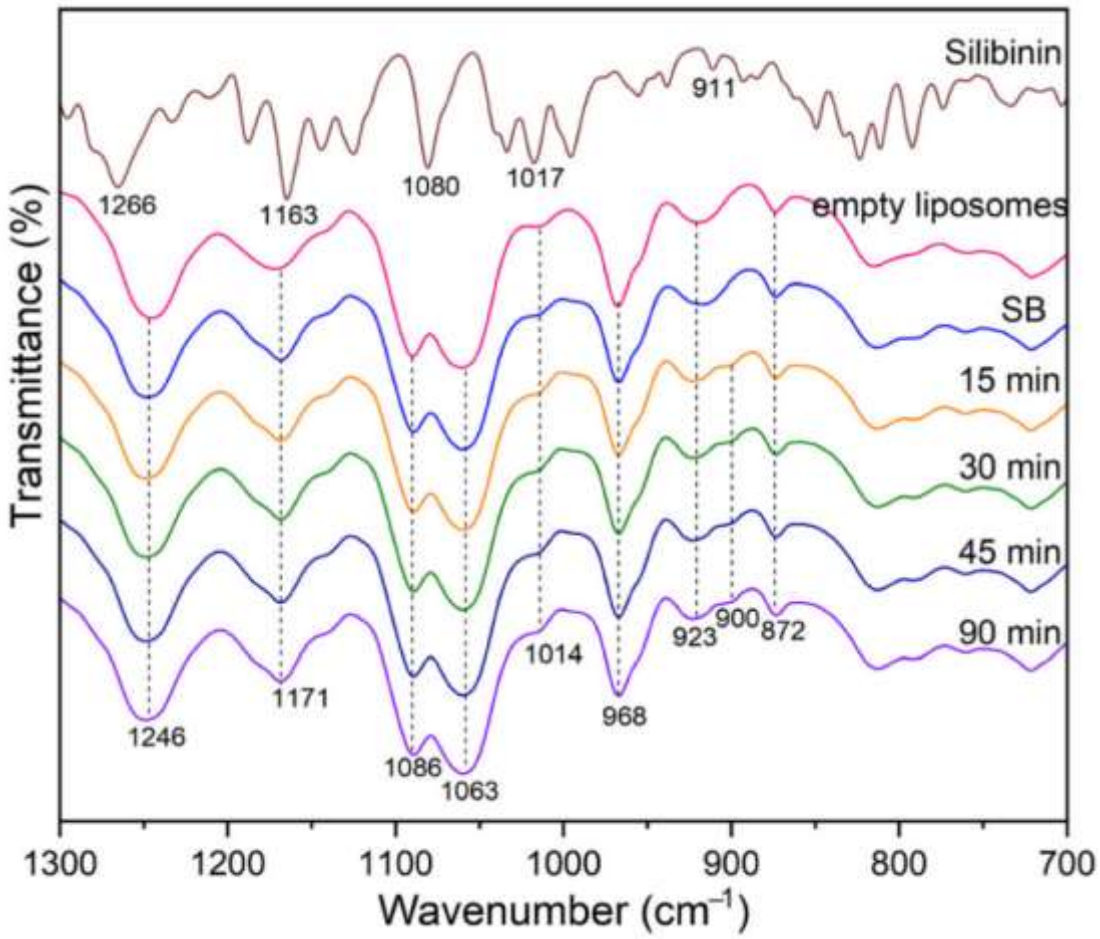

Figure 23. Time-dependent UV-induced variations in the Fourier transform infrared absorption bands of liposomes containing silibinin (700-1300 cm^{-1})

Ultraviolet treatment of phosphatidylcholine, empty lipid particles, and liposome vesicles with silibinin resulted in distinct changes in spectra associated with UV-induced structural modifications of the treated materials, as exemplified for silibinin-loaded liposomes.

These changes included:

1) A reduction in the intensity of the mode (3009 cm^{-1}), corresponding to disappearance of C–H stretching vibrations (Figure 22)

2) Alterations in the peak structure within the 1600-1750 cm^{-1} region, attributed to carbonyl stretching vibrations originating from ester, carboxyl, and aldehyde functional groups (Fig. S3, Supplementary Materials)

3) The emergence of weak shoulder bands in the 800-1300 cm^{-1} region (Figure 23 and Supplementary Materials - Fig. S6)

Because the UV-induced radical reactions led to subtle peak shifts, minor intensity changes, or the formation of weak new bands, two complementary analytical approaches were applied: peak deconvolution and quantitative analysis of peak areas as indicators of functional group evolution within the studied systems.

There is no change related to the mode at 1735 cm^{-1} (ester carbonyl group in phospholipids), indicating a high resistance of this functional group to oxidative degradation. The appearance of small shoulder bands at approximately 900 cm^{-1} and 800 cm^{-1} (Supplementary Materials - Fig. S1) suggests hydroperoxide species' formation, while the intensities/positions of the remaining peaks remained largely the same. The data derived from deconvolution analysis were summarized in Table S1 (Supplementary Materials).

An increase in oxygen-containing functional groups was evidenced by the growth of band area (1704 cm^{-1}) with increasing UV exposure time (up to 30 min). A similar effect has been noticed for multilamellar vesicles with silibinin, although to a lesser extent, indicating antioxidant, *i.e.*, radical-scavenging capacity of silibinin within the liposomal bilayer.

As shown in Figure 24, ultrasound waves did not induce detectable alterations within the FT-IR spectrum of silibinin-entrapped liposomal particles. Nevertheless, ultrasonic treatment may influence lipid spheres' properties; however, the extent of these effects is strongly determined by the ultrasound settings used (Sun et al., 2024b).

In the present study, the relatively short sonication time (15 min), combined with intermittent pauses, likely prevented bilayer degradation caused by cavitation while enabling the intended decrease of vesicle diameter. Extended sonication time, in contrast, may induce phase transitions and membrane expansion, leading to both chemical and physical alterations of the phospholipid bilayer (Sun et al., 2024b).

The preservation of FT-IR spectral features after sonication indicates that the chemical integrity of silibinin and the phospholipid bilayer remained intact. This suggests that the applied sonication protocol effectively reduced particle size without compromising molecular interactions within the vesicles. Maintaining structural stability is particularly important for ensuring consistent encapsulation efficiency and predictable release profiles of the bioactive compound. These results demonstrate that carefully controlled ultrasonic treatment can optimize liposomal formulations by improving physical characteristics while preserving both chemical composition and functional performance. Furthermore, the retention of characteristic FT-IR peaks after sonication highlights the resilience of both silibinin and the lipid components under mechanical stress. This stability supports the hypothesis that ultrasonic energy can be finely tuned to achieve smaller, more uniform vesicles without inducing chemical degradation. Such control over vesicle size and integrity is critical for enhancing the reproducibility of encapsulation and the reliability of subsequent release studies. In addition, these findings suggest that ultrasonic processing can be integrated into scalable production methods while maintaining the therapeutic potential of bioactive-loaded liposomes. The combination of physical optimization and chemical preservation underscores the utility of sonication in advanced liposomal formulation design.

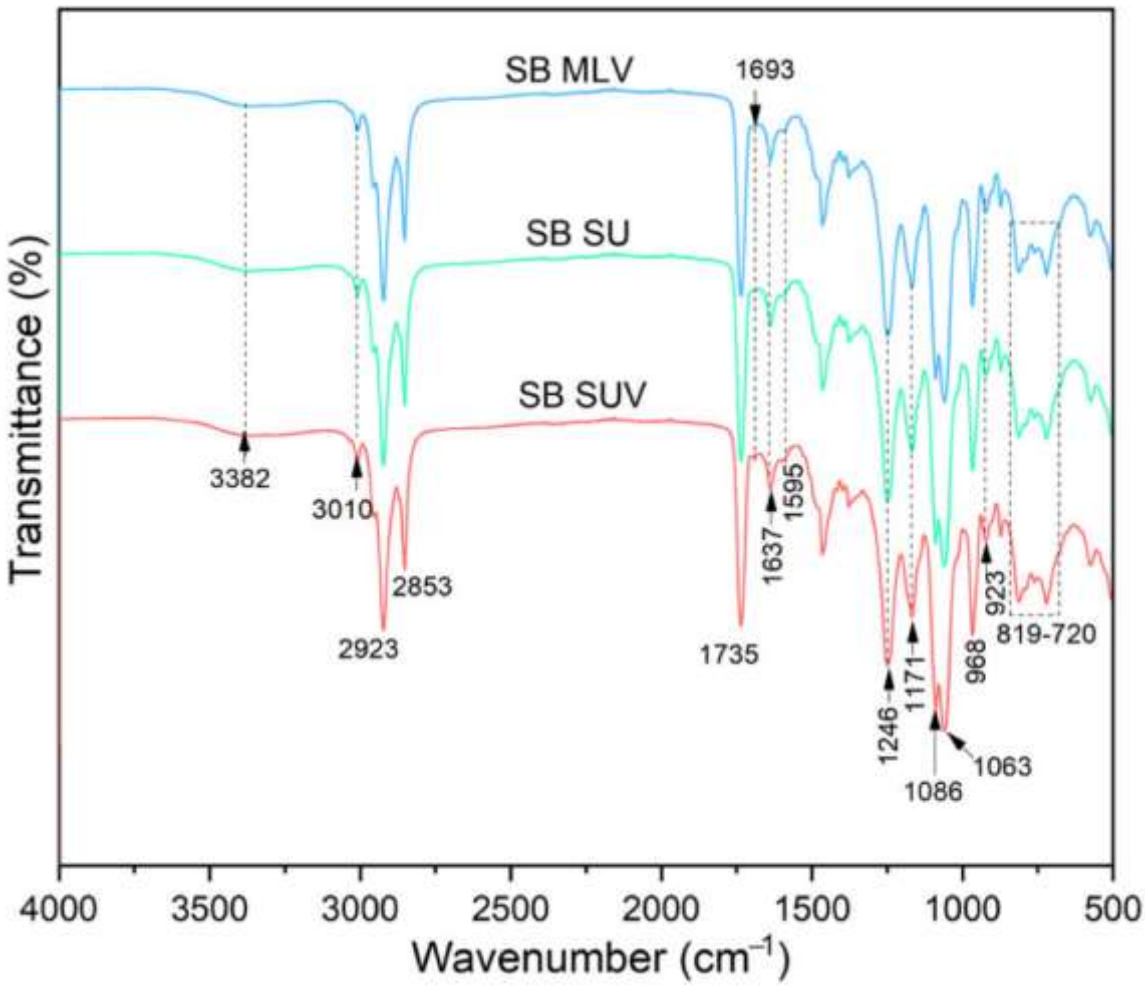

Figure 24. Fourier-transform infrared analysis performed on silibinin-encapsulated liposomes, including MLVs - multilamellar liposomes, liposomes exposed to UV irradiation, and SUVs - small unilamellar liposomes

Numerous studies have demonstrated that silibinin acts as an effective sensitizer of ultraviolet-A-triggered oxidative damage and apoptosis, while also providing substantial protection in ultraviolet-mediated injury to the epidermal layer (Dhanalakshmi et al., 2004; Matsumura and Ananthaswamy, 2004; Narayanapillai et al., 2012; Singh and Agarwal, 2002; Singh and Agarwal, 2009). Given that silibinin was incorporated into liposomes, carriers whose components may be vulnerable to ultraviolet exposure, ultrasound waves, as well as freeze drying, the stability and potential alterations in chemical features of silibinin under these conditions were not investigated. UV irradiation was not applied to free silibinin because previous research has confirmed both its stability after ultraviolet exposure and its beneficial properties (Singh and Agarwal, 2002; Singh and Agarwal, 2009). Similarly, lyophilization was not relevant for free silibinin, as this process is not typically employed for powdered compounds like silibinin. Finally, sonication of silibinin in its powdered form was not feasible with the ultrasonic probe used for liposome processing. These considerations emphasize that the evaluation of silibinin stability and bioactivity is particularly relevant within the context of liposomal encapsulation, where external processing conditions may affect both the carrier and the loaded compound.

4.6. Data on Raman spectroscopy of liposomes containing silibinin

Raman spectroscopy was employed to examine potential interactions among silibinin, Ph, silibinin-loaded liposomes, and their ultraviolet-treated or ultrasound wave-treated forms. The spectrum of silibinin and phospholipids was provided in Fig. S7 (Supplementary Materials). Figure 25 presents the spectrum of multilamellar-large particles containing silibinin, ultraviolet-exposed particles containing silibinin, as well as sonicated lipid spheres containing silibinin, with all samples lyophilized to meet the instrument's operational requirements.

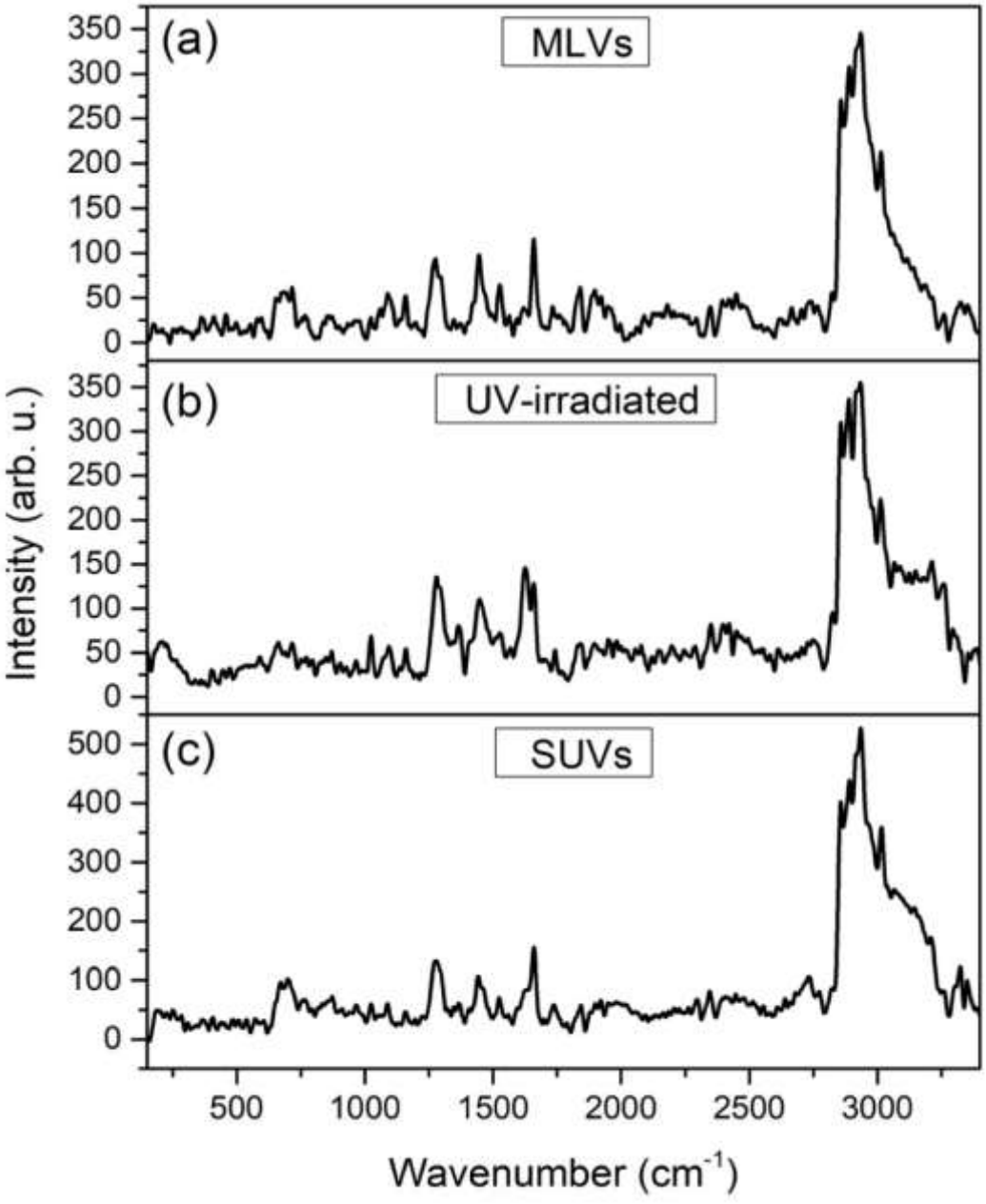

Figure 25. Raman spectroscopy analysis of silibinin-loaded liposomes: (a) MLVs - multilamellar particles, (b) ultraviolet-exposed particles, and (c) SUVs - sonicated unilamellar particles

The Raman spectrum of MLVs containing silibinin (Figure 25a) closely resembled those of Ph (Supplementary Materials - Fig. S7a), both exhibiting characteristic phospholipid bands. When encapsulated compounds primarily display peaks corresponding to the carrier, such as lipid membrane within liposomal vesicles containing silibinin, this proves effective entrapment of active substance (Medina-Torres et al., 2016). The Raman features observed for phospholipids and multilamellar vesicles containing silibinin (Supplementary Materials - Fig. S7a and Fig. 25a) can be attributed to palmitic acid or stearic acid esters (400-500 cm^{-1}) (Czamara et al., 2015), symmetric C–N stretching of choline in the phospholipid headgroup (approximately 720 cm^{-1}) (Jovanović et al., 2023b), the signature stearic acid peak (approximately 850 cm^{-1}) (Czamara et al., 2015), stretching of C–C=O (approximately 979 cm^{-1}) (Batinić, et al., 2020), skeletal vibrations of C–C (approximately 1027 cm^{-1}) (Jovanović et al., 2023b), symmetric PO_2^- stretching (approximately 1079 cm^{-1}), as well as stretching of PO_2^-, asymmetric (approximately 1200 cm^{-1}) (Šeremet et al., 2022), C–H bands (in lipid acyl chains) correspond to twisting of CH_2, *in-plane* (approximately 1280 cm^{-1}) and scissoring of CH_2 (approximately 1450 cm^{-1}) (Qiu et al., 2019; Vasić et al., 2021). Further, N–O stretching band (~1525 cm^{-1}), followed by stretching mode of C=C (~1670 cm^{-1}), was observed in both spectra (Jovanović et al., 2023b), while the ester carbonyl (C=O) peak (approximately 1750 cm^{-1}) arises from the linkage between glycerol and fatty acids (Lee and Bain, 2005). Peaks between 2100-2750 cm^{-1} originate from phospholipids, appearing more intense in MLVs than in Ph. Bands at around 2849 cm^{-1} are related to C–H stretching (symmetric and asymmetric) in the CH_2 and CH_3 groups within the alkyl chains. A 3016 cm^{-1} peak is attributed to stretching of N–CH_3 (Jovanović et al., 2023b; Lee and Bain, 2005). The mode at around 3350 cm^{-1} reflects bound water (Jovanović et al., 2023b).

The Raman spectrum of pure silibinin (Supplementary Materials - Fig. S7b) aligns with literature reports for 500-1700 and 3000-3500 cm^{-1} spectral ranges (Solís-Gómez et al., 2019; Tan et al., 2014), whereas signals between 2000-2800 cm^{-1} may arise from minor impurities. Upon UV irradiation, notable changes were observed in the spectrum of developed liposomal formulations with silibinin, particularly in the 500-1600 cm^{-1} region, where peak intensities increased (Figure 25b). This enhancement is consistent with previous reports showing elevated peak intensities in UV-exposed liposomes relative to untreated samples (Jovanović et al., 2023a). FT-IR analysis corroborated these alterations, particularly in the 800-1300 cm^{-1} region, as well as in the 1600-1750 cm^{-1} region, reflecting structural modifications of the peaks. Additional changes were detected around 2000 cm^{-1} and 3100-3250 cm^{-1}. The 3015 cm^{-1} peak in silibinin-loaded MLVs shifted below 3000 cm^{-1} following UV exposure, which was also evident in FT-IR spectra (Section 4.5. *Data on Fourier transform infrared spectroscopy of liposomes containing silibinin*).

In contrast, ultrasound treatment of silibinin-loaded liposomes primarily affected peak intensities without causing notable shifts in Raman band positions (Figure 25c). Previous work showed that sonication can increase the intensity and shift stretching of CH_2 and C=O bands (around 2900-200 and around 1750 cm^{-1}) to high wavenumbers because of unsaturated fatty acid components sensitive to oxidation (Chotphruethipong et al., 2021). The absence of such shifts in silibinin-containing liposomes may be attributed to the compound's antioxidant activity, as polyphenols are known to inhibit lipid oxidation effectively (Sun et al., 2024b).

4.7. Data on antiradical potential of liposomes containing silibinin

Liposomal vesicles serve as delivery systems for antioxidant molecules, enhancing their bioavailability and enabling controlled release, while also providing protection against oxidative degradation of the liposome itself (Guldiken et al., 2018). Here, the radical scavenging abilities of multilamellar silibinin-entrapped lipid particles, UV-exposed liposomal spheres, freeze-dried particles, as well as sonicated particles loaded by silibinin were assessed using ABTS and DPPH assays, as well as in a cellular model with induced reactive oxygen species, as detailed in Section 4.9. *Data on the antioxidant effect of liposomes containing silibinin on H_2O_2-induced oxidative stress of keratocytes*. The results obtained from the ABTS/DPPH tests were summarized in Figure 26.

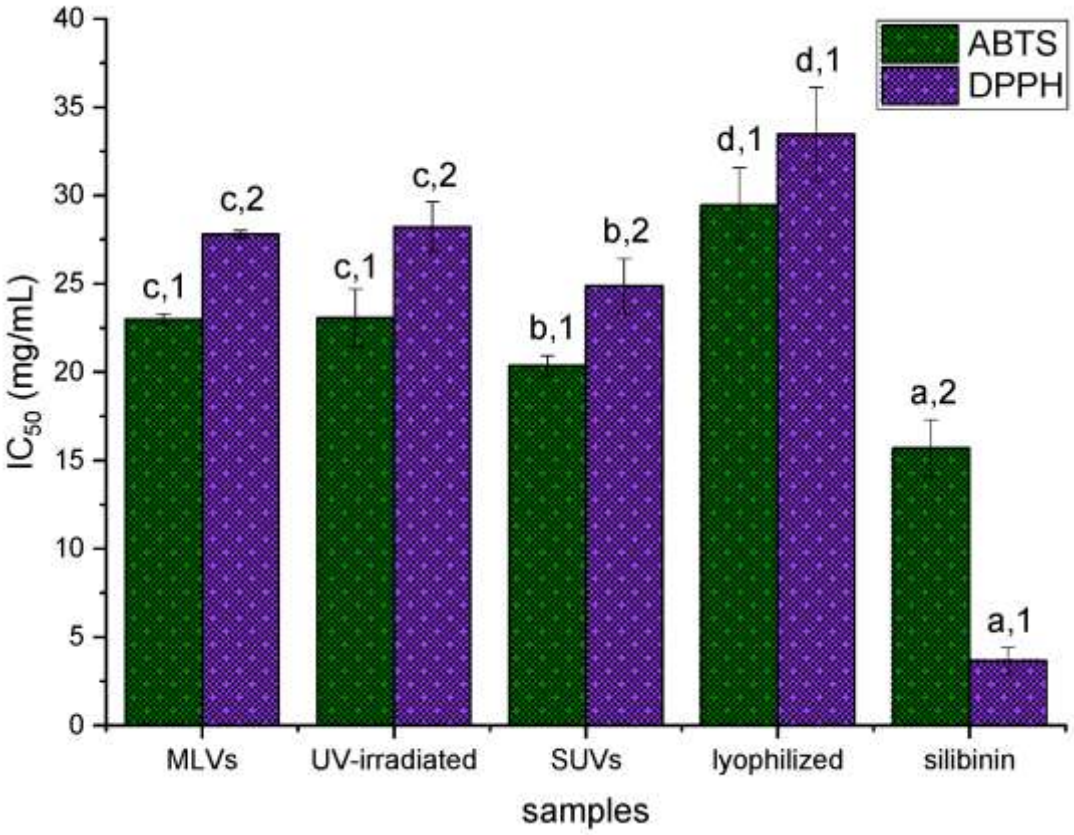

Figure 26. Antioxidant (antiradical) activity of silibinin-loaded liposomal formulations (MLVs - multilamellar vesicles, ultraviolet-treated sample, SUVs - sonicated sample, and freeze-dried particles) and free silibinin, determined in the ABTS and DPPH methods. Data with the same letter or number indicates no difference

Anti-ABTS abilities of the silibinin-loaded sample were approximately 22.99, 23.08, 20.36, and 29.44 mg of pure silibinin per mL of liposome formulation (Figure 26). Similarly, the DPPH assay yielded IC_{50} values of approximately 27.80, 28.21, 24.86, and 33.46 mg/mL (Figure 26). For comparison, the IC_{50} values of vitamin C were approximately 0.217 mg/mL (ABTS assay) and approximately 0.052 mg/mL (DPPH assay). Ultraviolet treatment did not significantly alter afore-mentioned ability of developed formulations with silibinin in either assay, whereas lyophilization markedly reduced their radical scavenging activity. Nevertheless, ultrasound treatment enhanced the potential of silibinin-loaded liposomal vesicles, as indicated by lower IC_{50} values. The anti-radical ability of free silibinin amounted to 15.69 ± 1.61 mg/mL (ABTS) and 3.65 ± 0.76 mg/mL (DPPH) (Figure 26).

UV irradiation did not significantly affect the liposome activity, highlighting the beneficial effect of the phospholipid carrier toward encapsulated molecules. In contrast, freeze-drying markedly reduced this liposome effect. Freezing at a low rate can disrupt the lipid bilayer due to the development of large ice crystals and can cause structural alterations through mechanical strain and osmotic forces, ultimately resulting in the leakage of the encapsulated antioxidants and, consequently, decreased entrapment efficiency (Yu et al., 2021), as observed for liposome particles with silibinin. Comparing the liposomal formulations obtained in this study, the lyophilized sample exhibited the lowest silibinin content. Furthermore, because the antioxidant assays were conducted after rehydration of the lyophilized liposomes, incomplete re-suspension and structural rearrangements of the liposomes may have contributed to the observed decrease in overall antioxidant activity (Yu et al., 2021). Sonicated vesicles also exhibited lower encapsulation efficiency compared to multilamellar particles and liposomes exposed to UV radiation. However, sonication appeared to enhance their antioxidant potential, likely due to the

increased surface area (present in smaller vesicles) interacting with reactive oxygen or nitric species. Pure silibinin displayed higher antioxidant activity in both assays (Figure 26). Overall, these findings indicate that the liposomal environment substantially influences the antioxidant capacity of silibinin.

4.8. Data on cytotoxic effect of liposomes containing silibinin on keratocytes

Considering the reported biological activities of silibinin on skin in previous studies (Matsumura and Ananthaswamy, 2004; Singh and Agarwal, 2002; Singh and Agarwal, 2009), the impact of the developed liposomal formulations on keratinocyte viability was evaluated. The data obtained is shown in Figure 27.

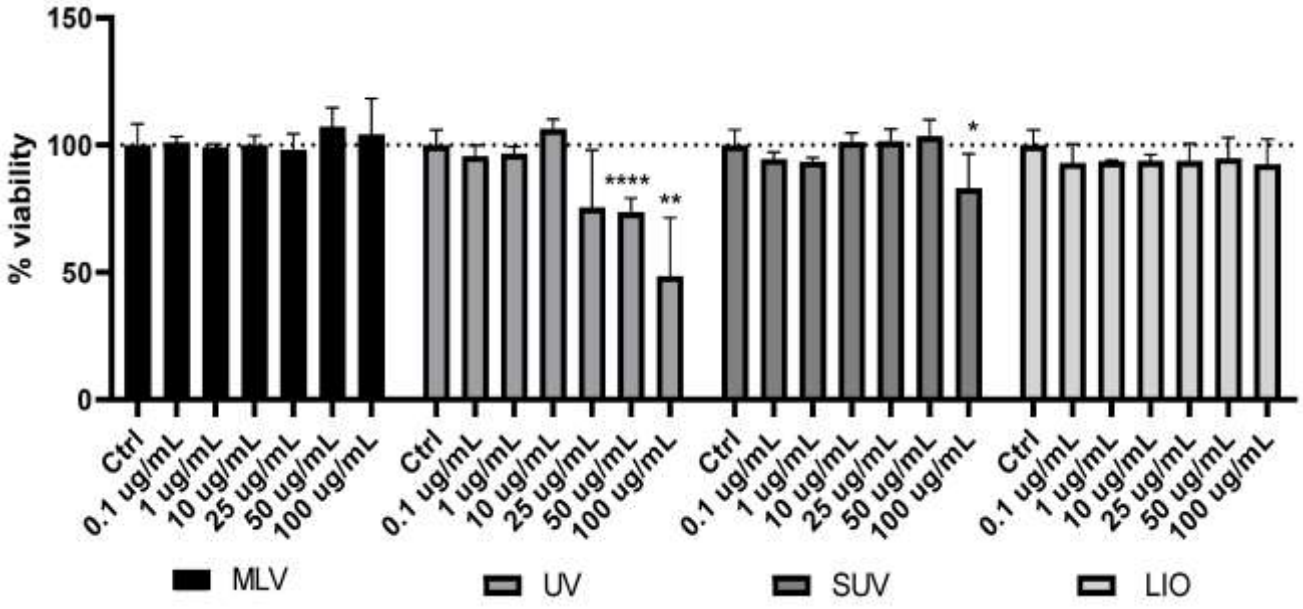

Figure 27. Cytotoxic effects of MLVs (multilamellar vesicles), ultraviolet-treated sample, freeze-dried formulation, as well as SUVs (sonicated vesicles) encapsulating silibinin (0.1-100 μg/mL), assessed by MTT test in human immortalized keratinocyte cell line.

Figure 27 illustrates the impact of multilamellar vesicles, ultraviolet-treated sample, freeze-dried formulation, as well as sonicated vesicles encapsulating silibinin on the human immortalized keratinocyte cell line. The effect of liposomal formulations showed various trends depending on liposome type. Specifically, multilamellar vesicles and freeze-dried formulation containing silibinin did not significantly affect keratinocytes at all tested ratios compared to untreated samples. In contrast, silibinin-loaded UV-irradiated liposomes showed the impact on the viability using higher amounts of the samples (over 25 μg/mL), with a marked, concentration-dependent reduction in viability noticed at 0.05 and 0.10 mg/mL. Small unilamellar vesicles caused a drop in viable cells, but only when using 0.10 mg/mL relative to control (Figure 27). The cytotoxic effects of empty liposomes were also observed (Supplementary Materials, Fig. S8), but only at a high phospholipid concentration of 1000 μg/mL.

MLVs and lyophilized silibinin-loaded liposomes did not significantly affect HaCaT cell viability, whereas UV-irradiated liposomes exhibited cytotoxic effects. SUVs also caused a notable drop in the viability of keratinocytes. These observations may be because of generation of reactive oxygen and nitric species, as well as peroxidation of lipid components within the liposomal suspensions induced under ultraviolet exposure or sonication process.

Ultraviolet exposure led to alterations in the chemical structure/profile within the liposomal bilayer, as demonstrated by performing spectrophotometric methods, including Raman or FT-IR (Sections 4.5. *Data on Fourier transform infrared spectroscopy of liposomes containing silibinin* and 4.6. *Data on Raman spectroscopy of liposomes containing silibinin*). Reactive oxygen or nitric species formed under sonication or ultraviolet treatment may modify structures of various proteins, trigger apoptosis, and stimulate cytokine recovery (causing skin inflammation) (Nakai and Tsuruta, 2021). Additionally, free radicals can activate transcription factors, whereas peroxidation of lipid components can trigger vascular endothelial growth factor expression within skin cells (Nakai eta al., 2011; Nakai and Tsuruta, 2021). Ferroptosis (programmed death of the cells) is also associated with free radical-induced lipid oxidation and contributes to the development of different disorders related to the skin (collagen-related diseases, psoriasis, as well as tumors) (Dixon et al., 2012).

Previous studies have reported that ultraviolet-treated lipid vesicles exhibit characteristic Raman modes at 834 cm^{-1} and 867 cm^{-1}, corresponding to stearic acid (Jovanović et al., 2023a). In the present study, FT-IR analysis confirmed bands between 800 cm^{-1} and 900 cm^{-1} in UV-irradiated liposomes, indicating the formation of hydroperoxide species, potentially oxidative derivatives of stearic acid. Literature reports that fatty acids (such as stearic acid) and their oxidized derivatives were lipotoxic and reduced growth and division of cells, providing death ot the cells, consistent with observed cytotoxicity in the presence of UV-irradiated liposomes against keratynocytes (Liu et al., 2018; Yang et al., 2020).

Cytotoxicity of empty liposomal particles is likely due to excessive phospholipid content, which has been shown to reduce HaCaT cell viability in other studies (Tran et al., 2022). For example, (HEK)-293 cell line treated with higher concentrations of lecithin-based systems (10-25%) displayed reduced viability, whereas 10-fold diluted formulations (0.12-0.5% final phospholipid concentration) were non-toxic (Płaczek et al., 2019). Additionally, one limitation of liposomal formulations is their susceptibility to degradation through hydrolysis of glycerol esters, as well as polyunsaturated lipid peroxidation, forming soluble derivatives with short chains and reducing liposome quality (Castañeda-Reyes et al., 2020).

4.9. Data on the antioxidant effect of liposomes containing silibinin on H_2O_2-induced oxidative stress of keratocytes

The activity of multilamellar vesicles, ultraviolet-exposed samples, freeze-dried particles, as well as sonicated formulations containing silibinin was also evaluated toward H_2O_2-triggred process of oxidation and production of radicals within HaCaT line. The data from the experiments is in Figure 28.

Figure 28 illustrates the impact of developed liposomal formulations on reactive oxygen species amounts within keratinocytes. After 24 h incubation without H_2O_2 exposure (Figure 28A), all silibinin-loaded liposomes did not significantly affect endogenous reactive oxygen species production. Empty liposomes were also tested, and only the highest phospholipid concentration (1000 μg/mL) induced increased reactive oxygen species, while lower concentrations had no effect (Fig. S9 - Supplementary Materials).

Following 2 h treatment with H_2O_2 (concentration of 200 μM), reactive oxygen species production approximately doubled within keratynocites (Figure 28B). Pre-incubation with silibinin-loaded liposomes reduced reactive oxygen species levels (dose-dependent trend), with lower levels generally being significantly effective. Specifically, multilamellar and ultraviolet-treated silibinin-entrapped liposomes efficiently reduced reactive oxygen species (0.1 μg/mL), whereas sonicated and freeze-dried samples were effective at both 0.1 or 1 μg/mL (Figure 28B). At 0.10 mg/mL, silibinin-loaded ultraviolet-exposed and sonicated formulations significantly reduced reactive oxygen species levels as well (Figure 28B).

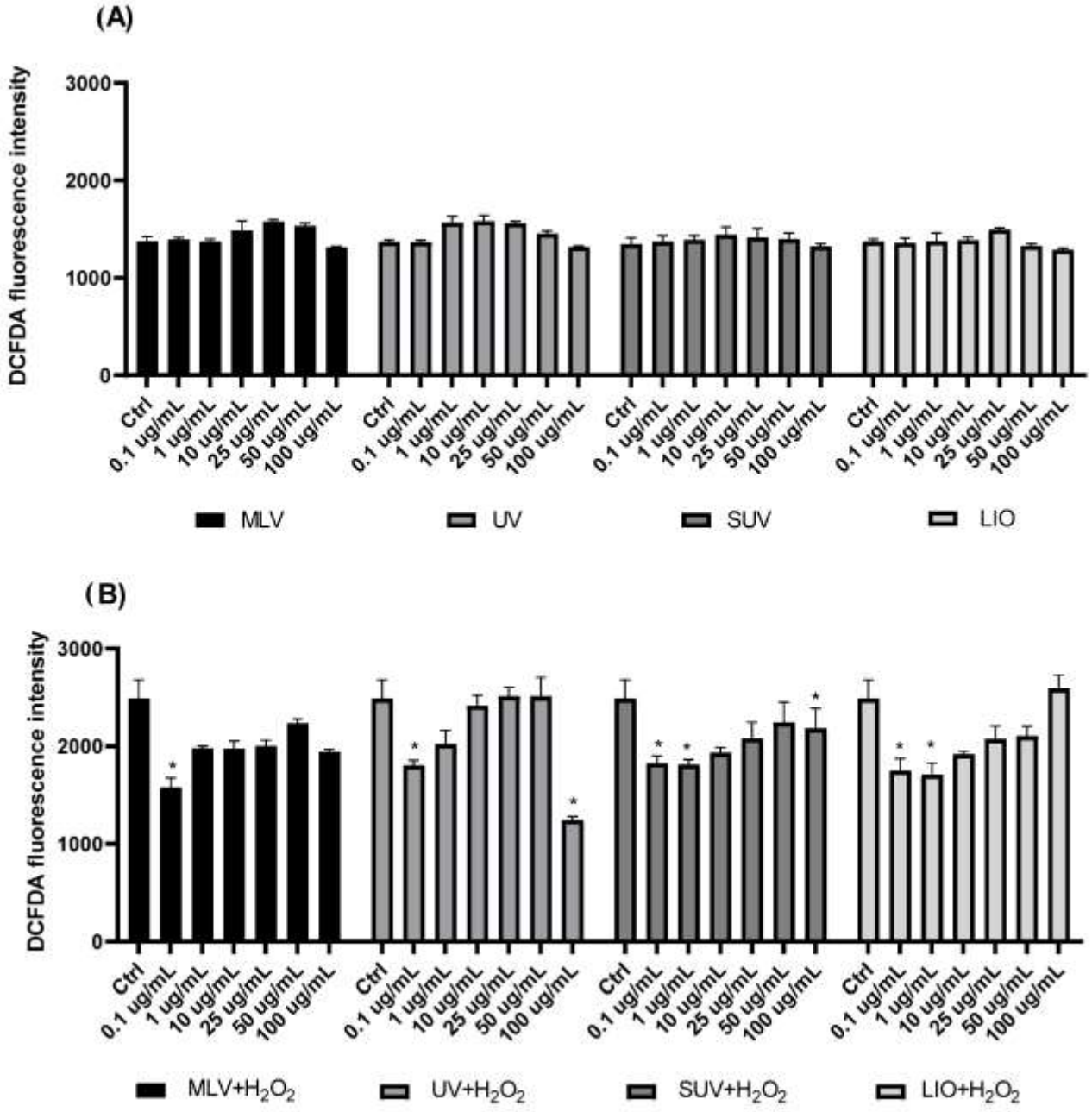

Figure 28. MLVs (multilamellar vesicles), ultraviolet-treated sample, freeze-dried formulation, as well as SUVs (sonicated vesicles) containing silibinin (0.1-100 μg/mL) impact on production of reactive oxygen species within keratinocytes: (A) the absence of hydrogen peroxide, (B) following hydrogen peroxide treatment; H2DCFDA assay.

Developed liposomes with silibinin treatment on HaCaT caused decreased amounts of reactive oxygen species levels than in HaCaT treated by hydrogen peroxide alone. Previous studies have shown that silibinin can decrease mitochondrial radical content (Li et al., 2022), although, according to Zhang et al. (2023), it may increase the generation of free radicals within cancer tissues and cells, promoting apoptosis and oxidative stress.

Here, silibinin-loaded MLVs and all modified silibinin-loaded liposomes significantly reduced reactive oxygen species amounts at 0.1 μg/mL, indicating that the liposome modification technique did not substantially affect their antioxidant potential. At higher concentrations, ultraviolet-treated and sonicated vesicles containing silibinin led to efficient reactive oxygen species reductions, likely reflecting the lower number of viable cells, as these formulations decreased cell viability in the MTT assay (Figure 27). The presence of unsaturated and other lipids in liposomal vesicles can render the membrane susceptible to UV-induced damage, as photon energy can generate reactive oxygen species *via* various mechanisms (electron redox reaction process, bond homolysis, the process of photolysis, high-energy irradiation, etc.), contributing to membrane disruption (Toopkanloo et al., 2020).

4.10. Data on the anti-inflammatory effect of liposomes containing silibinin on keratocytes

MIF, IL-1β, and COX-2 are central mediators of inflammatory signaling in skin cells, playing pivotal roles in cytokine regulation and immune responses. Exploring the influence of liposomes loaded with bioactive compound silibinin to these markers provides insight into their potential to modulate inflammation at the cellular level. Pre-treatment with liposomal formulations allows evaluation of both basal and LPS-induced inflammatory responses, highlighting the protective and inhibitory capacity of the encapsulated bioactive compound. Understanding how different liposome processing methods, such as UV irradiation, lyophilization, and sonication, affect anti-inflammatory activity is crucial for optimizing formulation design and therapeutic efficacy.

Since cyclooxygenase-2, interleukin-1 beta, and macrophage migration inhibitory factor are key regulators of responses related to inflammation within cells of the skin, the effect of the treatment by multilamellar vesicles, ultraviolet-treated sample, freeze-dried formulation, as well as sonicated vesicles at the concentration of 10 μg/mL (all formulations contained silibinin) was evaluated within HaCaT exposed to LPS.

As shown in Figure 29, bacterial lipopolysaccharide exposure triggered the increase in interleukin-1 beta and macrophage migration inhibitory factor levels, while COX-2 levels exhibited only a slight rise compared to untreated controls. In cells treated with liposomal formulations (in the absence of lipopolysaccharide), a slight cyclooxygenase-2 inhibition was observed for sonicated and freeze-dried samples with silibinin, whereas interleukin-1 beta expression was moderately decreased by silibinin-loaded SUVs. Control experiments with empty lipid particles (vesicles containing only phospholipids/the absence of bioactive silibinin) at 10 μg/mL did not alter cyclooxygenase-2, interleukin-1 beta, and macrophage migration inhibitory factor expression compared to untreated cells (Fig. S10 - Supplementary Materials).

Developed silibinin-loaded liposomal formulations significantly reduced MIF levels after 24 h incubation in the absence of LPS (Figure 29). In LPS-challenged cells, pre-treatment with prepared liposomes significantly suppressed macrophage migration inhibitory factor expression compared to bacterial lipopolysaccharide, showing the inhibition by silibinin-loaded liposomes on this cytokine (Figure 29). Regarding IL-1β, only silibinin-loaded lyophilized liposomes induced a significant reduction in protein expression, whereas other formulations showed a non-significant decreasing trend (silibinin-loaded SUVs also tended to reduce IL-1β) (Figure 29). COX-2 levels did not change significantly upon LPS exposure; therefore, no notable effect of liposome pre-treatment on COX-2 expression was observed (Figure 29).

All silibinin-loaded liposomes significantly decreased MIF expression within keratinocytes following a 24-hour period in the LPS absence (Figure 29). Similarly, in LPS-stimulated cells, all four liposomal formulations retained their inhibitory effect on MIF expression, demonstrating that both unmodified and modified liposomes effectively suppressed MIF levels (Figure 29). These results indicate that post-processing changes did not alter MIF-inhibitory ability of developed liposomal formulations with silibinin. Previous research has also shown that silibinin reduces MIF levels in tumor-associated macrophages (Ramasamy et al., 2013).

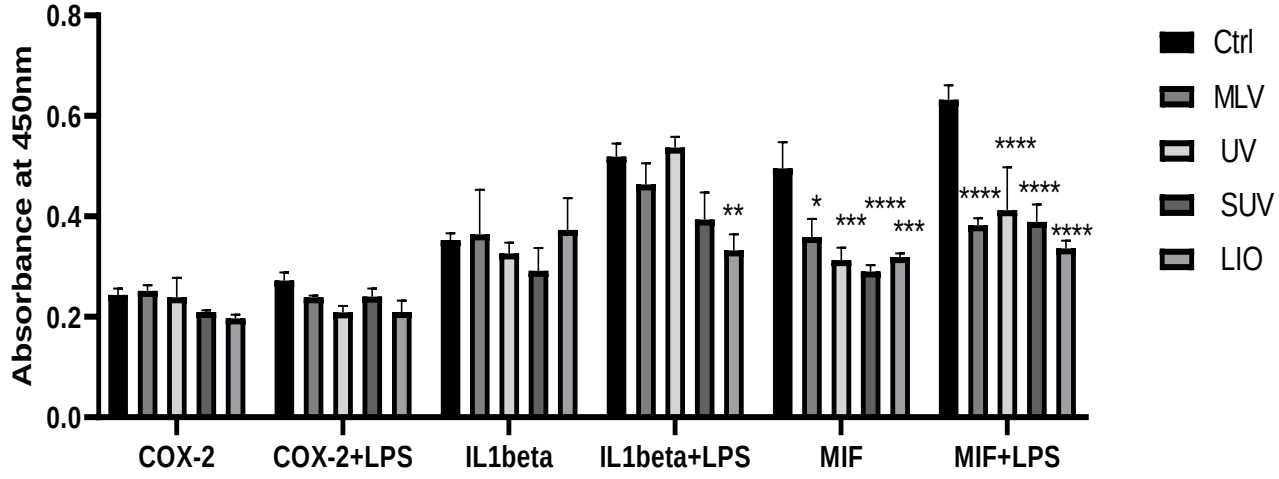

Figure 29. MLVs (multilamellar vesicles), ultraviolet-treated sample, freeze-dried formulation, as well as SUVs (sonicated vesicles) containing silibinin (10 μg/mL) impact cyclooxygenase-2, interleukin-1β, and macrophage inhibitory factor within keratynocytes, in the presence and absence of lipopolysaccharide (LPS). Protein levels were measured using cell-ELISA.

Regarding IL-1β expression, the presence of freeze-dried vesicles effectively decreased interleukin-1β levels within LPS-exposted cells, while sonicated vesicles exerted a non-significant decreasing manner. Multilamellar and ultraviolet-treated liposomes did not affect IL-1β expression. Liposome size appears to be a critical factor for skin delivery, as smaller vesicles (*e.g.*, SUVs and lyophilized liposomes) can penetrate various skin layers, increasing the release, as well as encapsulated compounds' efficacy (Castañeda-Reyes et al., 2020). Reduced vesicle size has been employed previously to improve therapeutic outcomes in conditions such as vitiligo (Castañeda-Reyes et al., 2020), and liposomes around 100 nm have been shown to enhance skin penetration and formulation efficacy (Peralta et al., 2018).

Although silibinin is known to reduce IL-1β levels and exert anti-inflammatory abilities within clinical settings, absence of significant IL-1β downregulation in some liposomal formulations may be due to encapsulation, resulting in prolonged or delayed release (Giorgi et al., 2012). Lyophilized liposomes and SUVs, which exhibited smaller particle sizes than MLVs and UV-irradiated liposomes, likely allowed for greater silibinin release due to higher surface area, explaining the enhanced interleukin-1β expression drop. Supporting this, literature reported that liposomal silibinin achieved superior anti-inflammatory effects compared to free silibinin *in vivo*, attributed to improved delivery and bioavailability after oral or parenteral administration (Yan et al., 2023).

These observations suggest that optimizing liposome size represents a key to boosting the therapeutic potential of encapsulated bioactives within skin applications. Smaller vesicles show larger ratios between volume and surface, enhancing faster and significantly efficient recovery of silibinin within desirable place. Moreover, particle size can influence cellular uptake and penetration through the *stratum corneum*, contributing to the observed differences in IL-1β modulation between tested samples. In conclusion, the data show the importance of carefully controlling liposomal characteristics to maximize anti-inflammatory efficacy while maintaining stability and biocompatibility.

4.11. Data on nuclear magnetic resonance spectroscopy of pullulan-isononanoate

NMR spectroscopy provides detailed structural and chemical information about molecules, making it an indispensable tool in the characterization of bioactive compounds and formulations. It allows precise identification of functional groups, molecular interactions, and conformational changes, ensuring the integrity and purity of the studied substances. The application of NMR enhances the reliability of experimental data and supports robust conclusions regarding molecular composition and behavior (Hernandez-Tenorio and Giraldo-Estrada, 2022).

Therefore, ^{1}H and ^{13}C NMR spectroscopy were applied to verify pullulan-isononanoate production. Pullulan-isononanoate structural representation is shown in Figure 30. The individual structural formulas of pullulan (labeled with residues A-C) and isononanoic acid are depicted in Supplementary Materials, Figures S11 and S12 (as 2D and 3D formulas). NMR techniques have previously been employed for detailed characterization of pullulan and isononanoic acid structures (McIntyre et al., 1993), as an essential method for investigation (Fig. S13, Fig. S14, Supplementary Materials). These residues are bonded by α-(1→4) D-glucosidic linkages. Further, they in turn were connected *via* α-(1→6) D-glucosidic bonds, in agreement with prior assignments reported in the literature (Arnosti and Repeta, 1995; McIntyre et al., 1993; Singh et al., 2021).

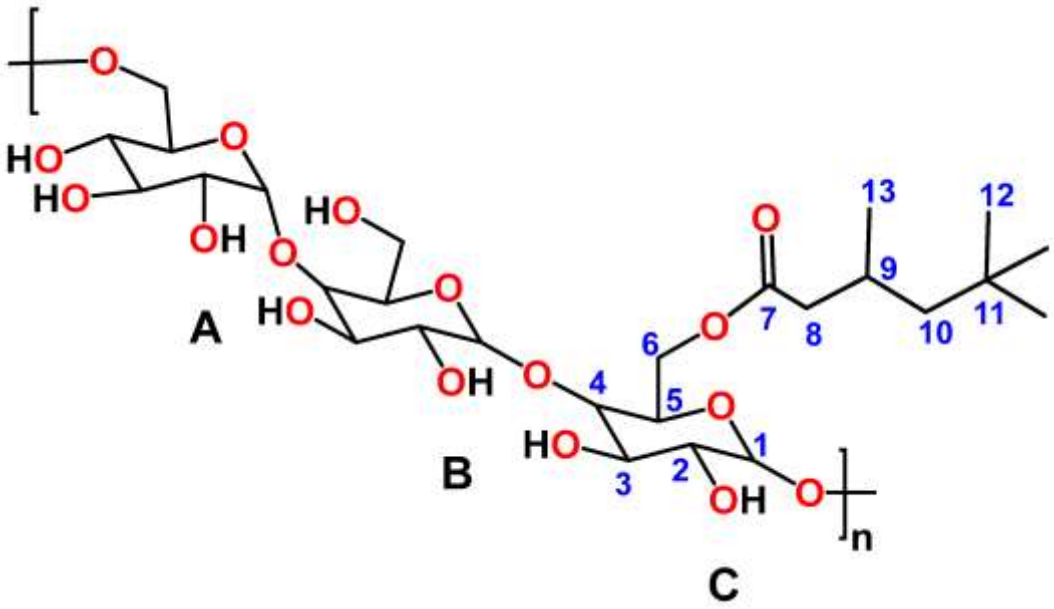

Figure 30. Structural formula of pullulan-isononanoate

Successful esterification with 3,5,5-trimethylhexanoic acid chloride was verified using both one-dimensional and two-dimensional nuclear magnetic resonance spectrometry experiments, alongside by comparing to previously reported papers (Hussain et al., 2017; Park et al., 2012). Proton (^{1}H) and carbon-13 (^{13}C) nuclear magnetic resonance spectrum of Pull-Iso were measured in dimethyl sulfoxide-d_6. Those were shown in two figures, namely, Figures 31-32, respectively, while two-dimensional spectra were presented in Fig. S15 (Supplementary Materials), confirming pullulan modification.

Combined use of NMR techniques allowed for the detailed assignment of proton and carbon signals, providing unambiguous proof of the effective isononanoate groups' introduction along backbone of pullulan. Correlation experiments, such as COSY and HSQC, further confirmed the connectivity between sugar residues and esterified moieties, supporting the structural integrity of the modified polymer. These spectroscopic analyses validate the efficiency of the esterification reaction and serve as a basis for correlating chemical modification with changes in thermal, mechanical, and functional properties of Pull-Iso. The results are consistent with previously reported modifications of pullulan, demonstrating the reproducibility and reliability of the applied synthetic strategy.

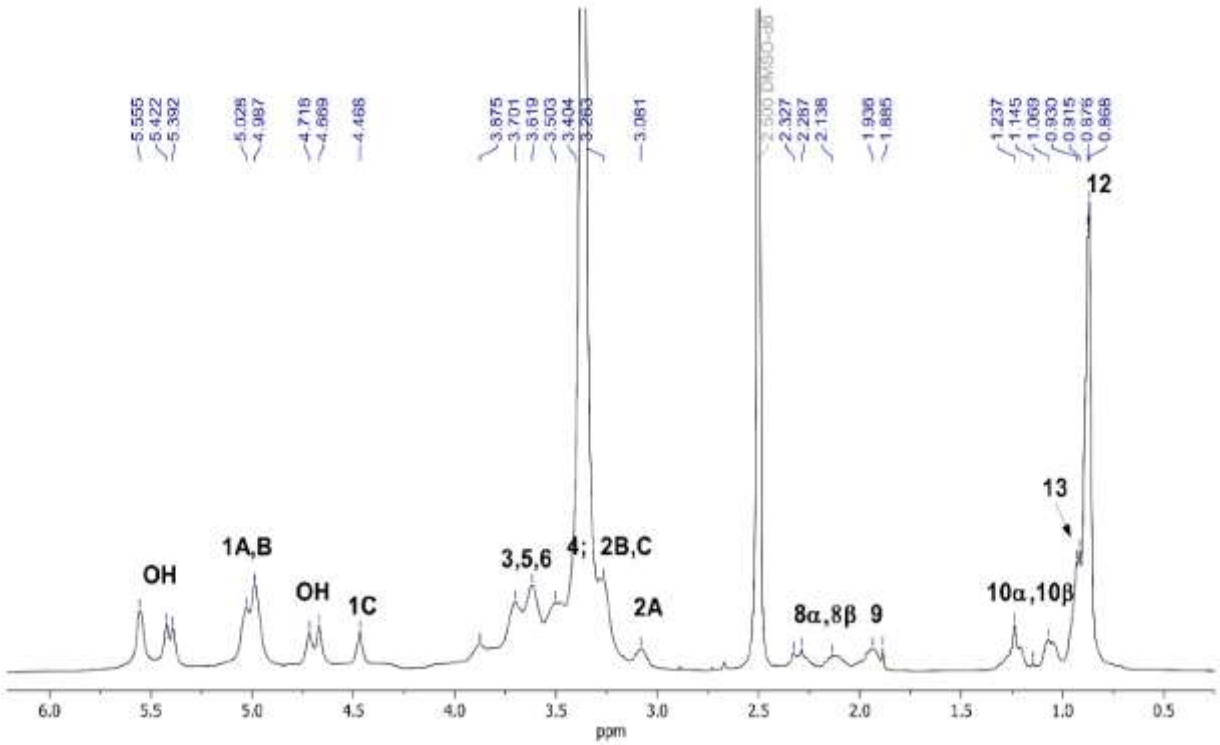

Figure 31. [1]H nuclear magnetic resonance spectra of developed pullulan-isononanoate

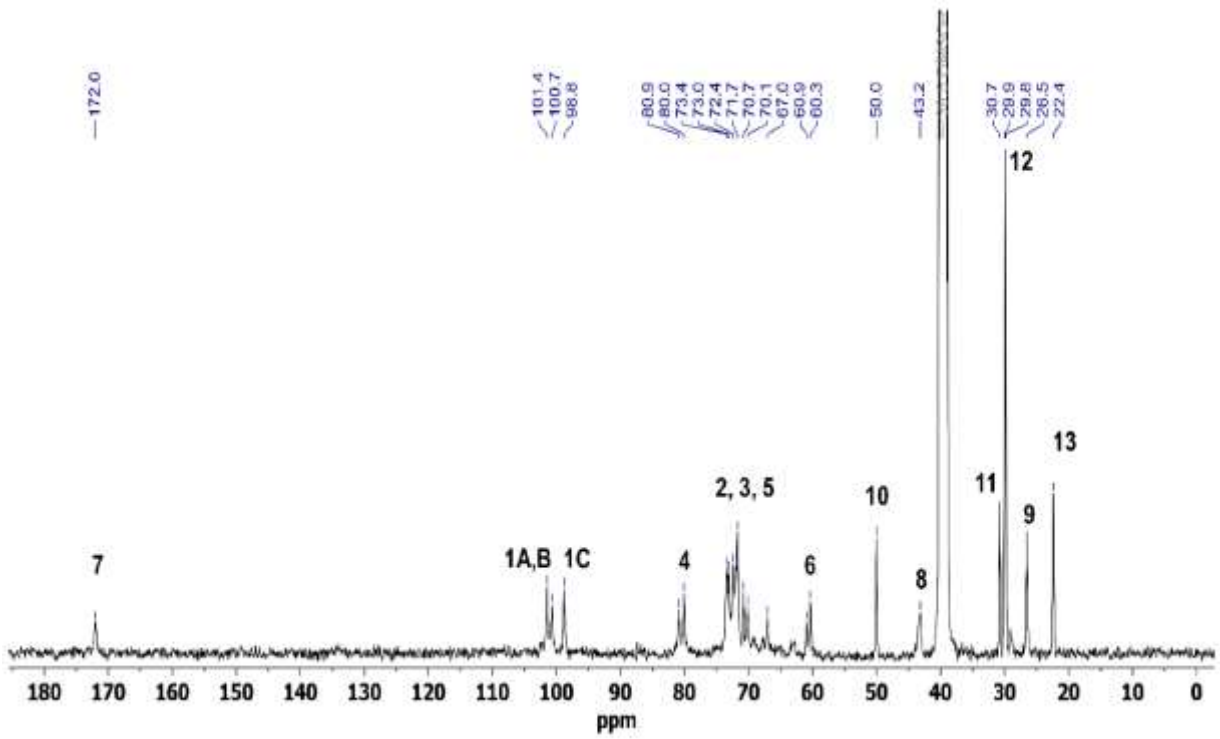

Figure 32. [1]C nuclear magnetic resonance spectra of developed pullulan-isononanoate

In the ^{1}H NMR spectrum, δH 0.83 resonance arises from terminal methyl protons (3H, H-12) in groups of isononanoate, whereas the methyl protons H-13 (3H) are observed at δH 0.92 (Figure 31 and Supplementary Materials - Fig. S13). Methylene protons within the aliphatic chain (H-10α and H-10β) resonate between δH 1.00-1.30. The signal at δH 2.13 (2H, H-8α) and the signal at δH 2.32 (H-8β) are attributed to groups of methylene positioned α to the carbonyl, whereas the signal at δH 1.94 is assigned to H-9 (1H). Further, the signal observed within δH 3.00-4.00 range arises from ring protons, whereas the signal at δH 4.25-5.75 corresponds to pullulan's hydroxyl and anomeric protons in backbone (α-(1→4) bond and α-(1→6) bond) (Figure 31 and Supplementary Materials - Fig. S13).

The observation of unreacted hydroxyl signals indicates that only a portion of the accessible hydroxyl groups underwent esterification. Anomeric protons H-1A and H-1B are observed at δH 5.02 and 4.99, respectively, whereas at signal δH 4.47 appears H-1C (Figure 32, Supplementary Materials - Fig. S13).

The ^{13}C NMR spectrum of Pull-Iso displays distinct peaks corresponding to both the carbohydrate skeleton and aliphatic side chains. Resonances appearing between δC 22.2 ppm and 50.6 ppm are assigned to methyl and methylene, as well as methine carbons within chains of isononanoate (Figure 32, Supplementary Materials - Fig. S14). At δC 60.3-101.4 ppm were linked to the oxygen-bearing carbons (in backbone of pullulan), such as anomeric centers, indicating that structures of polysaccharides remain intact (Figure 32, Supplementary Materials - Fig. S14). A peak (δC 172.0 ppm) corresponds to the moieties of ester carbonyl carbon, confirming efficient integration of residues from isononanoate within framework of pullulan (Figure 32, Supplementary Materials - Fig. S12, Fig. S14, and Fig. S16). Taken together, the 1D and 2D NMR data provide clear evidence that modification of hydroxyl group of pullulan by 3,5,5-trimethylhexanoic acid led to formation of isononanpullulan.

Pullulan-isononanoate showed 0.264 g KOH/g of SV, measured according to method explained in Section 3.12. *Determination of the degree of esterification by potentiometric titration*. The EV, calculated as SV - AV, had a value of 0.252 g KOH/g, suggesting the following: roughly 0.81 esterification of the hydroxyl groups in each anhydroglucose unit by 3,5,5-trimethylhexanoic acid was achieved.

Taken together, the NMR spectra and potentiometric titration data confirm that pullulan is efficiently esterified by 3,5,5-trimethylhexanoic acid, resulting in a chemically modified biopolymer with approximately 81% of available hydroxyl groups substituted. These results showed preserved polysaccharide backbone integrity while efficiently incorporating aliphatic ester moieties, providing a foundation for subsequent functional and formulation studies.

4.12. Data on differential scanning calorimetry of developed pullulan-isononanoate

DSC is an essential tool for evaluating the thermal behavior of modified materials intended for film applications. It provides critical information on glass transition, crystallinity, and thermal stability, which directly influence the mechanical performance, flexibility, and processability of polymer films. By analyzing thermal transitions and degradation temperatures, DSC allows researchers to predict how modified polymer films will behave under heat or during storage, helping to ensure their long-term performance and reliability. Additionally, DSC analysis enables the identification of potential interactions between polymer chains and incorporated bioactive compounds, which can alter the thermal behavior of the material. Subtle changes in melting or crystallization patterns revealed by DSC can indicate modifications in polymer microstructure or compatibility with additives. Namely, incorporating DSC data into the study provides a comprehensive understanding of the material's thermal properties, guiding formulation optimization for enhanced performance in film applications.

Therefore, thermogram obtained in DSC analysis of pullulan-isononanoate is created to investigate how esterification affects its phase-transition characteristics (Figure 33).

The thermal analysis of Pull-Iso reveals significant modifications in its polymer chain dynamics compared to native pullulan. Specifically, the observed glass transition temperature (T_g) provides insight into how esterification with isononanoic acid influences chain mobility, segmental flexibility, and overall thermal behavior of the modified polymer (as described in detail below).

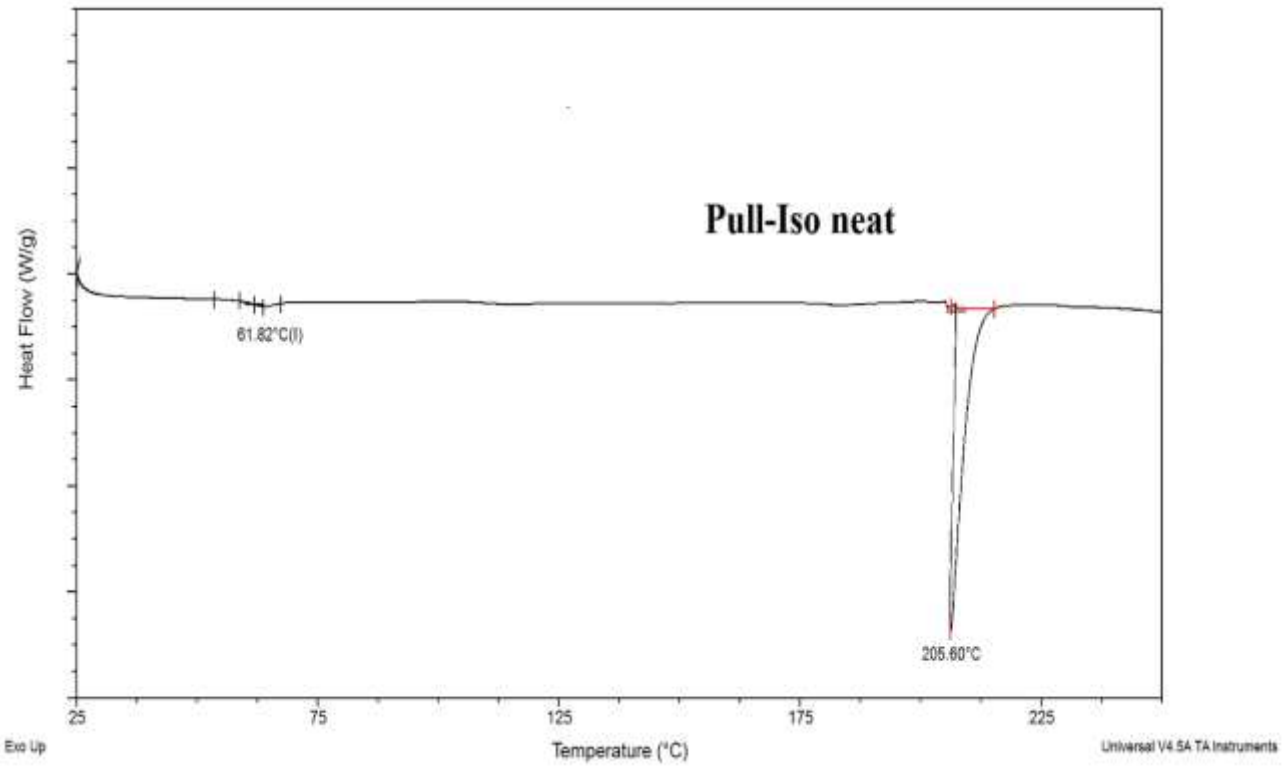

Figure 33. Differential scanning calorimetry curve of developed pullulan-isononanoate

T_g (glass transition temperature) of pullulan-isononanoate appeared at ~61°C, considerably reduced compared to unmodified sample, which exceeds 120°C, which alters due to the changes in molecular weight, as well as content of moisture (Simões et al., 2024). This decrease in T_g corresponds to side chains' introduction along backbone of pullulan, which creates additional unoccupied volume and enhances mobility of segments from polymer. Being an amorphous polysaccharide, pullulan lacks crystalline regions and therefore does not display a sharp melting point (Farris et al., 2014). Increasing the length of the acyl group in pullulan esters results in a gradual drop in T_g, reflecting greater chain flexibility due to the incorporation of longer, more pliable substituents. In the present study, esterification with isononanoic acid produced a macromolecule exhibiting a glass transition temperature (T_g) positioned intermediate to pullulan valerate (67°C) and pullulan hexanoate (46°C), as documented by Enomoto-Rogers et al. (2015), whereas pullulan octanoate and decanoate presented T_g measurements of 42°C and 35°C, correspondingly. This tendency is consistent with anticipated behavior because isononanoic acid possesses a six-carbon backbone. These observations indicate that thermotropic behavior of pullulan-isononanoate may be finely adjusted by selecting the appropriate reagents for esterification, such as carboxylic acid, acyl halide, etc. Additionally, the distinct endothermic peak (~207°C) corresponds to initiation of thermal degradation of the esterified polymer.

4.13. Data on the encapsulation efficiency of silibinin/smoke tree extract-loaded liposomes

EE is a key parameter in evaluating liposomal formulations, as it reflects the proportion of active compounds successfully entrapped within the vesicles. High EE is crucial for ensuring effective delivery, protecting sensitive molecules from degradation, and controlling their release. Factors such as lipid composition, vesicle size, preparation method, and solubility of the active compound significantly influence EE (Jovanović et al., 2018). Thus, entrapment efficiency of total polyphenols, including both silibinin and other phenolic constituents from the ethanol smoke tree extract, was evaluated in Folin-Ciocalteu method.

An analysis revealed a large portion of target molecules efficiently loaded into lipid vesicles (~87.1%); the majority of extracted smoke tree compounds were entrapped within vesicular carriers. The observed EE suggests that the bioactive molecules are effectively retained within the liposomes. Polyphenols are particularly challenging to encapsulate due to their hydrophilic nature and chemical instability. Achieving high EE ensures that the majority of polyphenolic compounds are retained within the liposomal core, protecting them from oxidation and enhancing their bioavailability. Efficient encapsulation of polyphenols in liposomes also allows their incorporation into functional films or other delivery systems without loss of activity. Optimizing the EE of polyphenols in liposomal systems is essential for maximizing their therapeutic potential, as it directly affects the stability, release profile, and biological efficacy of the final formulation (Mignet et al., 2013).

4.14. Data on dynamic light scattering analysis of silibinin/smoke tree extract-loaded liposomes

The storage behavior of liposomal formulations containing silibinin/smoke tree extract was tested for 60 days by analyzing key variables (particle diameter, distribution, as well as surface charge) (Figure 34). The assessment of vesicle dimensions and colloidal stability was performed by DLS, the standard quantitative assay for testing of liposomal particles, which provides a mean diameter of whole particles (their hydrated forms) (Bhattacharjee et al., 2016). Consequently, results obtained by DLS and transmission electron microscopy cannot be directly compared, and DLS is considered more appropriate for evaluating liposomal systems designed for biomedical use (Danaei et al., 2018; Leitgeb et al., 2012).

Pronounced increase of vesicle diameter was observed in the 30-day period, rising from ~1979 to ~4220 nm, while moderate reduction was observed on the 60th day (~3763.67 nm) (as shown in Figure 34A). This trend reflects the dynamic nature of the structure of the particles within water environments. The relatively narrow distribution, *i.e.*, lower index of polydispersity (approximately 0.340), indicates the presence of a fairly uniform sphere size instead of irregular aggregates of phospholipids. The enlargement of vesicles can be attributed to fusion or clustering processes, which are commonly reported in liposomal systems during storage, as well as to destabilization of the lipid bilayer caused by chemical phenomena, such as oxidation, hydrolysis, or phase transitions. Additionally, water uptake into the membrane or internal compartment may result in vesicle swelling (Grit and Crommelin, 1993; Levin and Idiart, 2004). After reaching maximum size at day 30, a decrease of approximately 10.8% was recorded, which may be explained by structural reorganization of the bilayer toward a more thermodynamically stable configuration, sedimentation or rupture of larger vesicles, and possible leakage of the encapsulated compounds, affecting vesicle structure/integrity and dimensions (Alshaer et al., 2023; Leirer et al., 2009). These observations indicate notable poor physical stability during the storage period, especially during the beginning stages. Although partial stabilization can happen following a 30-day period, formulations still exhibit considerable size variability, which could influence release kinetics and biological performance. Therefore, the detected instability further supports the incorporation of liposomes within pullulan-isononanoate film samples. The particle dimensions surpass those generally regarded as optimal for dermal resorption; therefore, delivery functions independently of the transport of intact particles through the *stratum corneum*. Alternatively, sizable multi-layered formations are anticipated to persist atop the epidermis, serving as storage depots that slowly dispense biologically active compounds. This non-infiltrative mechanism of effect for standard liposomal carriers has been extensively described in various papers (Elsayed et al., 2007; Honeywell-Nguyen et al., 2005).

Furthermore, the main function of liposome-based encapsulation lies in safeguarding delicate biologically active compounds, including silibinin/extracted polyphenols from the smoke tree wooden sections, against breakdown, while guaranteeing their regulated release following integration into the polymer film framework.

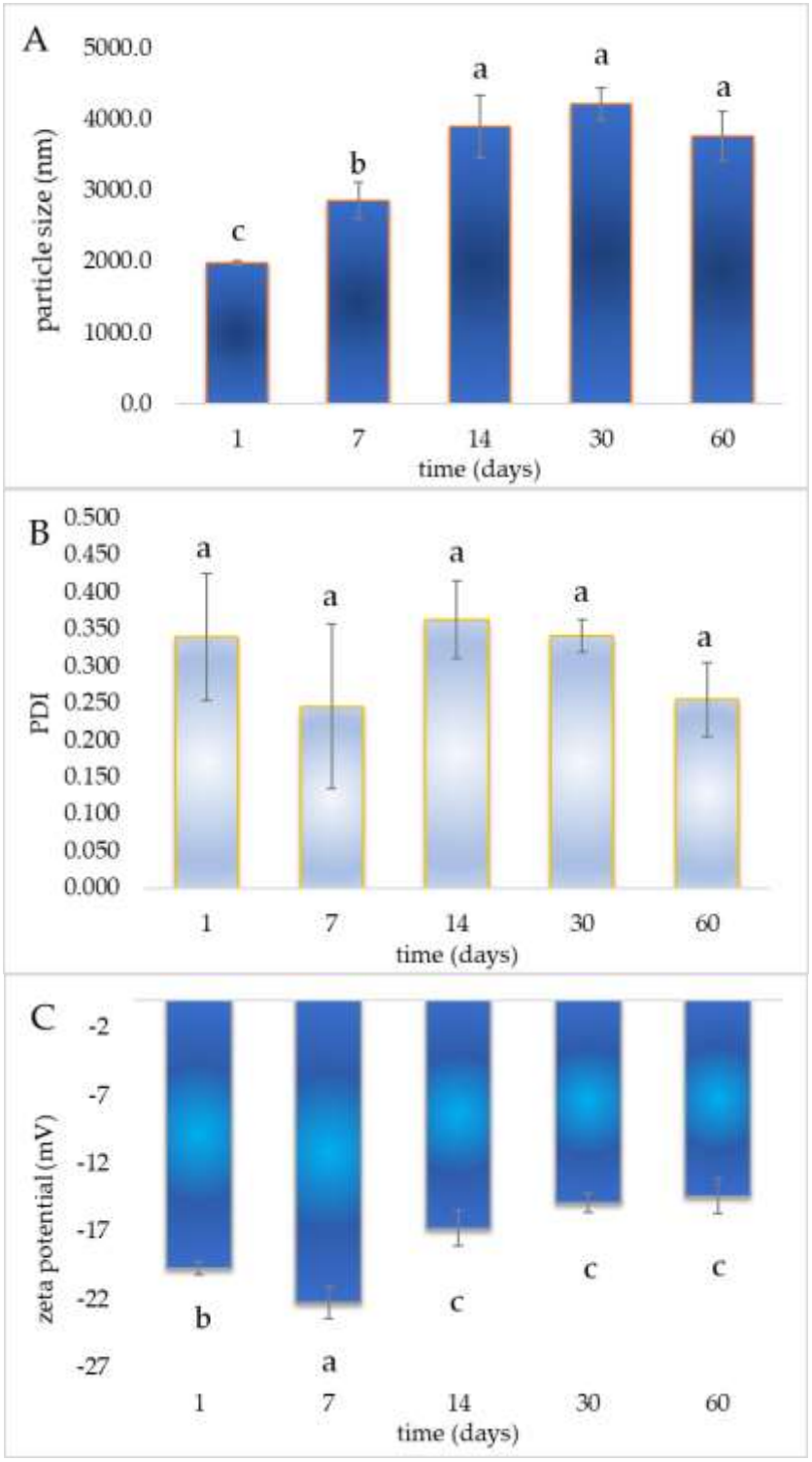

Figure 34. Dynamic light scattering analysis of silibinin/smoke tree extract-entrapped liposomal spehres during storage in the fridge (60-day period): (A) liposome size, (B) liposome size distribution, (C) surface charge of liposomal particles; the same letters above bars represent the absence of significant differences.

In this work, liposomes were deliberately applied without any post-preparation size-modification procedures to maintain their original multilamellar architecture and initial structural stability. Probe sonication was intentionally excluded, since ultrasonic processing can introduce titanium contaminants from the probe tip into lipid dispersions, which may compromise formulation purity and reduce biocompatibility. This methodological decision is consistent with earlier *in vitro* findings, where the biological performance of multilamellar lipid particles (MLVs) and sonicated vesicles (SUVs) generated *via* probe sonication, both loaded with silibinin, was evaluated using skin cell models (Karkad et al., 2024). Those experiments revealed that silibinin-loaded SUVs induced marked cytotoxic responses, whereas MLVs with silibinin exhibited no detectable toxic effects. Notably, both vesicle types retained significant ability to neutralize free radicals and prevent inflammation responses, indicating that larger multilamellar vesicles are better options in the case of topical delivery while preserving biological efficacy.

Index of polydispersity serves as a descriptor of particle size uniformity, where values below 0.3 correspond to narrow distributions. Additionally, values above this threshold indicate increased heterogeneity (Alshaer et al., 2023). The PDI measured on day 1 (~0.340) and day 14 (~0.360) reflects broad population, *i.e.*, variability in the formation of particles, as well as fusion phenomena at the beginning stages (as shown in Figure 34B). Further, reduced PDI values were recorded on day 7 (approximately 0.250) and day 60 (approximately 0.260), both falling below the 0.3 limit, which indicates improved size uniformity. The smallest variability was observed on day 30 (~0.340), implying a transient stability-maintaining interval within intermediate storage conditions. Although minor fluctuations in PDI occurred throughout the observation period, no progressive destabilization trend was evident. Such variations may be linked to limited fusion or fragmentation processes, lipid membrane reorganization, and settling of bigger vesicular particles, which may alter the distribution of the population without markedly affecting mean diameter (Bhattacharjee, 2016). Overall, despite initial heterogeneity, the data suggest enhanced colloidal stability after prolonged storage, likely driven by gradual lipid rearrangement and narrowing of the size distribution. The measured data did not show significant processes of aggregation and loss of structural integrity within the 60-day period.

Surface charge evolution was evaluated by monitoring zeta potential at several time points, yielding initial values: ~-19.9, -22.4, -16.8, -14.9, -14.5 mV (as shown in Figure 34C). The measurements reveal the progressive decrease of negative charge intensity over time. Surface charges are widely recognized as indicators in electrostatic stabilization of colloidal systems, including liposomal dispersions. Typically, absolute values exceeding 30 mV are associated with strong repulsive forces and high stability, whereas 10-30 mV values showed medium stability; data close to 0 evidence a high risk of the aggregation process (Yang et al., 2023). In this case, although the intensity of the negative electrostatic charge diminished gradually, it remained within the moderate stability range throughout storage, indicating adequate electrostatic repulsive forces to inhibit the significant particle aggregation process. An observed reduction in surface charge may result from partial screening effects, surface group rearrangements, ion adsorption from surrounding solvent, or mild particle association (Honary and Zahir, 2013). Despite the downward trend, the zeta potential values never approached neutrality, supporting sustained stability against flocculation or particle settling during 60 days. While a charge decrease merits attention for long-term storage considerations, the overall electrostatic profile remains acceptable for the intended application. Furthermore, the zeta potential results reinforce the occurrence of well-structured liposomal bilayer spheres instead of undefined aggregated particles.

Finally, physicochemical assessments of liposomal vesicles following the encapsulation within film formulations were not performed, since re-dispersing the films would require mechanical disruption that could damage vesicle structure. In addition, polymeric and matrielas used for the film preparations can interfere with light scattering analysis, making it difficult to attribute size and surface charge data specifically to liposomes.

4.15. Data on the chemical characterization of the extract from the smoke tree wooden sections

Ethanol extract formulation obtained from wooden part of the smoke tree showed the high polyphenol amount. Polyphenol yield was determined to be 188.92 ± 4.12 mg GAE per g of plant material, indicating a rich presence of polyphenols. In addition, the total flavonoid content reached 70.76 ± 2.18 mg CE per g of plant material, suggesting that flavonoids represent a significant fraction of the phenolic constituents. These results confirm that the wooden part of the smoke tree was the valuable source of phenolics.

Previous research using the HPLC/DAD method reported that ethanolic extract of smoke tree contained a diverse profile of flavonoids (Pašić et al., 2025). Among these compounds, fustin and sulfuretin were identified as the dominant constituents. Other flavonoids, including butin, fisetin, taxifolin, and butein, were detected in lower but still notable amounts. According to Pavlov (2025), fustin and sulfuretin represented the most abundant bioflavonoids identified in ethanol infusion of smoke tree heartwood.

Chemical characterization of the smoke tree extract (determined in the present doctoral thesis and literature data) revealed a complex phytochemical profile dominated by phenolic constituents. Chromatographic and spectrophotometric analyses confirmed content of multiple flavonoid molecules, as well as related phenolics, indicating that its extracts represent important sources of bioactives. The diversity/abundance of these substances strongly depends on both herbal solid and applied extraction conditions. Ethanolic extracts exhibited an increased degree of chemical complexity, reflecting the efficient solubilization of phenolic compounds from the woody plant tissue. Such a profile supports the potential of smoke tree extracts for further biological and pharmacological investigations.

To achieve a higher yield of total flavonoids, polyphenols, or specific target compounds, optimization of the extraction process is essential. Key parameters that require adjustment include solvent type and concentration, extraction time, temperature, ratio between matrix and medium, particle size of solids, and applied technique for isolation.

The yield of the extraction process, a percentage of material recovered from the sample, is an important indicator of efficiency of extraction procedure. The extraction process resulted in a yield of 6% in the case of smoke tree extract, indicating the proportion of the target compound successfully isolated from the raw material. Extraction yield provides valuable insight into the efficiency and selectivity of the method, highlighting how much of the desired compound can be obtained from the source material. The observed extraction yield may be altered by multiple parameters (solvents, temperature, and duration, which collectively determine the effectiveness of the process. Here, extraction yield amounted to 6% demonstrates the content of total extractable constituents isolated, which is critical for evaluating both process efficiency and potential scalability.

4.16. Data on Fourier transform infrared spectroscopy of silibinin/smoke tree extract-loaded liposomes and pullulan-isononanoate-based films

FT-IR spectroscopy (powerful spectroscopic method) was employed in order to characterize molecular structures and functional groups in both pure compounds and complex formulations. By comparing the spectra of individual components with those of liposomal formulations, it is possible to identify specific interactions, confirm the incorporation of active molecules, and assess potential structural modifications. In this study, FT-IR analysis was employed to elucidate the molecular features of the extracted molecules from the smoke tree wooden sections, phospholipid molecules, silibinin, as well as their corresponding liposomal carriers and Pull-Iso films.

The FT-IR spectra of silibinin, smoke tree extract, phospholipid molecules, unloaded lipid spheres, as well as liposomal formulation containing smoke tree extract/silibinin were presented in Figure 35. The spectra graph of silibinin exhibits absorption mode (3200-3400 cm^{-1} range), corresponding to stretching vibrations of O–H (phosphatidylcholines'/silibinin's molecular structures are shown in Supplementary Materials, Fig. S2). A weaker band at 3050-3000 cm^{-1} is assigned to aromatic stretching

of C–H. Two distinct modes (2800-2900 cm^{-1}) correspond to aliphatic CH_2 and CH_3 functionalities stretching vibrations, asymmetric and symmetric. The prominent band (~1629 cm^{-1}) represents keto groups' C=O stretching, while absorptions ~1599, ~1510, and ~1449 cm^{-1} represent skeletal vibration (C=C, aromatic), as well as bending (CH_2). Bands (1270-1050 cm^{-1}) are associated with stretching vibration of C–O (phenolic, ether, as well as alcoholic groups). Finally, a region from 900-700 cm^{-1} corresponds to aromatic deformation vibration (*out-of-plane*, C–H bonds).

The FT-IR spectral unit of smoke tree extract displays a more intricate composition, indicative of a variety of phytochemicals, including flavonoid, phenol-carboxylic acid, tannic, and other phenolic constituents (Figure 35). The mode (3300-3400 cm^{-1}) corresponds to stretching vibration (O–H, phenolic and alcoholic functionalities). Modes (approximately 2919-2949 cm^{-1}) are due to $–CH_3$ and $–CH_2$ functionalities (stretching, asymmetric/symmetric, aliphatic). At approximately 1669 cm^{-1}, aromatic stretching (skeletal, C=C) related to polyphenol constituents is observed with modes (~1595 and ~1510 cm^{-1}) representing vibrations of C=C within condensed tannin aromatic ring. At ~1453 cm^{-1}, aliphatic and aromatic functionalities of vibration from C–H bending appear, whereas a mode (approximately 1369-1379 cm^{-1}) represents deformation of C–H/bending of O–H. The stretching of C–O (phenolic functionalities) is observed within 1230-1260 cm^{-1} range, whereas vibrations of C–O–C and C–O are from alcohol components, ether molecules, as well as polysaccharides (approximately 1029 and 1090 cm^{-1}). The modes (approximately 815 and 970 cm^{-1}) correspond to aromatic C–H bonds (bending, *out-of-plane*).

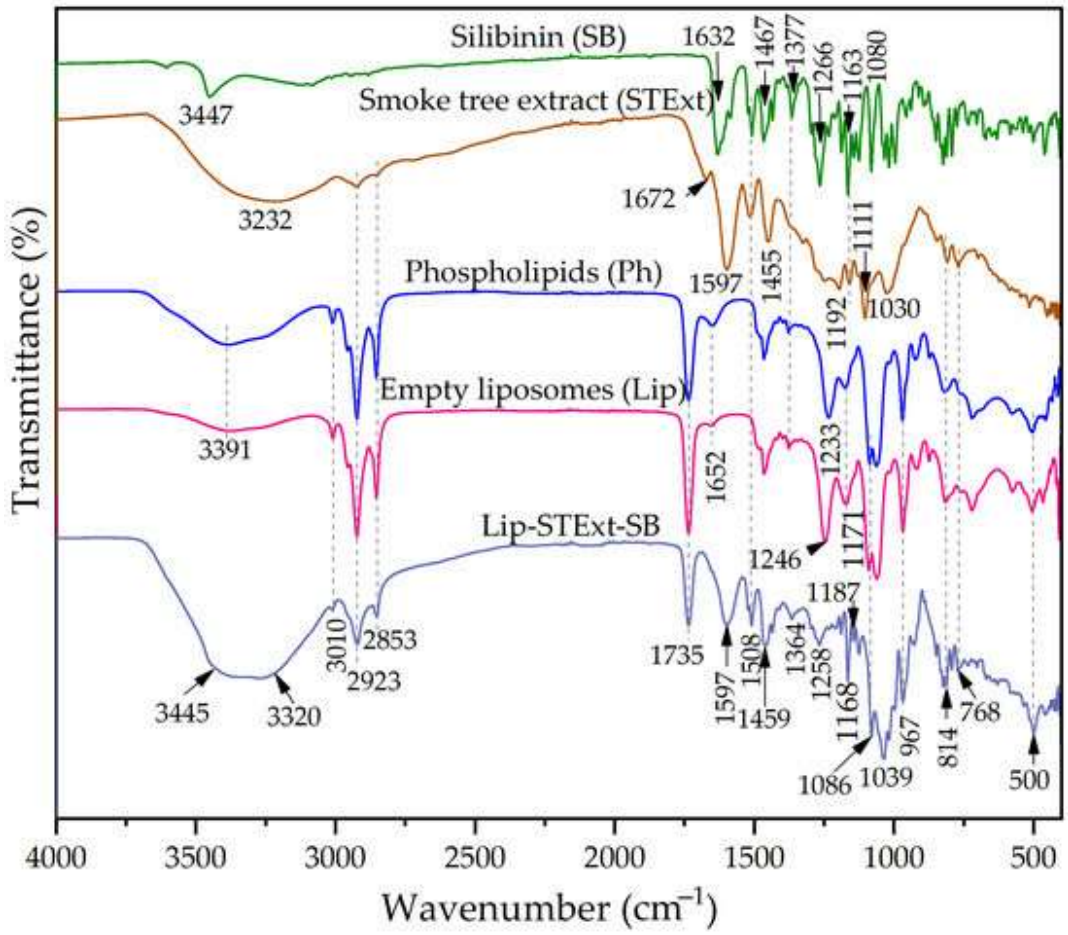

Figure 35. Fourier transform infrared spectroscopy analysis of pure SB (silibinin), STExt (dried smoke tree extract), Ph (pure phospholipids employed for the liposome development), Lip (unloaded liposomes), and Lip-STExt-SB (liposomes containing silibinin/smoke tree extract)

Phospholipid compounds represent molecules consisting of glycerol esterified by 2 fatty acids, as well as polar group (as shown in Fig. S2a, Supplementary Materials). Phospholipids' FT-IR spectral unit showed absorption modes corresponding to aliphatic or functional groups incorporating phosphate moieties (Figure 35). A mode (~3009 cm^{-1}) is attributed to stretching vibrations (=C–H and $=CH_2$). An area between ~2919 and 2849 cm^{-1} is related to the methylene group ($–CH_2$) stretching (C–H, asymmetric/symmetric, from long chains of fatty acids). A peak (approximately 1737 cm^{-1}) arises from stretching vibrations (C=O, ester carbonyl functionalities). It confirms ester bonds within glycerol. Scissoring vibration of CH_2 is at approximately 1465-1470 cm^{-1}, while a band at approximately 1369-1379 cm^{-1} shows terminal methyl group symmetric bending and *in-plane* O–H bending (phenolic and alcohol functionalities). The peak (approximately 1250 cm^{-1}) is P=O stretching (asymmetric), characterized by the phosphate headgroup.

Plain lipid spheres containing these phospholipid molecules exhibited the same modes, confirming that liposomal preparation does not chemically alter the phospholipid structure (Figure 35). In contrast, the FT-IR spectral unit from liposomal vesicles containing silibinin-extract showed a peak shift, as well as additional peaks, indicating effective encapsulation of bioactives (Figure 35). The modes (approximately 3343 and 3319 cm^{-1}) correspond to stretching of O–H (alcoholic/phenolic functionalities from silibinin or smoke tree extract).

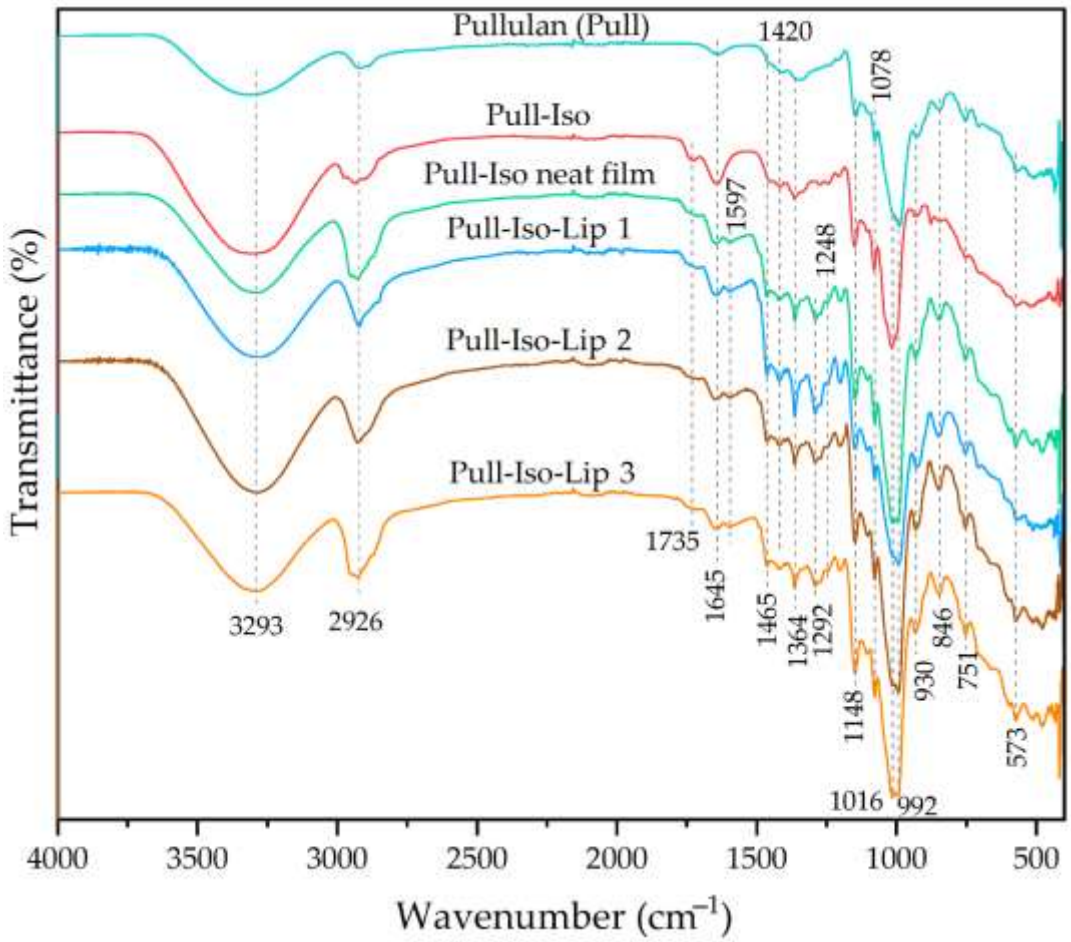

Figure 36. Fourier transform infrared spectroscopy analysis of pure Pull (pullulan), developed pullulan-isononanoate, pullulan-isononanoate empty film sample, as well as pullulan-isononanoate films with different concentrations of liposomes containing silibinin/smoke tree extract.

Absorptions (~1595, 1510, as well as 1460 cm^{-1}) were assigned to aromatic stretching vibration (C=C) from tannin molecules or different polyphenolics and bending vibration of C–H (aliphatic $–CH_2$ functionalities from the aromatic structure). Several silibinin peaks overlap those from smoke tree extract; the observed shifts suggest particular interactions occurring among smoke tree components and the liposome membrane. The mentioned alterations imply that water-soluble phenolic molecules tend to interact primarily with the hydrophilic domains of the phospholipid membrane, indicating adsorption at the vesicle interface rather than incorporation into the non-polar interior of the bilayer.

These interactions between liposome surfaces and hydrophilic bioactives may affect the stability and controlled recovery profile, as well as overall encapsulated compounds' bioavailability. Furthermore, FT-IR data provide valuable insight into the molecular environment of silibinin and smoke tree extract within the liposomal system, supporting the design of effective delivery formulations.

The pullulan FT-IR spectra displayed the mode at ~3299 cm^{-1} (stretching vibration of O–H from glucose repeating units hydroxyl functionalities (Figure 36). Modes among 2799 and 2919 cm^{-1} were C–H stretching (asymmetric/symmetric, $–CH_2$ functionalities from polysaccharides). Modes at approximately 1410-1420 cm^{-1} and around 1369-1379 cm^{-1} were attributed to scissoring and deformation bendings of C–H from methylene functionalities. A peak at approximately 1153-1159 cm^{-1} corresponds to stretching of C–O–C (asymmetric) in α-glucan (glycosidic links), while modes (1099-1019 cm^{-1}) are related to stretching of C–O, as well as the skeletal vibration of C–O–C. Signals (919-949 cm^{-1}) indicate bonds of α-1,6 glycoside, and a mode (849-869 cm^{-1}) confirms the unit of α-linked glucose.

These characteristic FT-IR bands confirm the preserved polysaccharide structure of neat pullulan, reflecting the integrity of its α-(1→4) and α-(1→6) glycosidic linkages. Such spectral information provides a reference for comparison with chemically modified or formulation-incorporated pullulan, allowing identification of structural changes resulting from functionalization or interaction with bioactive compounds.

Esterification of pullulan resulted in the drop of the band intensity (a mode assigned to –OH stretching, around 3300 cm^{-1}), reflecting incomplete ester formation of hydroxyl functionalities (Figure 36). Modes appeared at approximately 1719-1734 cm^{-1} were ester group C=O stretching, verifying that isononanoate chains were successfully attached. The increase in C–H stretching modes around 2919-28549 cm^{-1} additionally confirms the aliphatic chain presence. Additionally, the slight displacement and decrease of glycosidic stretching of C–O–C peaks (approximately 1150-1020 cm^{-1}) suggest structural rearrangement of the pullulan backbone due to substitution.

The FT-IR spectra of film formulations prepared (pure pullulan-isononanoate), as well as pullulan-isononanoate with silibinin/smoke tree extract-loaded liposomes, retained all characteristic ester-related bands, confirming that the chemical modification of pullulan was preserved during film formation (Figure 36). Broadening of the –OH stretching modes and minor displacement within the stretching of C–O–C region suggest the formation of hydrogen bonding between molecules, as well as supplementary physical intermolecular reactions inside bio-bades film formulations. Additionally, the mode observed at ~1643-1649 cm^{-1} represents the bending vibration of H–O–H from implemented water, indicating the presence of residual moisture in the films.

These observations indicate that the incorporation of liposomes did not disrupt the fundamental chemical structure of the modified pullulan matrix. Subtle shifts and broadening in the spectral bands suggest enhanced molecular interactions, which may contribute to improved mechanical cohesion and film integrity. The presence of residual water, as indicated by the H–O–H bending vibration, could also influence flexibility and facilitate controlled release of encapsulated bioactives. The FT-IR analysis confirms that both chemical modification and intermolecular interactions are maintained, supporting the development of stable, functional films for biomedical applications.

4.17. Data on optical microscopy of pullulan-isononanoate-based films with silibinin/smoke tree extract-loaded liposomes

Optical microscopy is widely employed for qualitative evaluation in surface morphology and internal microstructure of polymer-based systems. It is the fast, non-destructive procedure. It enables direct visualization of particle distribution, aggregation phenomena, and phase separation in composite materials, making it particularly useful for preliminary assessment of filler or carrier dispersion within film matrices (Sawyer et al., 2008). Although its resolution is limited compared to electron microscopy, optical microscopy provides valuable information under near-native conditions, without the need for extensive sample preparation or vacuum environments. This allows observation of hydrated or semi-hydrated systems, which is especially relevant for biopolymer and liposomal formulations (Venkateshaiah et al., 2020). Furthermore, optical imaging is frequently used to detect heterogeneities, defects, and structural irregularities that may influence the mechanical barrier or release properties of polymeric films. Changes in transparency, roughness, and the presence of microdomains can be directly correlated with formulation composition and processing conditions. In the context of liposome-loaded films, optical microscopy offers an efficient method to monitor vesicle dispersion and stability within the polymer network, providing essential insight into the compatibility between lipid carriers and biopolymer matrices. Namely, the technique represents an important complementary tool to mechanical and physicochemical analyses for understanding structure-property relationships in composite delivery systems (Sawyer et al., 2008; Venkateshaiah et al., 2020).

Thus, optical micrographs of the pure pullulan-isononanoate film and pullulan-isononanoate film preparations containing incorporated silibinin/smoke tree polyphenols-entrapped lipid vesicles at different amounts were shown in Figure 37.

Microscopic analysis provides critical insight into the distribution and integration of liposomal dispersions within biopolymer matrices. Such observations allow for the evaluation of how liposome concentration influences film microstructure, uniformity, and potential phase separation.

The micrographs reveal how increasing liposome content can lead to aggregation or clustering, which may compromise film homogeneity and mechanical integrity. Smaller, well-dispersed vesicles are observed to integrate more uniformly within the polymer network, minimizing phase separation and enhancing overall film performance. These observations underscore the importance of balancing liposome loading and particle size to achieve optimal structural and functional properties in biopolymer-liposome film samples.

Here, microscopy is employed in the determination of optimal liposomes' loading of liposomes in Pull-Iso-based films and to correlate structural features with their corresponding mechanical performance (as described in detail below).

In addition, optical microscopy provides a rapid means to evaluate the effects of processing parameters, such as casting and drying conditions, on the uniformity of liposome distribution. Observed variations in microstructure can help identify optimal formulation strategies that prevent aggregation while preserving film flexibility. The technique also allows correlation of visible microdomains or surface irregularities with potential changes in barrier properties and controlled release behavior. By comparing films with different liposome loadings, it is possible to determine the threshold at which particle clustering begins to negatively affect film performance. Optical microscopy can guide the selection of liposome sizes and concentrations that achieve a homogeneous dispersion without compromising the integrity of the polymer network. Such visual assessments complement quantitative analyses, ensuring that structural observations align with the mechanical and functional performance of the films. Therefore, these insights support the rational design of pullulan-isononanoate films with balanced mechanical strength and efficient bioactive delivery.

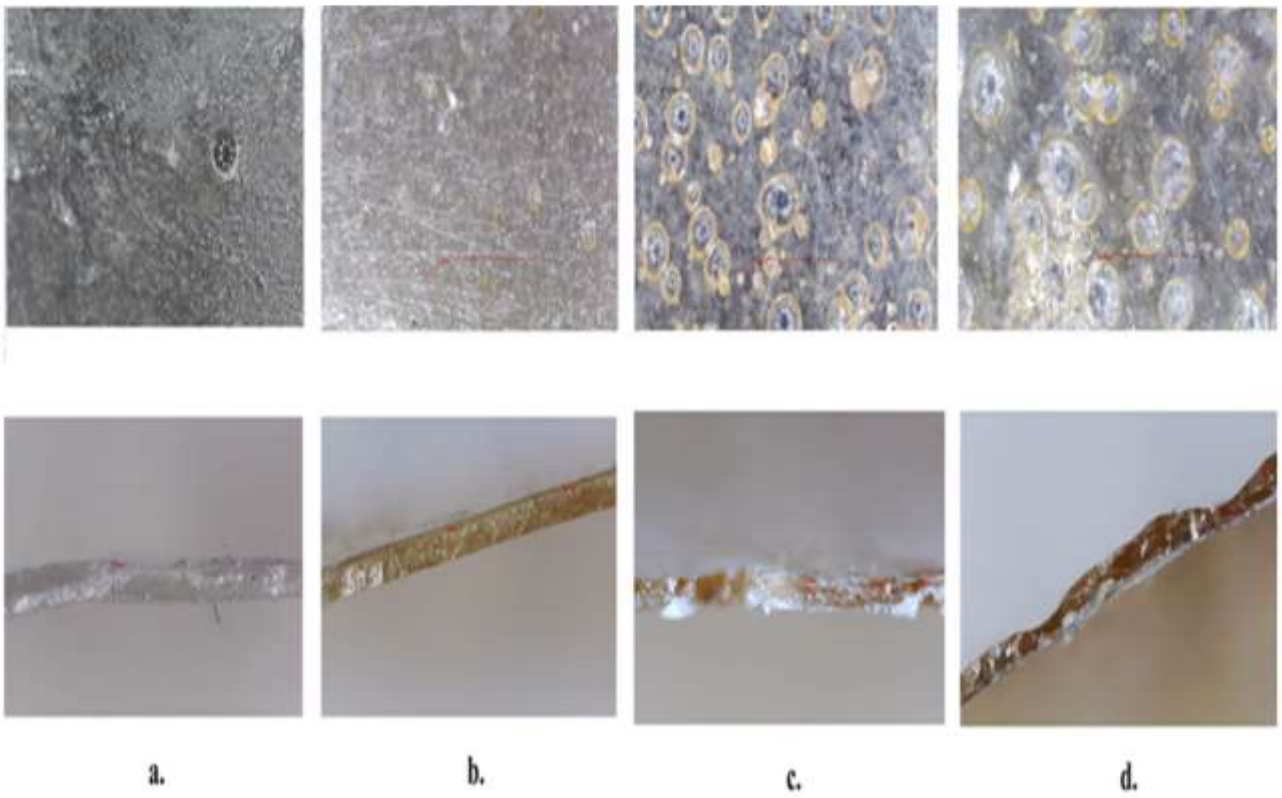

Figure 37. Images of optical micrography: (a) pullulan-isononanoate empty film sample, (b), (c), and (d) pullulan-isononanoate films with different concentrations of liposomes containing silibinin/smoke tree extract

The microscopic observations indicate that the most effective and homogeneous integration of liposomes was reached in pullulan-isononanoate-liposomes 2 formulation, which contained 25% of liposomal sample relative to the polymer mass (Figure 37). When the liposome concentration was increased beyond this level, pronounced aggregation and merging of vesicles became evident, leading to a decline in film uniformity and a subsequent reduction in mechanical performance. In these samples, intermolecular and interparticle attractive interactions between liposomes dominated over interactions with the polymer chains, resulting in phase separation and impaired dispersion within the matrix. These microstructural features are in good agreement with the mechanical behavior discussed in Section 4.20. *Data on the mechanical characteristics of developed pullulan-isononanoate-based films*, confirming that excessive liposome loading compromises the structural integrity of the films.

4.18. Data on water contact angle analysis of developed pullulan-isononanoate-based films

Upon initial exposure to water, Pull-Iso sample showed 79.5° ± 2.2 of the contact angle, confirming the moderately lipophilic area. By comparison, an unmodified bio-based film formulation prepared using pullulan showed a much-decreased value 39.2° ± 0.9, showing film inherently hydrophilic nature. An increase in hydrophobicity is connected to esterification of pullulan, which introduces lipophilic alkenyl functionalities in place of hydroxyl groups, thereby reducing complete material surface energy (Niu et al., 2019). Given that human skin typically has a water contact angle over 100°, the lipophilic alterations in pullulan can improve surface interaction compatibility among formulation and the site of the application, such as skin, conceivably enhancing adhesion and overall performance in wound dressing applications (Ginn et al., 1968).

The liposomal population addition to the pullulan-isononanoate material gradually increased surface wettability. Specifically, pullulan-isononanoate-liposomes 1 and pullulan-isononanoate-liposomes 2 samples showed the following values of the contact angle: 69.3° ± 2.2 and 63.1° ± 1.5, respectively, indicating that the liposomal components reduce hydrophobicity. Interestingly, using a higher content of liposomal dispersion (pullulan-isononanoate-liposomes 3), the contact angle slightly increased to 80.6°, likely due to liposome aggregation, which exposes hydrophobic regions on the film surface. These results suggest that liposome incorporation can modulate surface properties, balancing hydrophilicity and hydrophobicity depending on vesicle content and distribution.

4.19. Data on content of moisture, swelling properties, as well as total soluble solids of developed pullulan-isononanoate-based films

Data of content of moisture, swelling properties, as well as total soluble solids were summarized within Table 3. The pullulan esterification reduces hydroxyl group amount, *i.e.*, functionalities capable of forming H-bonds (Ding et al., 2022), leading to markedly reduced content of moisture and total soluble solids of pullulan-isononanoate formulation than unmodified pullulan. A swelling ratio was not measured in the case of the film formulation prepared from pure/unmodified pullulan, because pullulan is fully dissolved upon contact with aqua.

Table 3. Content of moisture analysis (expressed as %), total soluble solid values (expressed as %), as well as the capacity of swelling (expressed as %) of pure pullulan (Pull) and developed pullulan-isononanoate (Pull-Iso)-based films (empty sample and samples containing different concentrations of silibinin/smoke tree extract-loaded liposomes)

Sample	Content of moisture	Total soluble solids	Capacity of swelling
Pullulan	12.5±1.1	95.5±1.2	Completely dissolved
Empty pullulan-isononanoate film	7.5±1.4	58.4±1.9	62.1±1.7
Pull-Iso-Lip 1 film	8.3±1.7	55.7±2.1	58.2±2.2
Pull-Iso-Lip 2 film	10.2±1.6	52.8±1.8	45.8±2.0
Pull-Iso-Lip 3 film	10.3±1.8	51.9±1.6	72.8±1.4

Incorporation of liposomes at moderate levels resulted in the minor reduction of swelling capacity and total soluble solids, whereas content of moisture showed a moderate increase. This behavior may be due to lipophilic nature of the tails from phospholipids, as well as the presence of entrapped silibinin, which both influence water-binding capacity and diffusion within the film. However, in the case of a high liposomal content, the aggregation process became pronounced, causing microvoids to form, which promoted site-specific moisture uptake, leading to an increase in content of moisture and capacity of swelling. Conversely, total soluble solids showed a progressive rise with increasing portion of liposomes, probably because of polymer matrix partial disruption, as well as the efflux of soluble substances from vesicle aggregates. The results are supported by findings obtained in the optical microscopy and mechanical tests (Sections 4.17. *Data on optical microscopy of pullulan-isononanoate-based films with silibinin/smoke tree extract-loaded liposomes* and 4.20. *Data on the mechanical features of developed formulations*, respectively), highlighting an impact of liposome incorporation on film microstructure and its interactions with water.

4.20. Data on mechanical features of developed formulations

The mechanical properties of pullulan-isononanoate film, as well as silibinin/smoke tree liposomal particles-entrapped film formulations are summarized in Table 4. Pure pullulan films are characterized by elevated tensile strength accompanied by modest elongation at break (equivalent testing parameters), consistent with literature reports (Ding et al., 2022). Chemical pullulan modification effectively influences pullulan mechanical features (detailed in Supplementary Materials - Table S1) (Horinaka et al., 2018; Zahedi et al., 2010). Completely substituted film formulations based on pullulan acetate and prepared by medium casting maintain the increased tensile strength, while showing a reduced value of the elongation at break, indicative of enhanced stiffness, as well as restricted molecular chain flexibility. Nevertheless, pullulan hexanoate, pullulan octanoate, or pullulan decanoate (esters of fatty acids and pullulan), developed through casting using organic medium excluding plasticizer substances, demonstrate significantly lower tensile strength or similarly decreased elongation at break (Enomoto-Rogers et al., 2015; Wang et al., 2016). The noticed declines related to the mechanical features with increasing lengths of alkyl chains are connected to heightened lipophilicity, disruption of intermolecular H-bonds, or reduced cohesive strength of the film.

Table 4. Break stress (expressed as MPa), strain (expressed as %) of empty pullulan film, developed pullulan-isononanoate-based formulations (*i.e.*, empty and samples containing different concentrations of silibinin/smoke tree extract-loaded liposomes)

Film	Stress	Strain
Empty Pullulan	22.75±1.2	3.68±1.1
Empty Pullulan-Isononanoate	20.97±1.1	10.97±0.9
Pull-Iso-Liposomes 1	10.85±2.4	2.46±2.1
Pull-Iso-Liposomes 2	8.79±2.7	2.39±2.5
Pull-Iso-Liposomes 3	5.26±2.4	1.73±2.7

In comparison to formulation prepared from unmodified pullulan, pullulan-isononanoate formulations exhibit decreased tensile stress at break, although having equal plasticizer substance amount. The observation is consistent with reports related to esters among polysaccharides and fatty acids. Namely, the presence of extended lipophilic chains typically weakens the cohesion between polymer chains within matrix (Enomoto-Rogers et al., 2015). Despite differences in structures and patterns (substitution type) compared to simple alkyl esters, pullulan-isononanoate films follow the same general tendency of decreasing tension with higher levels of hydrophobic substitution. Nevertheless, their tensile strength remains considerably higher compared to pullulan ester cast from an organic medium, highlighting influence of water casting conditions and plasticizer choice. Notably, pullulan-isononanoate formulations exhibit tensile strengths up to an order of magnitude higher in comparison to formulations prepared by pullulan esters, such as pullulan decanoate, octanoate, or hexanoate. It exhibits relatively low tensile strengths (in the MPa range) of esters containing long chains.

In pullulan-isononanoate-based formulations, the liposome addition leads to decline in mechanical performance, reflected by decreases of stenght and break. This effect becomes more pronounced with increasing amount of the added liposomal dispersion, resulting in significant decreases of the above-mentioned variables. An impact of phospholipid additives on film behavior depends strongly on their chemical nature, concentration, and degree of integration within polymer network. For example, literature data reported that fatty acid addition to *Pistacia vera* L. formulations with globulin caused substantial weakening. Namely, break decreased ~36-71%, while strength also declined (Zahedi et al., 2010). The observed behavior was attributed to the perturbation of interactions among proteins by fatty acid components (with small molecular weight), facilitating separations of the phases and weakening the structural integrity of the network. Conversely, epoxidized *Ricinus communis* L. oil increased the

features of the formulation containing *Glycine max* (L.) Merr. proteins, nearly doubling strength and increasing breaking strain (~24%) (Wang et al., 2016). This enhancement is attributed to the formation of H-bonds among proteins and epoxide-functionalized chains, enhancing interfacial adhesion and facilitating the transmission of stress throughout the network.

In conclusion, the incorporation of hydrophobic modifications and lipid-based additives significantly influences the mechanical performance of pullulan-derived films. While Pull-Iso films exhibit reduced tensile strength compared to unmodified pullulan, they maintain superior mechanical properties relative to many long-chain pullulan esters due to optimized aqueous casting and plasticizer selection. The addition of liposomes introduces heterogeneities and potential phase separation, leading to further decreases in tensile strength and elongation, particularly at higher loadings. The conclusions emphasize an essential impact of liposome-polymer compatibility, additive concentration, and molecular interactions in determining the structural integrity and functional features of bio-based/polymer film formulations.

4.21. Data on the antiradical potential of developed silibinin/extract-entrapped liposomal population and pullulan-isononanoate-based films

Evaluation of the antiradical potential provides essential findings of bioactive-entrapped formulation's anti-radical potential. Silibinin and smoke tree extract possess significant antioxidant activity, which can be modulated by encapsulation within liposomal carriers. Assessing the antiradical activity of liposomes and liposome application within pullulan-isononanoate film formulations allows for determination of how formulation strategies influence bioactive availability and stability. Such analyses are crucial for predicting the functional efficacy of these composite systems in pharmaceutical, cosmetic, or biomedical applications.

The combination of silibinin and smoke tree extract within prepared film formulations is anticipated to elicit synergistic outcomes as a result of the complementary actions of the polyphenolic compounds present. Therefore, the abilities of Pull-Iso-based films and silibinin/extract-entrapped liposomes to neutralize radicals were tested in the ABTS and DPPH methods (Figure 38).

The antiradical activity of silibinin/extract-loaded liposomes and corresponding pullulan-isononanoate films was evaluated to determine the retention of bioactive functionality after formulation. Encapsulation within liposomes is expected to protect sensitive polyphenolic compounds from oxidative degradation, thereby enhancing their stability during processing and storage. Both ABTS and DPPH assays were employed to provide complementary measurements of radical scavenging capacity under different conditions. The results indicate that liposomal carriers effectively preserve antioxidant activity compared to free compounds in solution. Incorporation of these liposomes into pullulan-isononanoate films allows for further stabilization while maintaining accessibility of the bioactives to reactive radicals. A concentration-dependent effect was observed, where higher loading of silibinin/extract generally resulted in increased antiradical potential. Interestingly, the combination of silibinin and smoke tree extract showed additive or synergistic effects, surpassing the activity of either component alone. Time-course measurements suggested that the films provide sustained antioxidant activity, which may be beneficial for applications requiring prolonged bioactive availability. These findings also highlight the importance of uniform liposome distribution within the polymer matrix to avoid localized depletion of antioxidant capacity. Overall, the study demonstrates that carefully designed liposomal incorporation into Pull-Iso films can effectively preserve and deliver the antiradical potential of sensitive plant-derived and therapeutic compounds.

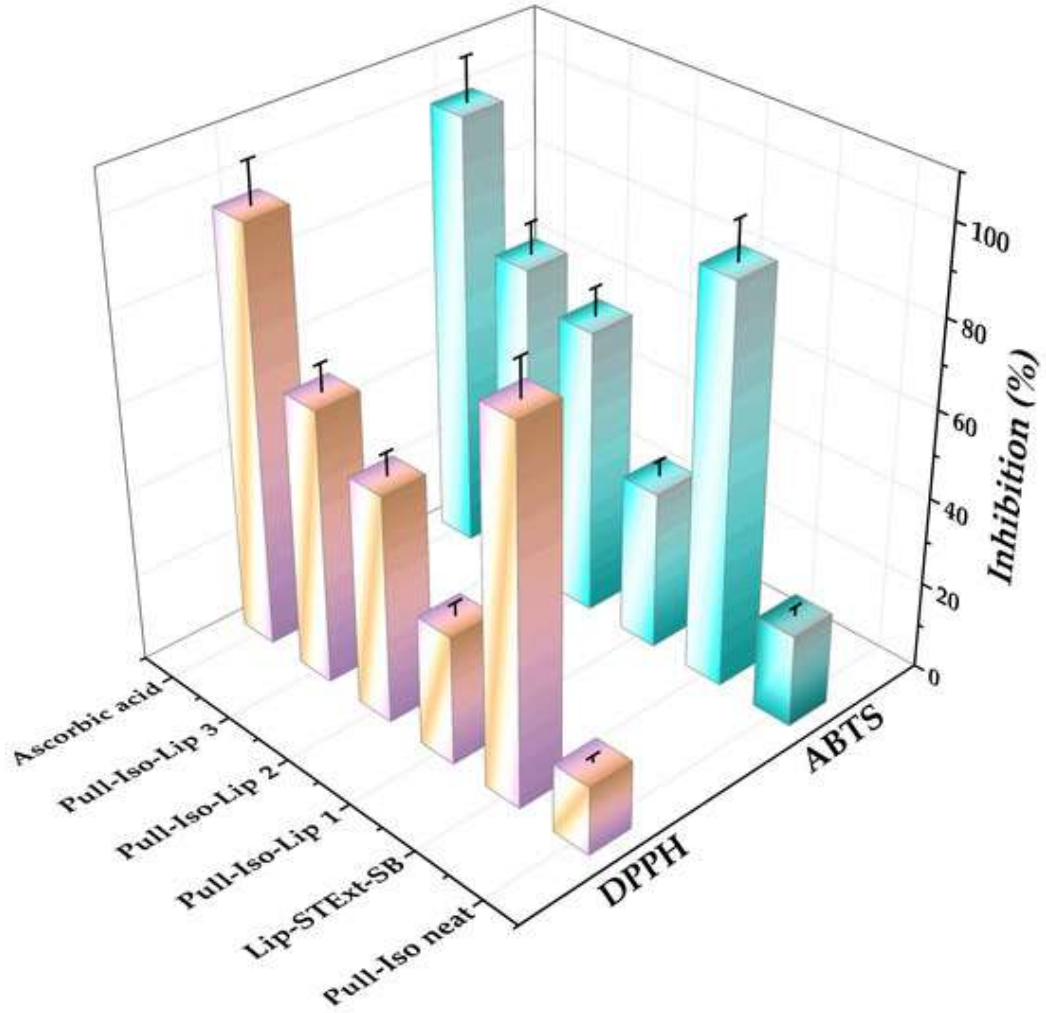

Figure 38. Antioxidant ability of silibinin/smoke tree extract-loaded liposomes (Lip-STExt-SB) and pullulan-isononanoate (Pull-Iso)-based films (empty sample and samples with different concentrations of liposomes)

As anticipated, vitamin C (positive control) exhibited the greatest antioxidant ability, validating the responsiveness and accuracy of the tests. Pullulan-isononanoate formulation in the absence of the liposomal dispersion (negative control sample) exhibited comparatively reduced antioxidant potential (approximately 21.24% for ABTS and approximately 15.83% for DPPH), reflecting the limited intrinsic antioxidant potential of pullulan. In contrast, liposomes containing silibinin and smoke tree extract exhibited substantial activity (approximately 91.3% ABTS and approximately 84.9% DPPH), highlighting the significant contribution of encapsulated polyphenols. Incorporation of various concentrations of silibinin and smoke tree extract-loaded liposomal systems within pullulan-isononanoate films resulted in the clear concentration-dependent increase in antioxidant activity. Pull-Iso-Lip 1 (250 mg of the liposomal dispersion) showed intermediate antioxidant capacity (approximately 36.55% ABTS and approximately 29.78% DPPH), indicating limited accessibility of bioactives entrapped in the formulation. Increasing the liposome content further enhanced radical neutralization: formulation with 500 mg liposomal dispersion reached approximately 65.58% and approximately 52.47% inhibition in ABTS and DPPH assays, respectively, while film with 750 mg of liposomal dispersion achieved the highest activity (approximately 72.53% ABTS and approximately 63.03% DPPH). These results confirm that a high level of liposomal particles' content allows higher entrapping and controlled recovery of phenolics, thereby improving a complete antioxidant ability of developed formulations.

According to Zare Mehrjerdi et al. (2025), silibinin primarily acts as the strong agent with antioxidant ability, mitigating stress induced by oxidant agents in damaged structures, while also exhibiting various activities, such as antibacterial, anti-inflammatory, etc. The polyphenolic mixture in smoke tree extract provides additional anti-inflammatory, antimicrobial, and antioxidant potential, as well as tissue-regenerative capacity (Marčetić et al., 2012; Pašić et al., 2025). This synergy likely arises from the complementary mechanisms of action: silibinin efficiently neutralizes oxidant agents while stabilizing membrane structures in the cells, whereas the diverse polyphenol substances of smoke tree extract can modulate inflammatory mediators and support extracellular matrix remodeling (as reported in the introduction section). Co-delivery of these bioactives in formulation can therefore offer wider protection and tissue-regenerative effect, enhancing the cutaneous regeneration potential more than films with individual components separately. Similar mutually enhancing effects of combined polyphenolic systems were reported for various topical formulations (Hoang et al., 2025; Radan et al., 2024).

Plant polyphenol substances were well-acknowledged for their strong antioxidant capacity, participating in reduction reactions and donating hydrogen, as well as neutralizing singlet oxygen (Grzesik et al., 2018). HPLC-DAD analysis of smoke tree extract revealed it to be rich in flavonoids (Pašić et al., 2025). Silibinin is also recognized for its potent antioxidant activity (Zare Mehrjerdi et al., 2024). Consistently, ABTS assay data was greater in comparison to the results from anti-DPPH ability across all samples, likely due to ABTS's higher sensitivity for lipophobic and hydrophobic agents and compatible with complex formulations, *e.g.*, liposomal population-encapsulated polymer matrices (Shahidi and Samarasinghe, 2025). The enhanced ABTS results suggest enhanced electron-transfer pathways driven by polyphenol compounds encapsulated within the carrier. In conclusion, these findings demonstrate that incorporating liposomes loaded with smoke tree extract and silibinin significantly enhances the Pull-Iso formulations' antioxidant potential according to the concentration-dependent trend. Formulations hold the capability to function as a bioactive matrix in biomedical applications or functional packaging, with antioxidant capacity that can mitigate oxidative stress or protect sensitive compounds from degradation.

The results clearly demonstrate that liposomal encapsulation of silibinin and smoke tree extract substantially improved capacity of pullulan-isononanoate formulations to neutralize free radicals compared to unmodified polymer matrices. The observed concentration-dependent increase in neutralization of radicals shows the influence of high liposomal concentration on the improved retention, as well as controlled polyphenols' recovery. The synergistic action of silibinin and smoke tree extract provides complementary mechanisms of free radical quenching, anti-inflammatory effects, and potential tissue-regenerative benefits. These findings highlight the promise of liposome-loaded Pull-Iso films as multifunctional materials with potential applications in wound healing, protective coatings, or active packaging systems.

5. CONCLUSIONS

➢ Silibinin, the bioactive compound characterized by strong antioxidant, antibacterial, antifungal, anti-inflammatory, and photoprotective effects, was successfully entrapped within liposomal spheres prepared from phospholipids to enhance physicochemical stability and facilitate its biological availability. Encapsulation enhanced silibinin solubility and protection from degradation, while providing a controlled release profile suitable for biomedical applications. This strategy also facilitates efficient delivery to target cells, improving functional outcomes.

➢ Liposomal formulation containing silibinin was additionally modified through ultraviolet treatment, exposure to ultrasound waves, as well as freeze-drying, and their effects on cytotoxic potential, together with antioxidant and inflammatory response reduction properties, storage stability, and FT-IR/Raman spectral profiles were investigated for the first time. These post-encapsulation treatments allowed systematic evaluation of how processing influences both structural integrity and bioactive efficacy. Comparative analysis of spectral data provided insight into potential chemical or physical changes induced by each modification.

➢ UV irradiation significantly altered liposome characteristics, rheology, and increased cytotoxicity in HaCaT cells, confirmed by FT-IR and Raman spectroscopy. The observed changes suggest that photochemical stress disrupts lipid bilayers, leading to compromised membrane integrity and altered functional properties. Consequently, UV treatment is unsuitable for sterilization when maintaining bioactivity and cell compatibility is critical.

➢ Freeze-drying decreased anti-ABTS and anti-DPPH ability, as well as encapsulation efficiency, but also caused an increase in the capacity of the sample to reduce inflammatory response, *i.e.*, a decrease in IL-1β production in LPS-stimulated HaCaT cells. The process likely induced minor structural changes in the lipid bilayer, reducing immediate antioxidant activity while facilitating the gradual release of silibinin for prolonged anti-inflammatory effects. Lyophilization thus represents a viable strategy for long-term storage without compromising therapeutic function.

➢ Sonication reduced EE, modified physical and rheological characteristics, slightly increased cytotoxicity, but significantly improved antioxidant activity and inhibition of IL-1β expression. Controlled sonication decreased particle size and increased surface area, promoting more efficient interaction of silibinin with reactive species and cellular targets. These changes highlight the balance between structural modification and functional enhancement achievable through ultrasonic processing.

➢ Throughout the storage period, all liposomal vesicles with entrapped silibinin (multilamellar, UV-irradated, freeze-dried, and SUVs) exhibited increased particle size and decreased absolute zeta potential values. These alterations reflect gradual aggregation and potential changes in surface charge over time, which may influence long-term stability, dispersibility, and bioactive release kinetics. Regular monitoring of these parameters is essential for estimating storage persistence and functional stability.

➢ Multilamellar and freeze-dried liposomal formulations containing silibinin maintained strong antioxidant activity within the keratinocyte line and an effect on the MIF suppression (reducing inflammatory response) and did not show cytotoxic effects. These formulations demonstrate an optimal balance between stability and biological efficacy, confirming their suitability for therapeutic applications. Preservation of cellular compatibility underscores the potential for safe topical or biomedical use.

➢ Ultraviolet exposure is not recommended in the case of sterilization of developed liposomes due to observed cytotoxicity, while freeze-drying is suitable for preventing hydrolytic and oxidative degradation while preserving bioactivity. These findings emphasize the need for careful selection of post-processing strategies to maintain both structural integrity and functional performance. Freeze-drying emerges as a practical approach for long-term storage and transport of bioactive liposomal formulations.

- The direct esterification of pullulan using 3,5,5-trimethylhexanoyl chloride led to the formation of branched pullulan-isononanoate, showing improved flexibility of the polymer structure. Attachment of lipophilic substituent chains not only increased polymer chain mobility but also enabled fine-tuning of physicochemical properties, making Pull-Iso suitable for advanced film-forming applications.

- Chemical modification reduced a glass transition point (T_g), indicating the promotion of greater free volume and chain segmental flexibility in the polymer. This decrease in T_g facilitates film processing and improves adaptability under mechanical stress, which is particularly important for flexible biomedical materials.

- Esterification increased hydrophobicity, as shown by a higher surface wettability angle and lower content of moisture and total soluble solid values at pH of ~5.5, simulating dermal attributes. Enhanced hydrophobicity improves barrier properties and reduces moisture uptake, supporting stability of incorporated bioactives during storage and application.

- Incorporation of liposomal particles containing *C. coggygria* extract/silibinin at a liposome amount of 750 mg improved coating wetting, preserving a water-repellent nature similar to human epidermis and supporting stickiness and ease of use. This balance ensures effective contact with skin surfaces, facilitating localized delivery of antioxidants and anti-inflammatory compounds without compromising wearer comfort.

- Microscopic examination and mechanical evaluation demonstrated that medium content liposomal addition (amount of 500 mg liposomes) yielded uniform structure and favorable stretching behavior, whereas greater content of liposomes caused their particle agglomeration and reduced tensile properties. These findings highlight the importance of optimizing liposomal vesicle content to maintain both structural integrity and functional performance in composite films.

- Silibinin/smoke tree extract-loaded liposome incorporation enhanced pullulan-isononanoate formulation anti-radical potential *via* promoting maintenance and managed liberation of phenolic constituents from smoke tree extract, as well as silibinin. ABTS scavenging activity was consistently higher than DPPH, suggesting efficient electron-transfer mechanisms. The observed dose-dependent enhancement confirms that controlled liposome incorporation can maximize bioactive efficacy while preventing rapid degradation of sensitive compounds.

- These findings indicate the potential of *C. coggygria* extract/silibinin-liposome-loaded pullulan-isononanoate formulations designed for functional packaging and healthcare purposes, particularly as flexible, bioactive-loaded wound dressings. Such films can simultaneously provide mechanical protection, sustained antioxidant delivery, and favorable skin interface properties, addressing multiple therapeutic needs.

- The study provides a comprehensive characterization of Pull-Iso, including chemical composition and heat resistance, as well as layer-forming efficiency in the presence of liposomal vesicles containing *C. coggygria* extract/silibinin, establishing a foundation to further develop multifunctional bioactive films. The integration of structural, mechanical, and bioactive analyses offers a complete framework for rational design of next-generation polymer-liposome composites.

- Future research will focus on optimizing lyophilization parameters (pressure, temperature, duration, cryoprotectants), comprehensive characterization and measurement of each extract component, assessment of liposome encapsulation efficiency and dispersion in films, *in vitro* assessment of biocompatibility with dermal area, bioactive compound delivery behavior, treatment effectiveness in wound repair, as well as investigating anti-aging and other skin-related effects in advanced cell-based models. Additionally, studies may explore synergistic interactions between silibinin and polyphenolic compounds under physiological conditions, long-term stability, and scale-up potential for clinical or industrial applications.

6. REFERENCES

1. Afaq, F.; Katiyar, S. K. Polyphenols: skin photoprotection and inhibition of photocarcinogenesis. Mini Reviews in Medicinal Chemistry 11(14) (2011), 1200–1215. https://doi.org/10.2174/13895575111091200
2. Agrawal, S.; Budhwani, D.; Gurjar, P.; Telange, D.; Lambole, V. Pullulan-based derivatives: Synthesis, enhanced physicochemical properties, and applications. Drug Delivery 29 (2022), 3328–3339. https://doi.org/10.1080/10717544.2022.2144544
3. Ahmad, U.; Akhtar, J.; Singh, S. P.; Ahmad, F. J.; Siddiqui, S. Silymarin nanoemulsion against human hepatocellular carcinoma: Development and optimization. Artificial Cells, Nanomedicine, and Biotechnology 46 (2018), 231–241. https://doi.org/10.1080/21691401.2017.1324465
4. Akbarzadeh, A.; Rezaei-Sadabady, R.; Davaran, S.; Joo, S.-W.; Zarghami, N.; Hanifehpour, Y.; Samiei, M.; Kouhi, M.; Nejati-Koshki, K. Liposome: Classification, preparation, and applications. Nanoscale Research Letters 8 (2013), 102. https://doi.org/10.1186/1556-276X-8-102
5. Aksoy, H.; Sancar, M.; Sen, A.; Okuyan, B.; Bitis, L.; Uras, F.; Akakin, D.; Cevik, O.; Kultur, S.; İzzettin, F. V. The effect of topical ethanol extract of *Cotinus coggygria* Scop. on cutaneous wound healing in rats. Natural Product Research 30 (2016), 452–455. https://doi.org/10.1080/14786419.2015.1019349
6. Aksoy, H.; Sen, A.; Sancar, M.; Sekerler, T.; Akakin, D.; Bitis, L.; Uras, F.; Kultur, S.; Izzettin, F. V. Ethanol extract of *Cotinus coggygria* leaves accelerates wound healing process in diabetic rats. Pharmaceutical Biology 54(11) (2016), 2732–2736. https://doi.org/10.1080/13880209.2016.1181660
7. Alshaer, W.; Nsairat, H.; Lafi, Z.; Hourani, O. M.; Al-Kadash, A.; Esawi, E.; Alkilany, A. M. Quality by design approach in liposomal formulations: Robust product development. Molecules 28 (2023), 10. https://doi.org/10.3390/molecules28010010
8. Apriliyani, M. W.; Purwadi, P.; Manab, A.; Apriliyanti, M. W.; Ikhwan, A. D. Characteristics of moisture content, swelling, opacity and transparency with addition of chitosan as edible films/coating based on casein. Advance Journal of Food Science and Technology 18 (2020), 9–14. https://doi.org/10.19026/ajfst.18.6041
9. Arnosti, C.; Repeta, D. J. Nuclear magnetic resonance spectroscopy of pullulan and isomaltose: Complete assignment of chemical shifts. Starch/Stärke 47 (1995), 67–71. https://doi.org/10.1002/star.19950470208
10. ASTM D3644-15R22. Standard Test Method for Acid Number of Styrene-Maleic Anhydride Resins. ASTM International: West Conshohocken, Pennsylvania, USA, 2022.
11. Baljak, J.; Dekanski, D.; Pirković, A.; Mitić, N.; Rašković, A.; Kladar, N.; Jovanović, A.A. Valorization of olive leaf extract *via* tailored liposomal carriers: comparative analysis of physicochemical features, antioxidant capacity, and stability. Pharmaceuticals 18 (2025), 1639. https://doi.org/10.3390/ph18111639
12. Batinić, P.; Đorđević, V.; Stevanović, S.; Balanč, B.; Marković, S.; Luković, N.; Mijin, D.; Bugarski, B. Formulation and characterization of novel liposomes containing histidine for encapsulation of a poorly soluble vitamin. Journal of Drug Delivery Science and Technology 59 (2020), 101920. https://doi.org/10.1016/j.jddst.2020.101920
13. Bhattacharjee, S. DLS and zeta potential - What they are and what they are not? Journal of Controlled Release 235 (2016), 337–351. https://doi.org/10.1016/j.jconrel.2016.06.017
14. Bojić-Trbojević, Ž.; Božić, M.; Vićovac, Lj. Steroid hormones modulate galectin 1 in the trophoblast HTR 8/SVneo cell line. Archives of Biological Sciences 60 (2008), 11–23. https://doi.org/10.2298/ABS0801011B
15. Bouarab, L.; Maherani, B.; Kheirolomoom, A.; Hasan, M.; Aliakbarian, B.; Linder, M.; Arab-Tehrany, E. Influence of lecithin-lipid composition on physico-chemical properties of nanoliposomes loaded

with a hydrophobic molecule. Colloids and Surfaces B: Biointerfaces 115 (2014), 197–204. https://doi.org/10.1016/j.colsurfb.2013.11.034

16. Bravo, L. Polyphenols: chemistry, dietary sources, metabolism, and nutritional significance. Nutrition Reviews 56 (1998), 317–333. https://doi.org/10.1111/j.1753-4887.1998.tb01670.x
17. Bruić, M.; Pirković, A.; Borozan, S.; Nacka Aleksić, M.; Jovanović Krivokuća, M.; Spremo Potparević, B. Antioxidative and anti-inflammatory effects of taxifolin in H_2O_2-induced oxidative stress in HTR 8/SVneo trophoblast cell line. Reproductive Toxicology 126 (2024), 108585. https://doi.org/10.1016/j.reprotox.2024.108585
18. Bruneel, D.; Schacht, E. Chemical modification of pullulan: 1. Periodate oxidation. Polymer 34 (1993), 2628–2632.
19. Buer, C. S.; Muday, G. K.; Đorđević, M. A. Flavonoids are differentially taken up and transported long distances in Arabidopsis. Plant Physiology 145 (2007), 478–490. https://doi.org/10.1104/pp.107.101824
20. Castañeda-Reyes, E. D.; Perea-Flores, M. de J.; Davila-Ortiz, G.; Lee, Y.; Gonzalez de Mejia, E. Development, characterization and use of liposomes as amphipathic transporters of bioactive compounds for melanoma treatment and reduction of skin inflammation: a review. International Journal of Nanomedicine 15 (2020), 7627–7650. https://doi.org/10.2147/IJN.S263516
21. Carvalho, L. T.; de Moraes, R. M.; Alves, G. M.; Lacerda, T. M.; dos Santos, J. C.; dos Santos, A. M.; Medeiros, S. F. Synthesis of amphiphilic pullulan-graft-poly(ε-caprolactone) *via* click chemistry. International Journal of Biological Macromolecules 145 (2020), 701–711. https://doi.org/10.1016/j.ijbiomac.2019.12.207
22. Cevc, G. Lipid vesicles and other colloids as drug carriers on the skin. Advanced Drug Delivery Reviews 56 (2004), 675–711. https://doi.org/10.1016/j.addr.2003.10.028
23. Chadorshabi, S.; Hallaj-Nezhadi, S.; Ghasempour, Z. Liposomal system based on lyophilization of a monophase solution for stabilization of bioactives from red onion skin. LWT - Food Science and Technology 172 (2022), 114174. https://doi.org/10.1016/j.lwt.2022.114174
24. Chen, C.; Han, D.; Cai, C.; Tang, X. An overview of liposome lyophilization and its future potential. Journal of Controlled Release 142 (2010), 299–311. https://doi.org/10.1016/j.jconrel.2009.10.024
25. Chen, C.; Han, D.; Zhang, Y.; Yuan, Y.; Tang, X. The freeze-thawed and freeze-dried stability of cytarabine-encapsulated multivesicular liposomes. International Journal of Pharmaceutics 387 (2010), 147–153. https://doi.org/10.1016/j.ijpharm.2009.12.017
26. Chen, B.-H.; Inbaraj, B. S. Nanoemulsion and nanoliposome based strategies for improving anthocyanin stability and bioavailability. Nutrients 11 (2019), 1052. https://doi.org/10.3390/nu11051052
27. Cheynier, V.; Comte, G.; Davies, K. M.; Lattanzio, V.; Martens, S. Plant phenolics: recent advances on their biosynthesis, genetics, and ecophysiology. Plant Physiology and Biochemistry 72 (2013), 1–20. https://doi.org/10.1016/j.plaphy.2013.05.009
28. Chotphruethipong, L.; Hutamekalin, P.; Sukketsiri, W.; Benjakul, S. Effects of sonication and ultrasound on properties and bioactivities of liposomes loaded with hydrolyzed collagen from defatted sea bass skin conjugated with epigallocatechin gallate. Journal of Food Biochemistry 45 (2021), e13809. https://doi.org/10.1111/jfbc.13809
29. Crozier, A.; Jaganath, I. B.; Clifford, M. N. Dietary phenolics: chemistry, bioavailability and effects on health. Natural Product Reports 26 (2009), 1001–1043. https://doi.org/10.1039/B802662A
30. Czamara, K.; Majzner, K.; Pacia, M. Z.; Kochan, K.; Kaczor, A.; Baranska, M. Raman spectroscopy of lipids: A review. Journal of Raman Spectroscopy 46 (2015), 4–20. https://doi.org/10.1002/jrs.4607
31. Čutović, N.; Marković, T.; Carević, T.; Stojković, D.; Bugarski, B.; Jovanović, A. A. Liposomal and liposomes-film systems as carriers for bioactives from *Paeonia tenuifolia* L. petals: Physicochemical characterization and biological potential. Pharmaceutics 15 (2023), 2742. https://doi.org/10.3390/pharmaceutics15122742

32. Danaei, M.; Dehghankhold, M.; Ataei, S.; Hasanzadeh Davarani, F.; Javanmard, R.; Dokhani, A.; Khorasani, S.; Mozafari, M. R. Impact of particle size and polydispersity index on the clinical applications of lipidic nanocarrier systems. Pharmaceutics 10 (2018), 57. https://doi.org/10.3390/pharmaceutics10020057
33. Dhanalakshmi, S.; Mallikarjuna, G. U.; Singh, R. P.; Agarwal, R. Silibinin prevents ultraviolet radiation-caused skin damages in SKH-1 hairless mice *via* a decrease in thymine dimer positive cells and an up-regulation of p53-p21/Cip1 in epidermis. Carcinogenesis 25 (2004), 1459–1465. https://doi.org/10.1093/carcin/bgh152
34. Ding, Z.; Chang, X.; Fu, X.; Kong, H.; Yu, Y.; Xu, H.; Shan, Y.; Ding, S. Fabrication and characterization of pullulan-based composite films incorporated with bacterial cellulose and ferulic acid. International Journal of Biological Macromolecules 219 (2022), 121–137. https://doi.org/10.1016/j.ijbiomac.2022.07.236
35. Dixon, S. J.; Lemberg, K. M.; Lamprecht, M. R.; Skouta, R.; Zaitsev, E. M.; Gleason, C. E.; Patel, D. N.; Bauer, A. J.; Cantley, A. M.; Yang, W. S.; Morrison, B. III; Stockwell, B. R. Ferroptosis: an iron-dependent form of nonapoptotic cell death. Cell 149 (2012), 1060–1072. https://doi.org/10.1016/j.cell.2012.03.042
36. Duceac, I. A.; Vereştiuc, L.; Coroaba, A.; Arotăriţei, D.; Coseri, S. All-polysaccharide hydrogels for drug delivery applications: Tunable chitosan bead surfaces *via* physical or chemical interactions using oxidized pullulan. International Journal of Biological Macromolecules 181 (2021), 1047–1062. https://doi.org/10.1016/j.ijbiomac.2021.04.128
37. Duffy, C.; Gafoor, S.; Richards, D.; Admadzadeh, H.; O'Kennedy, R.; Arriaga, E. Determination of properties of individual liposomes by capillary electrophoresis with postcolumn laser-induced fluorescence detection. Analytical Chemistry 73 (2001), 1855–1861. https://doi.org/10.1021/ac0010330
38. Elsayed, M. M. A.; Abdallah, O. Y.; Naggar, V. F.; Khalafallah, N. M. Lipid vesicles for skin delivery of drugs: Reviewing three decades of research. International Journal of Pharmaceutics 332 (2007), 1–16. https://doi.org/10.1016/j.ijpharm.2006.12.005
39. Emam, H. E.; Mohamed, A. L. Controllable release of povidone-iodine from networked pectin-carboxymethyl pullulan hydrogel. Polymers 13 (2021), 3118. https://doi.org/10.3390/polym13183118
40. Encyclopaedia Britannica. Smoke tree (*Cotinus* spp.) botanical overview. Encyclopaedia Britannica. https://www.britannica.com/plant/smoke-tree (accessed on 3rd February 2026)
41. Enomoto-Rogers, Y.; Iio, N.; Takemura, A.; Iwata, T. Synthesis and characterization of pullulan alkyl esters. European Polymer Journal 66 (2015), 470–477. https://doi.org/10.1016/j.eurpolymj.2015.03.007
42. Erceg, T.; Rackov, S.; Terek, P.; Šovljanski, O.; Šuput, D.; Travičić, V.; Hadnađev, M. Synergistic effects of bilayer edible coatings: Protein-based and cocoa butter/linseed oil formulation for enhanced food preservation. International Journal of Biological Macromolecules 306 (2025), 141500. https://doi.org/10.1016/j.ijbiomac.2025.141500
43. Erdoğan, Ü.; Uğur, Ş. S. Chitosan-enriched milk thistle extract-loaded liposomes anchored on nonwoven cotton fabric with antioxidant, anti-aging and UV protective effects. International Journal of Biological Macromolecules 304(Pt 2) (2025), 140963. https://doi.org/10.1016/j.ijbiomac.2025.140963
44. Fang, Z.; Bhandari, B. Encapsulation of polyphenols - a review. Trends in Food Science & Technology 21 (2010), 510–523. https://doi.org/10.1016/j.tifs.2010.08.003
45. Farris, S.; Uysal Unalan, I.; Introzzi, L.; Fuentes-Alventosa, J. M.; Cozzolino, C. A. Pullulan-based films and coatings for food packaging: Present applications, emerging opportunities, and future challenges. Journal of Applied Polymer Science 131 (2014), 40539. https://doi.org/10.1002/app.40539

46. Fraternale, D.; Ricci, D. Chemical composition and antimicrobial activity of the essential oil of *Cotinus coggygria* Scop. from Italy. Journal of Essential Oil Bearing Plants 17 (2014), 366–370. https://doi.org/10.1080/0972060X.2014.895192
47. Froude, V. E.; Zhu, Y. Dielectrophoresis of functionalized lipid unilamellar vesicles (liposomes) with contrasting surface constructs. Journal of Physical Chemistry B 113 (2009), 1552–1558. https://doi.org/10.1021/jp808454w
48. García-Lafuente, A.; Guillamón, E.; Villares, A.; Rostagno, M. A.; Martínez, J. A. Flavonoids as anti-inflammatory agents: implications in cancer and cardiovascular disease. Inflammation Research 2009, 58(9), 537–552. https://doi.org/10.1007/s00011-009-0037-3
49. García-Viñuales, S.; Ilie, I. M.; Santoro, A. M.; Romanucci, V.; Zarrelli, A.; Di Fabio, G.; Caflisch, A.; Milardi, D. Silybins inhibit human IAPP amyloid growth and toxicity through stereospecific interactions. Biochimica et Biophysica Acta - Proteins and Proteomics 1870 (2022), 140772. https://doi.org/10.1016/j.bbapap.2022.140772
50. Ghanbarzadeh, S.; Valizadeh, H.; Zakeri-Milani, P. The effects of lyophilization on the physico-chemical stability of sirolimus liposomes. Advanced Pharmaceutical Bulletin 3 (2013), 25–29. https://doi.org/10.5681/apb.2013.005
51. Ginn, M. E.; Noyes, C. M.; Jungermann, E. The contact angle of water on viable human skin. Journal of Colloid and Interface Science 26 (1968), 146–151. https://doi.org/10.1016/0021-9797(68)90306-8
52. Giorgi, V. S.; Peracoli, M. T.; Peracoli, J. C.; Witkin, S. S.; Bannwart-Castro, C. F. Silibinin modulates the NF-κB pathway and pro-inflammatory cytokine production by mononuclear cells from preeclamptic women. Journal of Reproductive Immunology 95 (2012), 67–72. https://doi.org/10.1016/j.jri.2012.06.004
53. Gomes, J.; Serrano, C.; Oliveira, C.; Dias, A.; Moldão, M. Thermal and light stability of anthocyanins from strawberry by-products non-encapsulated and encapsulated with inulin. Acta Scientiarum Polonorum Technologia Alimentaria 20(1) (2021), 79–92. https://doi.org/10.17306/J.AFS.0878
54. Grit, M.; Crommelin, D. J. A. The effect of aging on the physical stability of liposome dispersions. Chemistry and Physics of Lipids 62 (1993), 113–122. https://doi.org/10.1016/0009-3084(92)90089-8
55. Grzesik, M.; Naparlo, K.; Bartosz, G.; Sadowska-Bartosz, I. Antioxidant properties of catechins: Comparison with other antioxidants. Food Chemistry 241 (2018), 480–492. https://doi.org/10.1016/j.foodchem.2017.08.117
56. Guldiken, B.; Gibis, M.; Boyacioglu, D.; Capanoglu, E.; Weiss, J. Physical and chemical stability of anthocyanin-rich black carrot extract-loaded liposomes during storage. International Food Research Journal 108 (2018), 491–497. https://doi.org/10.1016/j.foodres.2018.03.071
57. Hamadou, A. H.; Huang, W. C.; Xue, C.; Mao, X. Formulation of vitamin C encapsulation in marine phospholipids nanoliposomes: Characterization and stability evaluation during long term storage. LWT - Food Science and Technology 127 (2020), 109439. https://doi.org/10.1016/j.lwt.2020.109439
58. Hernandez-Tenorio, F.; Giraldo-Estrada, C. Characterization and chemical modification of pullulan produced from a submerged culture of *Aureobasidium pullulans* ATCC 15233. Polymer Testing 114 (2022), 107686. https://doi.org/10.1016/j.polymertesting.2022.107686
59. Hoang, T. X.; Dang, N. M.; Bae, K. G.; Kim, J. Y. Anti-inflammatory and antioxidant effects of topical formulations containing plant extracts, methylsulfonylmethane, and Peptiskin® in *in vitro* models of arthritis. Pharmaceuticals 18 (2025), 1270. https://doi.org/10.3390/ph18091270
60. Honary, S.; Zahir, F. Effect of zeta potential on the properties of nano-drug delivery systems - A review (Part 1). Tropical Journal of Pharmaceutical Research 12 (2013), 255–264. https://doi.org/10.4314/tjpr.v12i2.19
61. Honeywell-Nguyen, P. L.; Bouwstra, J. A. Vesicles as a tool for transdermal and dermal delivery. Drug Discovery Today: Technologies 2 (2005), 67–74. https://doi.org/10.1016/j.ddtec.2005.05.003

62. Horinaka, J.; Hashimoto, Y.; Takigawa, T. Optical and mechanical properties of pullulan films studied by uniaxial stretching. International Journal of Biological Macromolecules 118 (2018), 584–587. https://doi.org/10.1016/j.ijbiomac.2018.06.127
63. Hosseini, S. F.; Ramezanzade, L.; Nikkhah, M. Nano-liposomal entrapment of bioactive peptidic fraction from fish gelatin hydrolysate. International Journal of Biological Macromolecules 105 (2017), 1455–1463. https://doi.org/10.1016/j.ijbiomac.2017.05.141
64. Huang, X.; Caddell, R.; Yu, B.; Xu, S.; Theobald, B.; Lee, L. J.; Lee, R. J. Ultrasound-enhanced microfluidic synthesis of liposomes. Anticancer Research 30 (2010), 463–466.
65. Hussain, M. A.; Abbas, K.; Lodhi, B. A.; Sher, M.; Ali, M.; Tahir, M. N.; Tremel, W.; Iqbal, S. Fabrication, characterization, thermal stability and nano-assemblies of novel pullulan–aspirin conjugates. Arabian Journal of Chemistry 10 (2017), S1597–S1603. https://doi.org/10.1016/j.arabjc.2013.06.001
66. Isailović, B. D.; Kostić, I. T.; Zvonar, A.; Đorđević, V. B.; Gašperlin, M.; Nedović, V. A.; Bugarski, B. M. Resveratrol-loaded liposomes produced by different techniques. Innovative Food Science & Emerging Technologies 19 (2013), 181–189. https://doi.org/10.1016/j.ifset.2013.03.006
67. ISO 3657:2023. Animal and Vegetable Fats and Oils – Determination of Saponification Value, 6th ed.; International Organization for Standardization (ISO): Geneva, Switzerland, 2023.
68. Jash, A.; Ubeyitogullari, A.; Rizvi, S. Liposomes for oral delivery of protein and peptide-based therapeutics: challenges, formulation strategies, and advances. Journal of Materials Chemistry B 9 (2021), 4773–4792. https://doi.org/10.1039/D1TB00126D
69. Jara-Quijada, E.; Pérez-Won, M.; Tabilo-Munizaga, G.; Lemus-Mondaca, R.; González-Cavieres, L.; Palma-Acevedo, A.; Herrera-Lavados, C. Liposomes loaded with green tea polyphenols – optimization, characterization, and release kinetics under conventional heating and pulsed electric fields. Food and Bioprocess Technology (2023), 1–13. https://doi.org/10.1007/s11947-023-03136-8
70. Jovanović, A. A.; Đorđević, V. B.; Zdunić, G. M.; Pljevljakušić, D. S.; Šavikin, K. P.; Gođevac, D. M.; Bugarski, B. M. Optimization of the extraction process of polyphenols from *Thymus serpyllum* L. herb using maceration, heat and ultrasound-assisted techniques. Separation and Purification Technology 179 (2017), 369–380. https://doi.org/10.1016/j.seppur.2017.01.055
71. Jovanović, A. A.; Balanč, B. D.; Ota, A.; Ahlin Grabnar, P.; Đorđević, V. B.; Šavikin, K. P.; Bugarski, B. M.; Nedović, V. A.; Poklar Ulrih, N. Comparative effects of cholesterol and β-sitosterol on the liposome membrane characteristics. European Journal of Lipid Science and Technology 120 (2018), 1800039. https://doi.org/10.1002/ejlt.201800039
72. Jovanović, A. A.; Balanč, B. D.; Đorđević, V. B.; Ota, A.; Skrt, M.; Šavikin, K. P.; Bugarski, B. M.; Nedović, V. A.; Poklar Ulrih, N. Effect of gentisic acid on the structural-functional properties of liposomes incorporating β-sitosterol. Colloids and Surfaces B: Biointerfaces 183 (2019), 110422. https://doi.org/10.1016/j.colsurfb.2019.110422
73. Jovanović, A. A.; Balanč, B.; Volić, M.; Pećinar, I.; Živković, J.; Šavikin, K. P. Rosehip extract-loaded liposomes for potential skin application: Physicochemical properties of non- and UV-irradiated liposomes. Plants 12 (2023), 3063. https://doi.org/10.3390/plants12173063
74. Jovanović, A. A.; Ćujić, D.; Stojadinović, B.; Čutović, N.; Živković, J.; Šavikin, K. Liposomal bilayer as a carrier of *Rosa canina* L. seed oil: Physicochemical characterization, stability, and biological potential. Molecules 28 (2023), 276. https://doi.org/10.3390/molecules28010276
75. Jovanović, A. A.; Karkad, A.; Pirković, A.; Dekanski, D.; Lupulović, D.; Novaković, M.; Marinković, A. Stability of *Cotinus coggygria* Scop. extract-loaded liposomes: The impact of storage on physical and antioxidant properties. Proceedings 119 (2025), 4. https://doi.org/10.3390/proceedings2025119004
76. Kalita, P.; Bhattacharyya, J.; Dutta, P. P.; Pachuau, L. Valorization of polyphenolic compounds *via* encapsulation: A review. Journal of Food Measurement and Characterization 2025 (2025). https://doi.org/10.1007/s11694-025-03852-z

77. Karkad, A.; Pirković, A.; Milošević, M.; Stojadinović, B.; Šavikin, K.; Marinković, A.; Jovanović, A. A. Silibinin-loaded liposomes: The influence of modifications on physicochemical characteristics, stability, and bioactivity associated with dermal application. Pharmaceutics 16 (2024), 1476. https://doi.org/10.3390/pharmaceutics16111476
78. Karkad, A.A.; Marinković, A.; Jovanović, A.; Simić, K.; Ivanović, S.; Milošević, M.; Erceg, T. Design and optimization of pullulan-isononanoate films with bioactive-loaded liposomes for potential biomedical use. Polymers 18 (2026), 305. https://doi.org/10.3390/polym18020305
79. Lazzari, M.; Chiantore, O. Drying and oxidative degradation of linseed oil. Polymer Degradation and Stability 65 (1999), 303–313. https://doi.org/10.1016/S0141-3910(99)00020-8
80. Lee, M.-K. Liposomes for enhanced bioavailability of water-insoluble drugs: *in vivo* evidence and recent approaches. Pharmaceutics 12 (2020), 264. https://doi.org/10.3390/pharmaceutics12030264
81. Lee, C.; Bain, C. D. Raman spectra of planar supported lipid bilayers. Biochimica et Biophysica Acta (BBA) - Biomembranes 1711 (2005), 59–71. https://doi.org/10.1016/j.bbamem.2005.02.006
82. Leirer, C. T.; Wunderlich, B.; Wixforth, A.; Schneider, M. F. Thermodynamic relaxation drives expulsion in giant unilamellar vesicles. Physical Biology 6 (2009), 016011. https://doi.org/10.1088/1478-3975/6/1/016011
83. Leitgeb, M.; Knez, Ž.; Primožič, M. Sustainable technologies for liposome preparation. Journal of Supercritical Fluids 165 (2020), 104984. https://doi.org/10.1016/j.supflu.2020.104984
84. Levin, Y.; Idiart, M. A. Pore dynamics of osmotically stressed vesicles. Physica A 331 (2004), 571–578. https://doi.org/10.1016/j.physa.2003.05.001
85. Lewis, R. N. A. H.; McElhaney, R. N. Structures of the subgel phases of n-saturated diacyl phosphatidylcholine bilayers: FTIR spectroscopic studies of $^{13}C{=}O$ and ^{2}H labeled lipids. Biophysical Journal 61 (1992), 63–77. https://doi.org/10.1016/S0006-3495(92)81816-7
86. Li, S.; Yi, J.; Yu, X.; Wang, Z.; Wang, L. Preparation and characterization of pullulan derivative/chitosan composite film for potential antimicrobial applications. International Journal of Biological Macromolecules 148 (2020), 258–264. https://doi.org/10.1016/j.ijbiomac.2020.01.080
87. Li, W.; Qu, X.; Kang, X.; Zhang, H.; Zhang, X.; Hu, H.; Yao, L.; Zhang, L.; Zheng, J.; Zheng, Y.; Zhang, J.; Xu, Y. Silibinin eliminates mitochondrial ROS and restores autophagy through IL6ST/JAK2/STAT3 signaling pathway to protect cardiomyocytes from doxorubicin-induced injury. European Journal of Pharmacology 929 (2022), 175153. https://doi.org/10.1016/j.ejphar.2022.175153
88. Li, X.; Zhao, S.; Chen, L.; Zhou, Q.; Qiu, J.; Xin, X.; Zhang, Y.; Yuan, W.; Tian, C.; Yang, J.; Yu, X. High-level production of pullulan from high concentration of glucose by mutagenesis and adaptive laboratory evolution of *Aureobasidium pullulans*. Carbohydrate Polymers 302 (2023), 120426. https://doi.org/10.1016/j.carbpol.2022.120426
89. Lidgate, D.; Hegde, S.; Maskiewicz, R. Conductivity measurement as a convenient technique for determination of liposome capture volume. International Journal of Pharmaceutics 96 (1993), 51–58. https://doi.org/10.1016/0378-5173(93)90211-W
90. Liu, Y.; Cheng, Y.; Li, J.; Wang, Y.; Liu, Y. Epoxy stearic acid, an oxidative product derived from oleic acid, induces cytotoxicity, oxidative stress, and apoptosis in HepG2 cells. Journal of Agricultural and Food Chemistry 66 (2018), 5237–5246. https://doi.org/10.1021/acs.jafc.8b01954
91. Liu, C.-H.; Jassey, A.; Hsu, H.-Y.; Lin, L.-T. Antiviral activities of silymarin and derivatives. Molecules 24 (2019), 1552. https://doi.org/10.3390/molecules24081552
92. Liu, C.; Dong, S.; Wang, X.; Xu, H.; Liu, C.; Yang, X.; Wu, S.; Jiang, X.; Kan, M.; Xu, C. Research progress of polyphenols in nanoformulations for antibacterial application. *Materials Today Bio* 21 (2023), 100729. https://doi.org/10.1016/j.mtbio.2023.100729
93. Lopez-Polo, J.; Silva-Weiss, A.; Giménez, B.; Cantero-López, P.; Vega, R.; Osorio, F. A. Effect of lyophilization on the physicochemical and rheological properties of food grade liposomes that encapsulate rutin. Food Research International 130 (2020), 108967. https://doi.org/10.1016/j.foodres.2019.108967

94. Luo, Z.; Murray, B. S.; Yusoff, A.; Morgan, M. R.; Povey, M. J.; Day, A. J. Particle-stabilizing effects of flavonoids at the oil-water interface. Journal of Agricultural and Food Chemistry 59 (2011), 2636–2645. https://doi.org/10.1021/jf1041855
95. Manach, C.; Scalbert, A.; Morand, C.; Rémésy, C.; Jiménez, L. Polyphenols: food sources and bioavailability. The American Journal of Clinical Nutrition 79 (2004), 727–747. https://doi.org/10.1093/ajcn/79.5.727
96. Marčetić, M.; Božić, D.; Milenković, M.; Malešević, N.; Radulović, S.; Kovačević, N. Antimicrobial, antioxidant and anti-inflammatory activity of young shoots of the smoke tree, *Cotinus coggygria* Scop. Phytotherapy Research 26 (2012), 1243–1252. https://doi.org/10.1002/ptr.4919
97. Matić, S.; Stanić, S.; Bogojević, D.; Vidaković, M.; Grdović, N.; Arambašić, J.; Dinić, S.; Uskoković, A.; Poznanović, G.; Solujić, S.; Mladenović, M.; Marković, J.; Mihailović, M. Extract of the plant *Cotinus coggygria* Scop. attenuates pyrogallol-induced hepatic oxidative stress in Wistar rats. Canadian Journal of Physiology and Pharmacology 89(6) (2011), 401–411. https://doi.org/10.1139/y11-043
98. Matić, S.; Stanić, S.; Mihailović, M.; Bogojević, D. *Cotinus coggygria* Scop.: An overview of its chemical constituents, pharmacological and toxicological potential. Saudi Journal of Biological Sciences 23(4) (2016), 452–461. https://doi.org/10.1016/j.sjbs.2015.05.012
99. Matsumura, Y.; Ananthaswamy, H. N. Toxic effects of ultraviolet radiation on the skin. Toxicology and Applied Pharmacology 195 (2004), 298–308. https://doi.org/10.1016/j.taap.2003.08.019
100. McIntyre, D. D.; Vogel, H. J. Structural studies of pullulan by nuclear magnetic resonance spectroscopy. Starch/Stärke 45 (1993), 401–405.
101. Medina-Torres, L.; Santiago-Adame, R.; Calderas, F.; Gallegos-Infante, J. A.; González-Laredo, R. F.; Rocha-Guzmán, N. E.; Núñez-Ramírez, D. M.; Bernad-Bernad, M. J.; Manero, O. Microencapsulation by spray drying of laurel infusions (*Litsea glaucescens*) with maltodextrin. Industrial Crops and Products 90 (2016), 1–8. https://doi.org/10.1016/j.indcrop.2016.06.009
102. Mignet, N.; Seguin, J.; Chabot, G. G. Bioavailability of polyphenol liposomes: A challenge ahead. Pharmaceutics 5 (2013), 457–471. https://doi.org/10.3390/pharmaceutics5030457
103. Mohammadi, M.; Ariafar, S.; Talebi-Ghane, E.; Afzali, S. Comparative efficacy of silibinin and nano-silibinin on lead poisoning in male Wistar rats. Toxicology 475 (2022), 153242. https://doi.org/10.1016/j.tox.2022.153242
104. Morais, H. A.; da Silva Barbosa, C. M.; Delvivo, F. M.; Mansur, H. S.; de Oliveira, M. C.; Silvestre, M. P. C. Comparative study of microencapsulation of casein hydrolysates in lipospheres and liposomes. Journal of Food Biochemistry 28 (2004), 21–41.
105. Mozafari, M. R.; Johnson, C.; Hatziantoniou, S.; Demetzos, C. Nanoliposomes and their applications in food nanotechnology. Journal of Liposome Research 18 (2008), 309–327. https://doi.org/10.1080/08982100802465941
106. Munin, A.; Edwards-Lévy, F. Encapsulation of natural polyphenolic compounds; a review. *Pharmaceutics* 3 (2011), 793–829. https://doi.org/10.3390/pharmaceutics3040793
107. Murru, C.; Badía-Laíno, R.; Díaz-García, M. E. Oxidative stability of vegetal oil-based lubricants. ACS Sustainable Chemistry & Engineering 9 (2021), 1459–1476. https://doi.org/10.1021/acssuschemeng.0c06988
108. Nakai, K.; Yoneda, K.; Ishihara, Y.; Ohmori, K.; Moriue, T.; Igarashi, J.; Kohno, M.; Kosaka, H.; Kubota, Y. Lipid peroxidation-induced VEGF expression in the skin of KKAy obese mice. Experimental Dermatology 20 (2011), 388–393. https://doi.org/10.1111/j.1600-0625.2010.01223.x
109. Nakai, K.; Tsuruta, D. What are reactive oxygen species, free radicals, and oxidative stress in skin diseases? International Journal of Molecular Sciences 22 (2021), 10799. https://doi.org/10.3390/ijms221910799
110. Narayanapillai, S.; Agarwal, C.; Tilley, C.; Agarwal, R. Silibinin is a potent sensitizer of UVA radiation-induced oxidative stress and apoptosis in human keratinocyte HaCaT cells. Photochemistry and Photobiology 88 (2012), 1135–1140. https://doi.org/10.1111/j.1751-1097.2011.01050.x

111. Narenji, M.; Talaee, M. R.; Moghimi, H. R. Investigating the effects of size, charge, viscosity and bilayer flexibility on liposomal delivery under convective flow. International Journal of Pharmaceutics 513 (2016), 88–96. https://doi.org/10.1016/j.ijpharm.2016.08.056
112. Nichols, J. A.; Katiyar, S. K. Skin photoprotection by natural polyphenols: anti-inflammatory, antioxidant and DNA repair mechanisms. Archives of Dermatological Research 302(2) (2010), 71–83. https://doi.org/10.1007/s00403-009-1001-3
113. Niu, B.; Shao, P.; Chen, H.; Sun, P. Structural and physicochemical characterization of novel hydrophobic packaging films based on pullulan derivatives for fruits preservation. Carbohydrate Polymers 208 (2019), 276–284. https://doi.org/10.1016/j.carbpol.2018.12.070
114. Novaković, M.; Vučković, I.; Janaćković, P.; Soković, M.; Filipović, A.; Tešević, V.; Milosavljević, S. Chemical composition, antibacterial and antifungal activity of the essential oils of *Cotinus coggygria* from Serbia. Journal of the Serbian Chemical Society 72(11) (2007), 1045–1051. https://doi.org/10.2998/JSC0711045N
115. Pan, M. H.; Lai, C. S.; Ho, C. T. Anti-inflammatory activity of natural dietary flavonoids. Food & Function 1(1) (2010), 15–31. https://doi.org/10.1039/c0fo00103a
116. Pandey, K. B.; Rizvi, S. I. Plant polyphenols as dietary antioxidants in human health and disease. Oxidative Medicine and Cellular Longevity 2 (2009), 270–278. https://doi.org/10.4161/oxim.2.5.9498
117. Park, J. S.; Park, J. K.; Nam, J. P.; Kim, J. A.; Nah, J. W. Preparation of pullulan-g-poly(L-lysine) and its evaluation as a gene carrier. Macromolecular Research 20 (2012), 667–672. https://doi.org/10.1007/s13233-012-0098-y
118. Pašić, I.; Novaković, M.; Tešević, V.; Milosavljević, S.; Petrović, N.; Stanojković, T.; Matić, I. Z. Exploring the anticancer potential of extracts and compounds from the heartwood of *Cotinus coggygria* Scop. wild growing in Serbia. BMC Complementary Medicine and Therapies 25 (2025), 36. https://doi.org/10.1186/s12906-025-04768-3
119. Păvăloiu, R. D.; Sha'at, F.; Neagu, G.; Deaconu, M.; Bubueanu, C.; Albulescu, A.; Sha'at, M.; Hlevca, C. Encapsulation of polyphenols from *Lycium barbarum* leaves into liposomes as a strategy to improve their delivery. Nanomaterials 11 (2021), 1938. https://doi.org/10.3390/nano11081938
120. Pavlov, D. Проучване на антиоксидантното, противовъзпалителното и противодиабетно действие на екстракти от *Cotinus coggygria* в експериментални модели с опитни животни и клетъчни култури (Investigation of the antioxidant, anti-inflammatory and antidiabetic activity of extracts from *Cotinus coggygria* in experimental animal models and cell cultures). PhD Thesis, 2015.
121. Peralta, M. F.; Guzmán, M. L.; Pérez, A. P.; Apezteguia, G. A.; Fórmica, M. L.; Romero, E. L.; Olivera, M. E.; Carrer, D. C. Liposomes can both enhance or reduce drugs penetration through the skin. Scientific Reports 8 (2018), 13253. https://doi.org/10.1038/s41598-018-31693-y
122. Petrović, S.; Tačić, A.; Savić, S.; Nikolić, V.; Nikolić, L.; Savić, S. Sulfanilamide in solution and liposome vesicles: *in vitro* release and UV stability studies. Saudi Pharmaceutical Journal 25 (2017), 1194–1200. https://doi.org/10.1016/j.jsps.2017.09.003
123. Pirković, A.; Vilotić, A.; Borozan, S.; Nacka-Aleksić, M.; Bojić-Trbojević, Ž.; Jovanović Krivokuća, M.; Battino, M.; Giampieri, F.; Dekanski, D. Oleuropein attenuates oxidative stress in human trophoblast cells. Antioxidants 12 (2023), 197. https://doi.org/10.3390/antiox12010197
124. Płaczek, M.; Wątróbska-Świetlikowska, D.; Stefanowicz-Hajduk, J.; Drechsler, M.; Ochocka, J. R.; Sznitowska, M. Comparison of the *in vitro* cytotoxicity among phospholipid-based parenteral drug delivery systems: emulsions, liposomes and aqueous lecithin dispersions (WLDs). European Journal of Pharmaceutical Sciences 127 (2019), 92–101. https://doi.org/10.1016/j.ejps.2018.10.018
125. Puri, A.; Loomis, K.; Smith, B.; Lee, J.-H.; Yavlovich, A.; Heldman, E.; Blumenthal, R. Lipid-based nanoparticles as pharmaceutical drug carriers: From concepts to clinic. Critical Reviews in Therapeutic Drug Carrier Systems 26 (2009), 523–580. https://doi.org/10.1615/critrevtherdrugcarriersyst.v26.i6.10

126. Qiu, J.; Hou, H.-Y.; Yang, I.-S.; Chen, X.-B. Raman spectroscopy analysis of free fatty acid in olive oil. Applied Sciences 9 (2019), 4510. https://doi.org/10.3390/app9214510
127. Rahdar, A.; Sayyadi, K.; Sayyadi, J.; Yaghobi, Z. Nano-gels: A versatile nano-carrier platform for drug delivery systems: A mini review. Nanomedicine Research Journal 4 (2019), 1–9. https://doi.org/10.22034/nmrj.2019.01.001
128. Radan, M.; Ćujić Nikolić, N.; Kuzmanović Nedeljković, S.; Mutavski, Z.; Krgović, N.; Stević, T.; Marković, S.; Jovanović, A.; Živković, J.; Šavikin, K. Multifunctional pomegranate peel microparticles with health-promoting effects for the sustainable development of novel nutraceuticals and pharmaceuticals. Plants 13 (2024), 281. https://doi.org/10.3390/plants13020281
129. Rahul, P. B.; Tiwari, R. K.; Dash, K. K.; Sharma, M. Recent advances in encapsulation of pomegranate peel extract and combination of wall materials: a review of encapsulation technologies, characterization and applications in the food industry. Sustainable Food Technology 3 (2025), 123–144. https://doi.org/10.1039/D4FB00196F
130. Ramasamy, K.; Deep, G.; Tyagi, A.; Agarwal, C.; Agarwal, R. Silibinin inhibits tumor associated macrophages-induced lung cancer cell growth and invasiveness by down-regulating macrophage migration inhibitory factor. Proceedings of the 104th Annual Meeting of the American Association for Cancer Research, Washington, DC, USA, 6–10 April 2013.
131. Rizkita, L. D.; Putri, R. G. P.; Farid, M.; Rizkawati, M.; Wikaningtyas, P. Liposome drug delivery in combating the widespread topical antibiotic resistance: A narrative review. Beni-Suef University Journal of Basic and Applied Sciences 13 (2024), 90. https://doi.org/10.1186/s43088-024-00545-2
132. Salem, Y.; Sunoqrot, S.; Rajha, H. N.; Abusulieh, S.; Afif, C.; Francis, H.; Touma, J. A.; Louka, N.; Maroun, R. G. Grape seed phenolic extracts encapsulation in polymeric nanoparticles: characterization and *in vitro* evaluation against skin melanoma. Journal of Drug Delivery Science and Technology 100 (2024), 106094. https://doi.org/10.1016/j.jddst.2024.106094
133. Sawyer, L. C.; Grubb, D. T.; Meyers, G. F. Polymer Microscopy, 3rd ed.; Springer: New York, USA, 2008. https://doi.org/10.1017/S1431927609090692
134. Schroeder, A.; Kost, J.; Barenholz, Y. Ultrasound, liposomes, and drug delivery: principles for using ultrasound to control the release of drugs from liposomes. Chemistry and Physics of Lipids 162(1–2) (2009) 1–16. https://doi.org/10.1016/j.chemphyslip.2009.08.003
135. Sebaaly, C.; Charcosset, C.; Stainmesse, S.; Fessi, H.; Greige-Gerges, H. Clove essential oil-in-cyclodextrin-in-liposomes in the aqueous and lyophilized states: From laboratory to large scale using a membrane contactor. Carbohydrate Polymers 138 (2016), 75–85. https://doi.org/10.1016/j.carbpol.2015.11.053
136. Sengupta, P.; Bose, A.; Sen, K. Liposomal encapsulation of phenolic compounds for augmentation of bio-efficacy: A review. Chemistry Select 8 (2021), 10447–10463. https://doi.org/10.1002/slct.202101821
137. Shaboyan, N. K.; Moghrovyan, A.; Dumanyan, K. H.; Chichoyan, N. Phytochemical analysis and antioxidant activity of *Cotinus coggygria* Scop. from Armenian flora. Pharmacognosy Journal 13 (2021), 933–941. https://doi.org/10.5530/pj.2021.13.120
138. Shahidi, F.; Ambigaipalan, P. Phenolics and polyphenolics in foods, beverages and spices: Antioxidant activity and health effects – A review. Journal of Functional Foods 18 (2015), 820–897. https://doi.org/10.1016/j.jff.2015.06.018
139. Shakibaei, M.; Harikumar, K. B.; Aggarwal, B. B. Resveratrol addiction: to die or not to die. Molecular Nutrition & Food Research 2009, 53(1), 115–128. https://doi.org/10.1002/mnfr.200800148
140. Scalbert, A.; Johnson, I. T.; Saltmarsh, M. Polyphenols: antioxidants and beyond. The American Journal of Clinical Nutrition 81 (2005), 215S–217S. https://doi.org/10.1093/ajcn/81.1.215S
141. Shade, C. W. Liposomes as advanced delivery systems for nutraceuticals. Integrative Medicine 15 (2016), 33–36.

142. Shahidi, F.; Samarasinghe, A. How to assess antioxidant activity? Advances, limitations, and applications of *in vitro*, *in vivo*, and *ex vivo* approaches. Food Production, Processing & Nutrition 7 (2025), 50. https://doi.org/10.1186/s43014-025-00326-z
143. Sharma, K.; Nilsuwan, K.; Ma, L.; Benjakul, S. Effect of liposomal encapsulation and ultrasonication on debittering of protein hydrolysate and plastein from salmon frame. Foods 12 (2023), 761. https://doi.org/10.3390/foods12040761
144. Silva, R.; Ferreira, H.; Little, C.; Cavaco-Paulo, A. Effect of ultrasound parameters for unilamellar liposome preparation. Ultrasonics Sonochemistry 17 (2010), 628–632. https://doi.org/10.1016/j.ultsonch.2009.10.010
145. Singh, R. P.; Agarwal, R. Flavonoid antioxidant silymarin and skin cancer. Antioxidants & Redox Signaling 4 (2002), 655–663. https://doi.org/10.1089/15230860260220166
146. Singh, R. P.; Agarwal, R. Cosmeceuticals and silibinin. Clinics in Dermatology 27 (2009), 479–484. https://doi.org/10.1016/j.clindermatol.2009.05.012
147. Singh, R. P.; Dhanalakshmi, S.; Tyagi, A. K.; Chan, D. C.; Agarwal, C.; Agarwal, R. Dietary feeding of silibinin inhibits advanced human prostate carcinoma growth in athymic nude mice and increases plasma insulin-like growth factor-binding protein-3 levels. Cancer Research 62 (2002), 3063–3069.
148. Singh, R. S.; Saini, G. K.; Kennedy, J. F. Pullulan production in stirred tank reactor by a color-variant strain of *Aureobasidium pullulans* FB-1. Carbohydrate Polymer Technologies and Applications 2 (2021), 100086.
149. Simões, A.; Ramos, A.; Domingues, F.; Luís, Â. Pullulan-Tween 40 emulsified films containing geraniol: Production and characterization as potential food packaging materials. European Food Research and Technology 250 (2024), 1721–1732. https://doi.org/10.1016/j.carpta.2021.100086
150. Solís-Gómez, A.; Sato-Berrú, R. Y.; Mata-Zamora, M. E.; Saniger, J. M.; Guirado-López, R. A. Characterizing the properties of anticancer silibinin and silybin B complexes with UV–Vis, FT-IR, and Raman spectroscopies: A combined experimental and theoretical study. Journal of Molecular Structure 1182 (2019), 109–118. https://doi.org/10.1016/j.molstruc.2019.01.042
151. Song, X.-Y.; Liu, P.-C.; Liu, W.-W.; Hayashi, T.; Mizuno, K.; Hattori, S.; Fujisaki, H.; Ikejima, T. Protective effects of silibinin against ethanol- or acetaldehyde-induced damage in liver cell lines involve repression of mitochondrial fission. Toxicology in Vitro 80 (2022), 105330. https://doi.org/10.1016/j.tiv.2022.105330
152. Srinivasan, V.; Chavan, S.; Jain, U.; Tarwadi, K. Liposomes for nanodelivery systems in food products. In Nanoscience for Sustainable Agriculture; Pudake, R., Chauhan, N., Kole, C., Eds.; 1st ed.; Springer: Cham, Switzerland, 2019; pp. 627–638. https://doi.org/10.1007/978-3-319-97852-9
153. Stojković, D.; Dragičević, N.; Ivanov, M.; Gajović, N.; Jurišević, M.; Jovanović, I.; Tomović, M.; Živković, J. New insights into the biological activities of *Cotinus coggygria* Scop. extracts: Antioxidant, antimicrobial, and gastroprotective potential. Pharmaceuticals 18(1) (2025), 98. https://doi.org/10.1016/j.sjbs.2015.05.012
154. Su, L.; Jia, Y.-L.; Fu, L.; Guo, K.; Xie, S. The emerging progress on wound dressings and their application in clinic wound management. Heliyon 9 (2023), e22520. https://doi.org/10.1016/j.heliyon.2023.e22520
155. Sun, X.; Ding, H.; Li, X. Disulfiram-loaded nanovesicle hydrogel promotes healing of diabetic wound. Journal of Translational Medicine 22 (2024), 1066. https://doi.org/10.1186/s12967-024-05875-4
156. Sun, L.; Wang, H.; Du, J.; Wang, T.; Yu, D. Ultrasonic-assisted extraction of grape seed procyanidins, preparation of liposomes, and evaluation of their antioxidant capacity. Ultrasonics Sonochemistry 105 (2024), 106856. https://doi.org/10.1016/j.ultsonch.2024.106856
157. Šeremet, D.; Štefančić, M.; Petrović, P.; Kuzmić, S.; Doroci, S.; Mandura Jarić, A.; Vojvodić Cebin, A.; Pjanović, R.; Komes, D. Development, characterization and incorporation of alginate-plant protein covered liposomes containing ground ivy (*Glechoma hederacea* L.) extract into candies. Foods 11 (2022), 1816. https://doi.org/10.3390/foods11121816

158. Tan, J. M.; Karthivashan, G.; Arulselvan, P.; Fakurazi, S.; Hussein, M. Z. Characterization and *in vitro* sustained release of silibinin from pH responsive carbon nanotube-based drug delivery system. Journal of Nanomaterials 2014 (2014), 439873. https://doi.org/10.1155/2014/439873
159. Tian, M.; Han, J.; Ye, A.; Liu, W.; Xu, X.; Yao, Y.; Li, K.; Kong, Y.; Wei, F.; Zhou, W. Structural characterization and biological fate of lactoferrin-loaded liposomes during simulated infant digestion. Journal of the Science of Food and Agriculture 99 (2019), 2677–2684. https://doi.org/10.1002/jsfa.9435
160. Toopkanloo, S. P.; Tan, T. B.; Abas, F.; Azam, M.; Nehdi, I. A.; Tan, C. P. Improving vesicular integrity and antioxidant activity of novel mixed soy lecithin-based liposomes containing squalene and their stability against UV light. Molecules 25 (2020), 5873. https://doi.org/10.3390/molecules25245873
161. Tran, H.-M.; Yang, C.-Y.; Wu, T.-H.; Yen, F.-L. Liposomes encapsulating morin: investigation of physicochemical properties, dermal absorption improvement and anti-aging activity in PM-induced keratinocytes. Antioxidants 11 (2022), 1183. https://doi.org/10.3390/antiox11061183
162. Vasić, D.; Špirović Trifunović, B.; Pećinar, I.; Paunović, D.; Popović-Đorđević, J. Chemical characterization of *Rosa canina* L. rosehip seed: Application of Raman spectroscopy and gas chromatography. Biology Life Science Forum 3 (2021), 50. https://doi.org/10.3390/IECAG2021-09674
163. Venkateshaiah, A.; Padil, V. V. T.; Nagalakshmaiah, M.; Waclawek, S.; Černík, M.; Varma, R. S. Microscopic techniques for the analysis of micro and nanostructures of biopolymers and their derivatives. Polymers 12 (2020), 512. https://doi.org/10.3390/polym12030512
164. Verdura, S.; Cuyàs, E.; Ruiz-Torres, V.; Micol, V.; Joven, J.; Bosch-Barrera, J.; Menendez, J. A. Lung cancer management with silibinin: A historical and translational perspective. Pharmaceuticals 14 (2021), 559. https://doi.org/10.3390/ph14060559
165. Wang, L.; Li, J.; Zhang, S.; Shi, J. Preparation and characterization of all-biomass soy protein isolate-based films enhanced by epoxy castor oil acid sodium and hydroxypropyl cellulose. Materials 9 (2016), 193. https://doi.org/10.3390/ma9030193
166. Wong-ekkabut, J.; Xu, Z.; Triampo, W.; Tang, I.-M.; Tieleman, D. P.; Monticelli, L. Effect of lipid peroxidation on the properties of lipid bilayers: A molecular dynamics study. Biophysical Journal 93 (2007), 4225–4236. https://doi.org/10.1529/biophysj.107.112565
167. Xi, X.; Wang, J.; Qin, Y.; You, Y.; Huang, W.; Zhan, J. The biphasic effect of flavonoids on oxidative stress and cell proliferation in breast cancer cells. Antioxidants 11 (2022), 622. https://doi.org/10.3390/antiox11040622
168. Yan, B.; Zheng, X.; Wang, Y.; Yang, J.; Zhu, X.; Qiu, M.; Xia, K.; Wang, Y.; Li, M.; Li, S.; Ma, X.; Xie, J.; Li, F.; Fu, T.; Li, W. Liposome-based silibinin for mitigating nonalcoholic fatty liver disease: dual effects *via* parenteral and intestinal routes. ACS Pharmacology & Translational Science 6 (2023), 1909–1923. https://doi.org/10.1021/acsptsci.3c00210
169. Yanagihara, S.; Kitayama, Y.; Yuba, E.; Harada, A. Preparing size-controlled liposomes modified with polysaccharide derivatives for pH-responsive drug delivery applications. Life 13 (2023), 2158. https://doi.org/10.3390/life13112158
170. Yang, D.; Wang, X.; Gan, L.; Zhang, H.; Shin, J.; Lee, K.; Hong, S. Effects of flavonoid glycosides obtained from a *Ginkgo biloba* extract fraction on the physical and oxidative stabilities of oil-in-water emulsions prepared from a stripped structured lipid with a low omega-6 to omega-3 ratio. Food Chemistry 174 (2015), 124–131. https://doi.org/10.1016/j.foodchem.2014.11.036
171. Yang, Y.; Huang, J.; Li, J.; Yang, H.; Yin, Y. Effects of stearic acid on proliferation, differentiation, apoptosis, and autophagy in porcine intestinal epithelial cells. Current Molecular Medicine 20 (2020), 157–166. https://doi.org/10.2174/1566524019666190917144127
172. Yang, K.; Tran, K.; Salvati, A. Tuning liposome stability in biological environments and intracellular drug release kinetics. Biomolecules 13 (2023), 59. https://doi.org/10.3390/biom13010059

173. Yao, W.; Liu, C.; Wang, N.; Zhou, H.; Shafiq, F.; Yu, S.; Qiao, W. O-nitrobenzyl liposomes with dual responsive release capabilities for drug delivery. Journal of Molecular Liquids 334 (2021), 116016. https://doi.org/10.1016/j.molliq.2021.116016
174. Yoon, G.; Park, W.; Yoo, I.-S. Solid lipid nanoparticles (SLNs) and nanostructured lipid carriers (NLCs): Recent advances in drug delivery. Journal of Pharmaceutical Investigation 43 (2013), 353–362. https://doi.org/10.1007/s40005-013-0087-y
175. Yu, J.-Y.; Chuesiang, P.; Shin, G.-H.; Park, H.-J. Post-processing techniques for the improvement of liposome stability. Pharmaceutics 13 (2021), 1023. https://doi.org/10.3390/pharmaceutics13071023
176. Zahedi, Y.; Ghanbarzadeh, B.; Sedaghat, N. Physical properties of edible emulsified films based on pistachio globulin protein and fatty acids. Journal of Food Engineering 100 (2010), 102–108. https://doi.org/10.1016/j.jfoodeng.2010.03.033
177. Zare Mehrjerdi, P.; Asadi, S.; Ehsani, E.; Askari, V. R.; Baradaran Rahimi, V. Silibinin as a major component of milk thistle seed provides promising influences against diabetes and its complications: A systematic review. Naunyn-Schmiedeberg's Archives of Pharmacology 397 (2024), 7531–7549. https://doi.org/10.1007/s00210-024-03172-x
178. Zhang, Z.; Li, X.; Sang, S.; McClements, D. J.; Chen, L.; Long, J.; Jiao, A.; Wang, J.; Jin, Z.; Qiu, C. A review of nanostructured delivery systems for the encapsulation, protection, and delivery of silymarin: An emerging nutraceutical. Food Research International 156 (2022), 111314. https://doi.org/10.1016/j.foodres.2022.111314
179. Zhang, H.; Kim, H.; Kim, S. Y.; Hai, H.; Kim, E.; Ma, L.; Kim, D.; Kim, C. Y.; Park, K.; Park, S.; Ko, J.; Kim, E.-K.; Kim, K.; Ryoo, Z. Y.; Yi, J.; Kim, M. O. Silibinin induces oral cancer cell apoptosis and reactive oxygen species generation by activating the JNK/c-Jun pathway. Journal of Cancer 14 (2023), 1875–1887. https://doi.org/10.7150/jca.84734
180. Zhang, H.; Lin, X.; Cao, X.; Wang, Y.; Wang, J.; Zhao, Y. Developing natural polymers for skin wound healing. Bioactive Materials 33 (2024), 355–376. https://doi.org/10.1016/j.bioactmat.2023.11.012
181. Zhao, F.; Li, X. Evaluation of immunomodulatory activity of silymarin extract from *Silybum marianum* in mice of health food. International Journal of Food Processing Technology 8 (2015), 278–282. https://doi.org/10.19026/ajfst.8.1508
182. Zheng, L.; Li, B.; Lin, P.; Zhang, X.; Zhang, C.; Zhao, B.; Wang, T. Sedimentation and precipitation of nanoparticles in power-law fluids. Microfluidics and Nanofluidics 15 (2013), 11–18. https://doi.org/10.1007/s10404-012-1117-1
183. Zhou, H.; Zheng, B.; McClements, D. J. Encapsulation of lipophilic polyphenols in plant-based nanoemulsions: impact of carrier oil on lipid digestion and curcumin, resveratrol and quercetin bioaccessibility. Food & Function 12 (2021), 3420–3432. https://doi.org/10.1039/D1FO00275A
184. Zuhair, R. A.; Abdullah, A.; Sahilah, A. M.; Dauqan, E. Antioxidant activity and physicochemical properties changes of papaya (*Carica papaya* L. cv. Hongkong) during different ripening stages. International Food Research Journal 20 (2013), 1653–1659.

7. SUPPLEMENTAL MATERIAL

These supplemental materials include visual representations that further illustrate the key trends and observations discussed in the study. The supplemental figures and graphical representations, as well as the table, present detailed results from FT-IR analysis and spectral deconvolution, NMR analysis, alongside data from cell-based assays, offering a comprehensive overview of both the structural characteristics and biological activity of the samples.

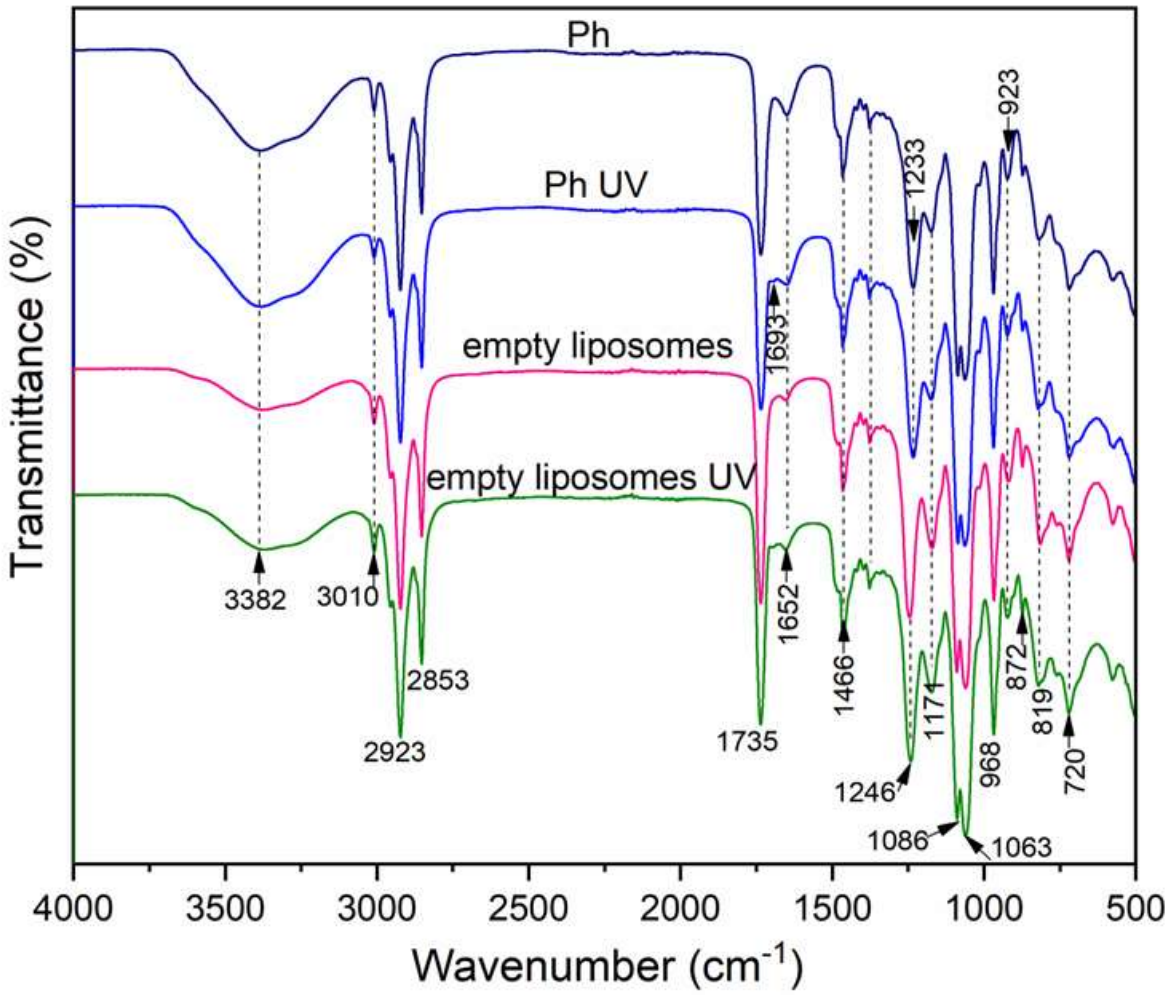

Figure S 1. Fourier transform infrared spectroscopy analysis of employed phospholipids for the liposome preparation (Phospholipon 90G, Ph), UV-exposed Phospholipon 90G (Ph UV), non-treated unloaded liposomes, and UV-exposed unloaded liposomes

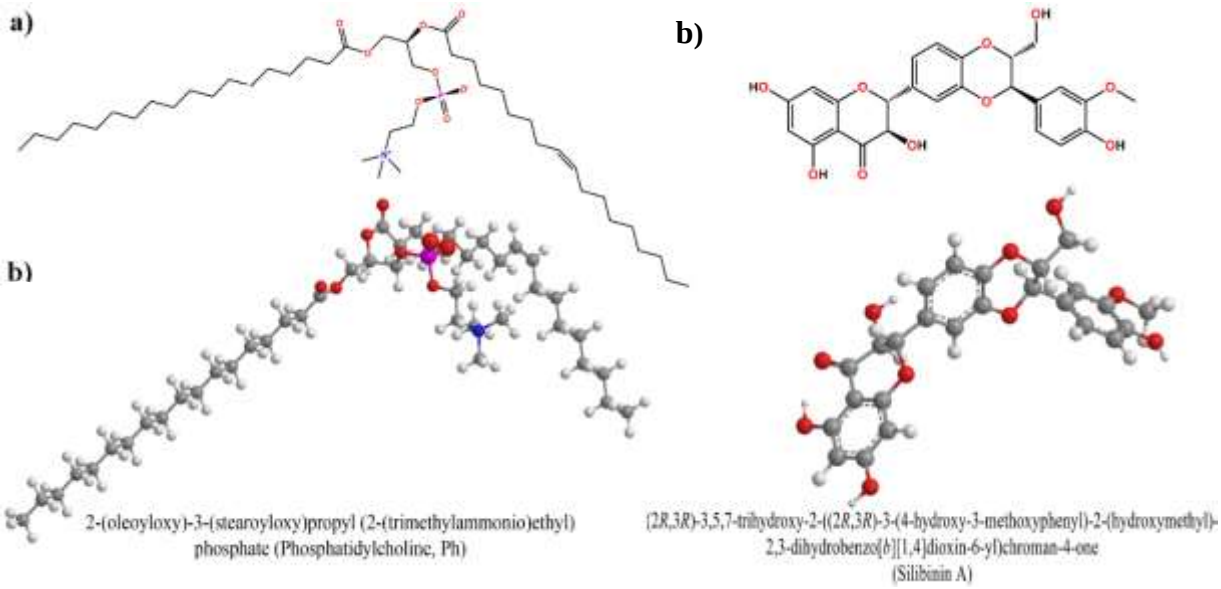

Figure S 2. The structure of (a) phosphatidylcholine and (b) silibinin A

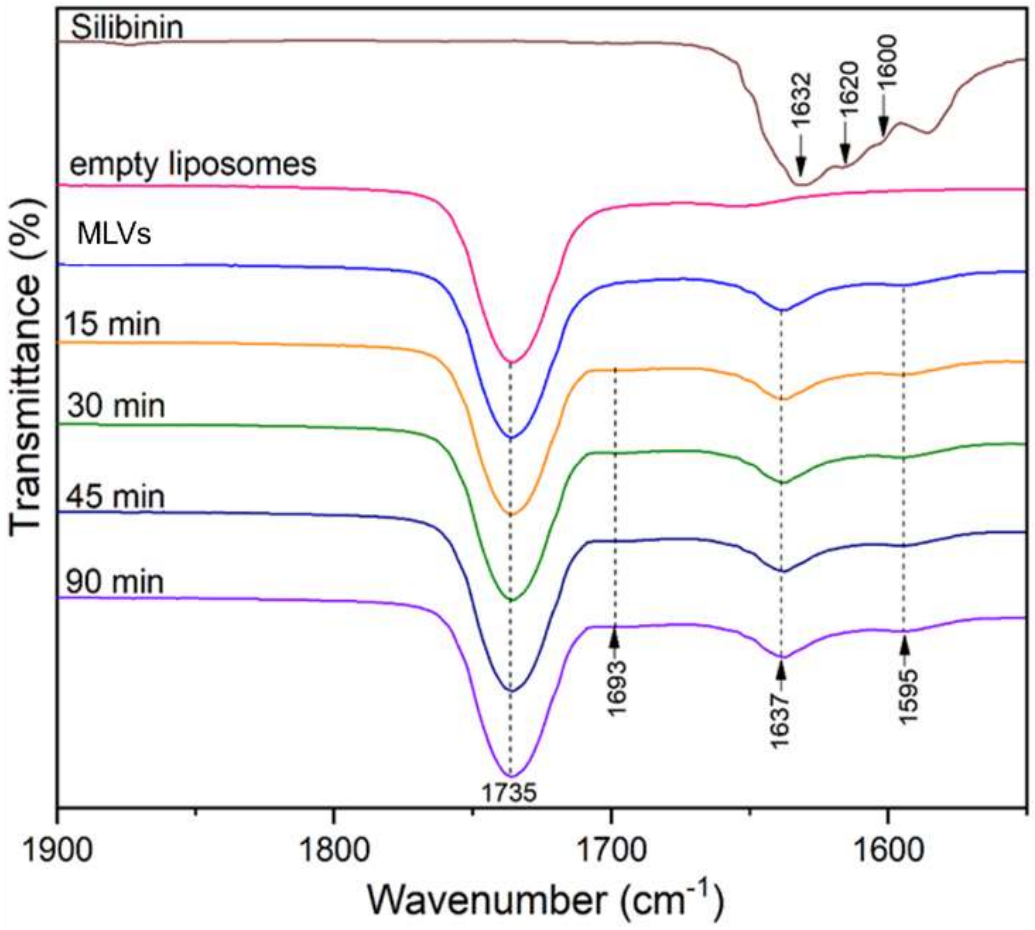

Figure S 3. Fourier transform infrared spectroscopy analysis of pure compound silibinin, loaded liposomal vesicles; liposomes containing silibinin, and UV-exposed liposomal particles with silibinin (during times of 15-90 min; the spectral region of 1550-1800 cm^{-1})

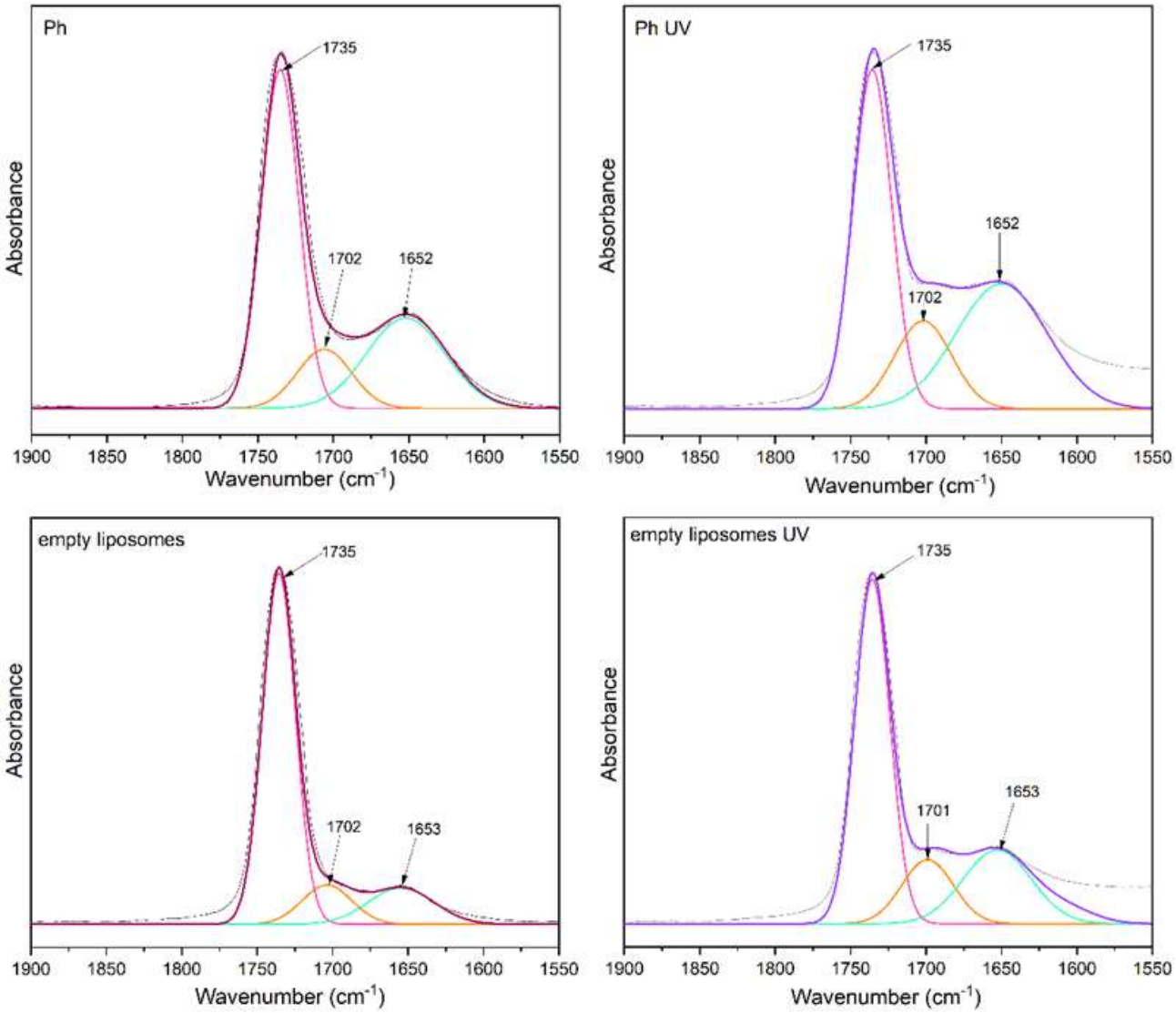

Figure S 4. Spectral deconvolution of the 1550-1800 cm^{-1} region for Phospholipon 90G (Ph) and unloaded liposomal particles, both prior to and following 30 min of ultraviolet (UV) exposure

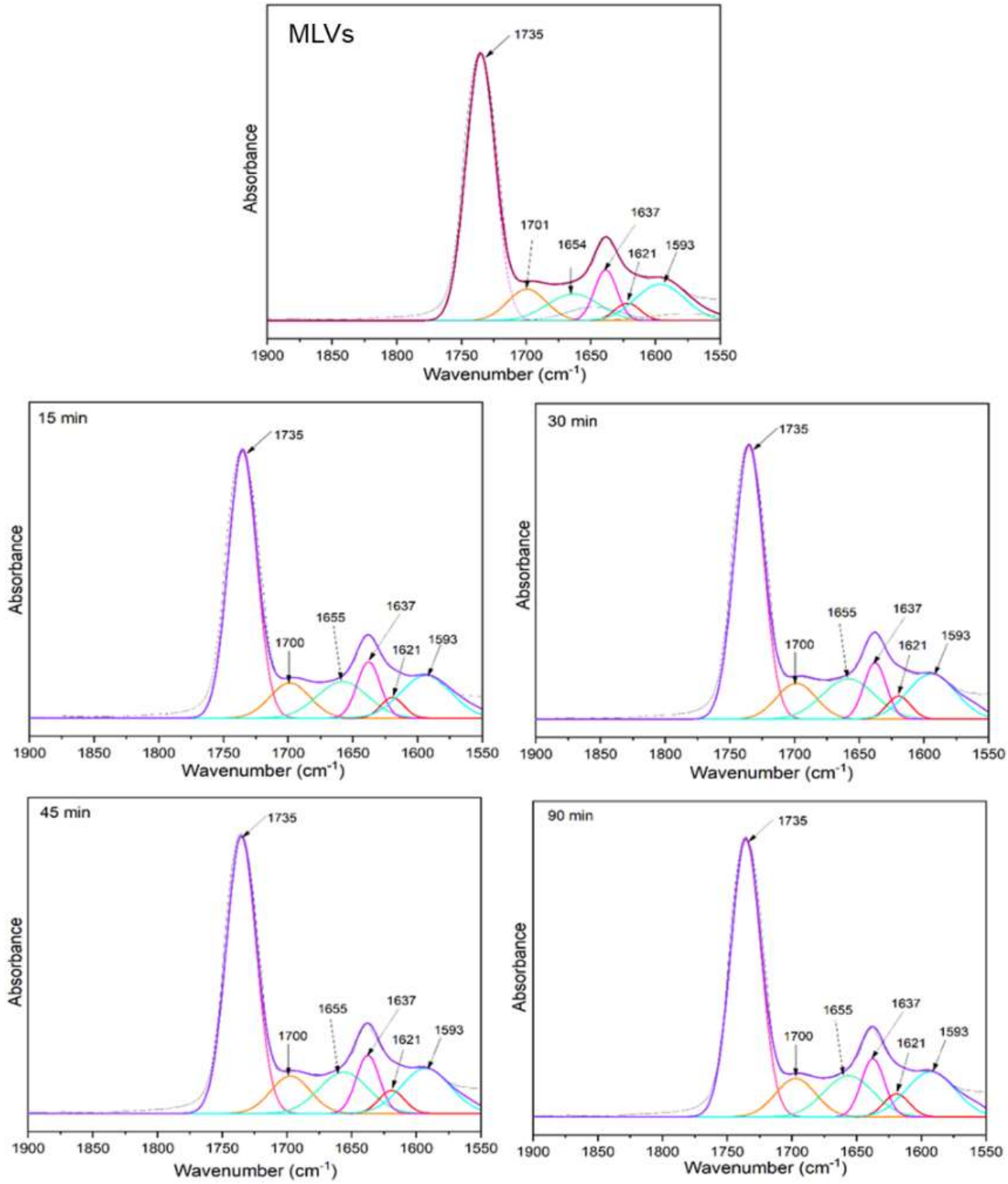

Figure S 5. Spectral deconvolution of the 1550-1800 cm^{-1} region for non-treated multilamellar liposomes (MLVs) containing silibinin and their ultraviolet-exposed paralles after times of 15 min, 30 min, 45 min, and 90 min

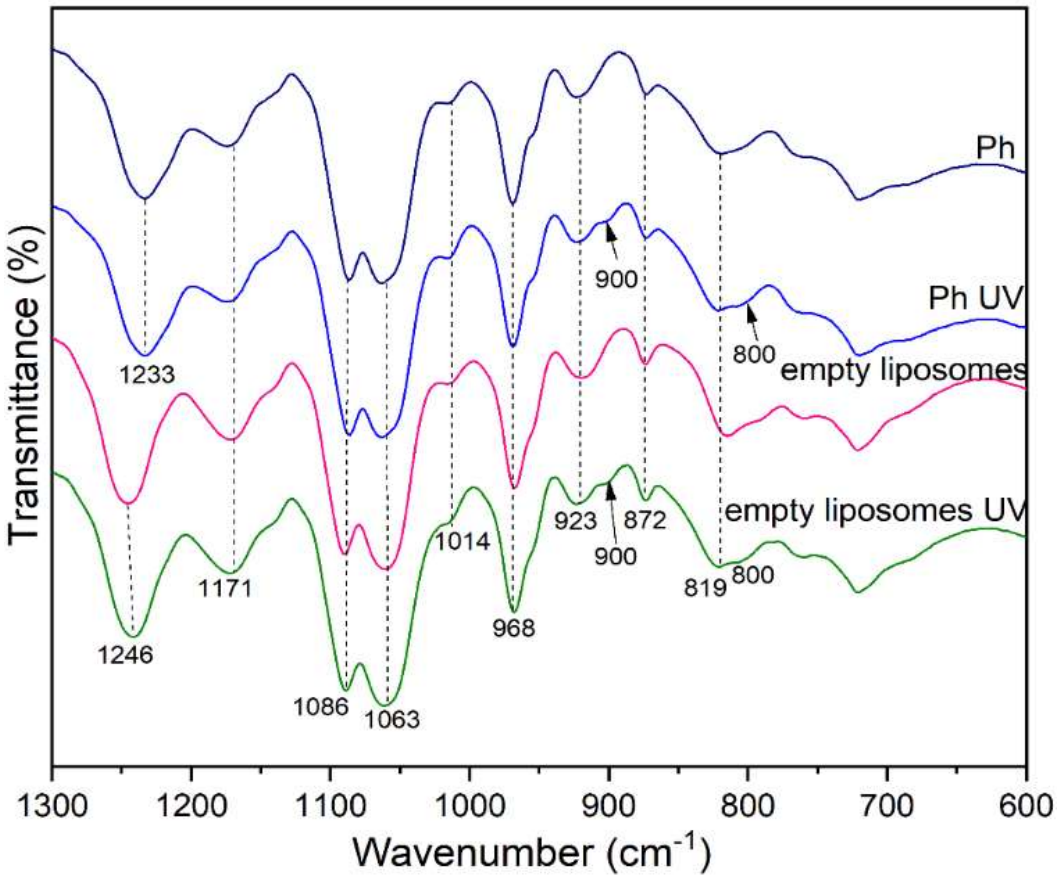

Figure S 6. Time-dependent ultraviolet (UV)-induced changes in the peaks of the 600-1300 cm^{-1} region monitored for Phospholipon 90G (Ph) and unloaded liposomal vesicles

Table S 1. Data from the deconvolution of Phospholipon 90G (Ph), plain liposomes, and multilamellar liposomal vesicles (MLVs) containing silibinin for both before and after the specified duration of ultraviolet (UV) exposure (15-90 min)

Samples	Deconvoluted peaks	X (cm^{-1})	Area (cm^2)	%
Ph	Peak 1	1735	791.67	55.3
	Peak 2	1702	198.82	13.9
	Peak 3	1652	440.40	30.8
Ph UV	Peak 1	1735	812.43	44.4
	Peak 2	1702	310.76	17.0
	Peak 3	1652	706.46	38.6
plain liposomes	Peak 1	1735	829.91	72.7
	Peak 2	1701	139.62	12.2
	Peak 3	1653	171.32	15.0
plain liposomes UV	Peak 1	1735	861.39	59.1
	Peak 2	1701	235.86	16.2
	Peak 3	1653	360.87	24.7
MLVs	Peak 1	1735	788.89	56.3
	Peak 2	1701	126.57	9.0
	Peak 3	1654	140.64	10.0
	Peak 4	1637	110.64	7.9
	Peak 5	1621	40.17	2.9
	Peak 6	1593	193.50	13.8
15 min	Peak 1	1735	811.94	51.7
	Peak 2	1700	155.54	9.9
	Peak 3	1655	181.86	11.6
	Peak 4	1637	140.38	8.9
	Peak 5	1621	51.40	3.3
	Peak 6	1593	230.21	14.5
30 min	Peak 1	1735	854.54	50.3
	Peak 2	1700	174.56	10.3
	Peak 3	1655	202.41	11.9
	Peak 4	1637	155.85	9.2
	Peak 5	1621	60.45	3.6
	Peak 6	1593	250.24	14.7
45 min	Peak 1	1735	888.94	49.0
	Peak 2	1700	185.90	10.4
	Peak 3	1655	215.41	12.1
	Peak 4	1637	165.76	9.3
	Peak 5	1621	63.36	3.5
	Peak 6	1593	263.99	14.8
90 min	Peak 1	1735	888.99	49.8
	Peak 2	1700	186.01	10.4
	Peak 3	1655	217.52	12.1
	Peak 4	1637	166.16	9.3
	Peak 5	1621	63.41	3.5
	Peak 6	1593	264.00	14.8

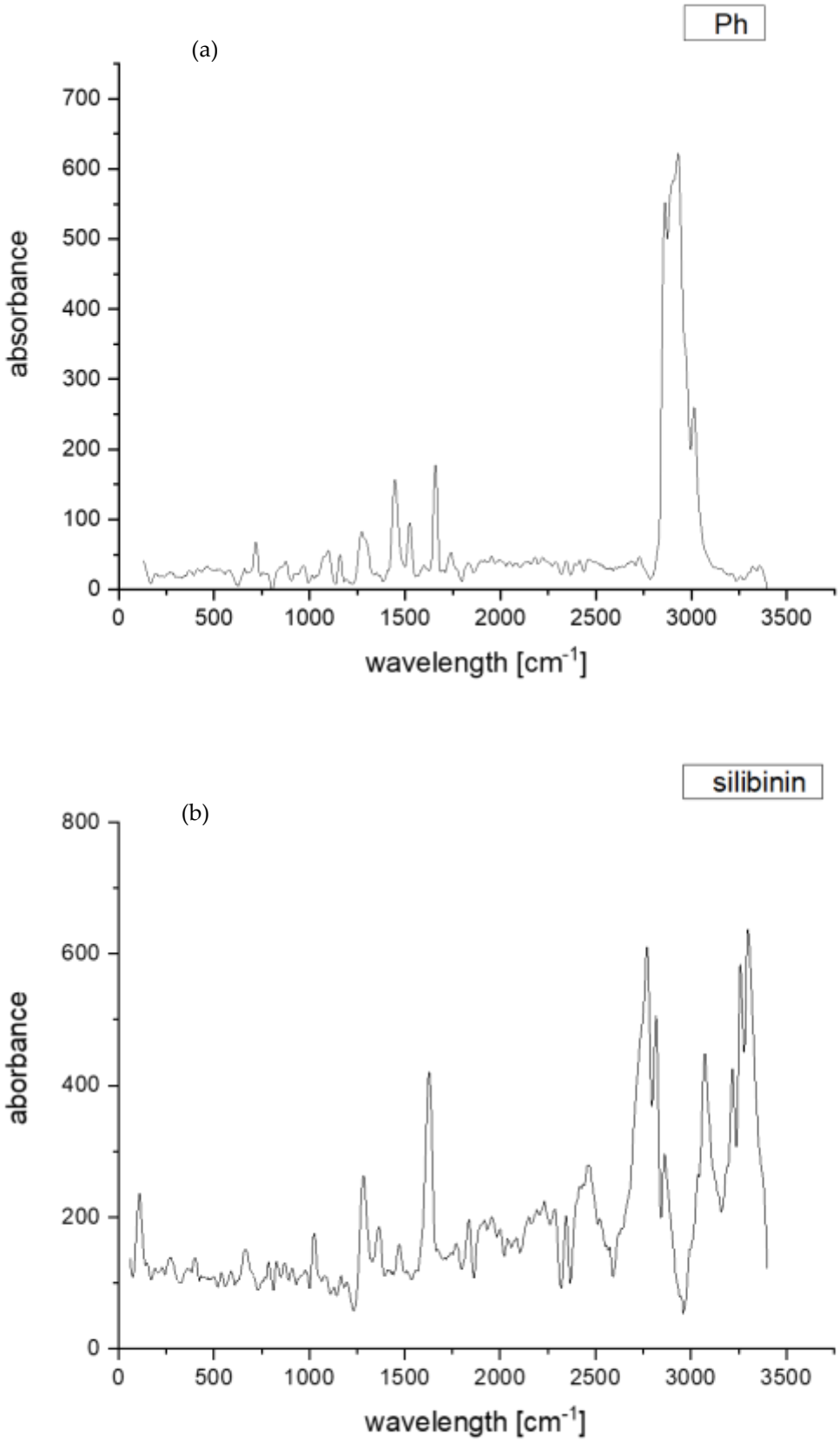

Figure S 7. Raman spectroscopy analysis of the phospholipids Phospholipon 90G used for the liposome preparation (a) and pure compound silibinin (b)

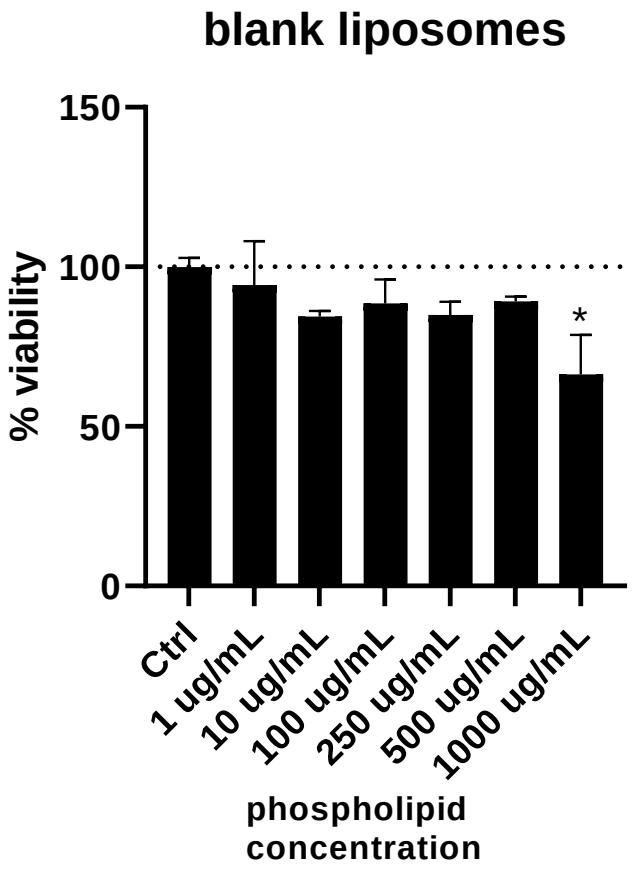

Figure S 8. HaCaT cell (immortalized human keratinocytes) viability after 24-h pre-treatment with unloaded liposomes at phospholipid concentrations of 1 μg/mL, 10 μg/mL, 100 μg/mL, 250 μg/mL, 500 μg/mL, and 1000 μg/mL, compared to untreated control cells (dashed line), using the MTT (3-(4,5-dimethylthiazol-2-yl)-2,5-diphenyltetrazolium bromide) assay. Results are shown as mean ± SEM (standard error of the mean) relative to the unexposed control; statistically significant differences (*$p < 0.05$) were determined by one-way ANOVA (analysis of variance) with Tukey's *post hoc* multiple comparisons.

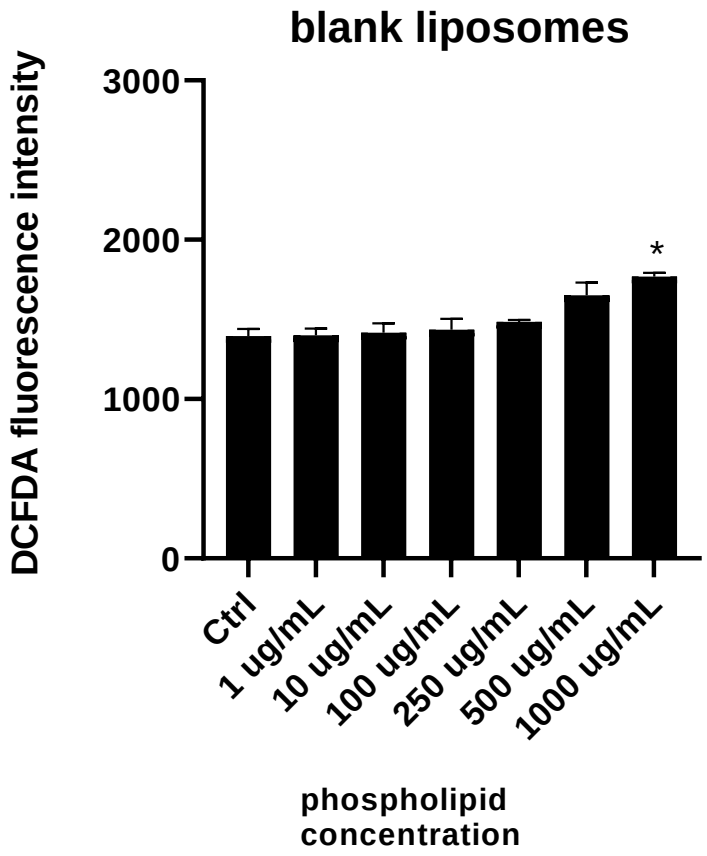

Figure S 9. The impact of 24-h pre-treatment with unloaded liposomes at phospholipid concentrations of 1 μg/mL, 10 μg/mL, 100 μg/mL, 250 μg/mL, 500 μg/mL, and 1000 μg/mL on reactive oxygen species (ROS) generation in HaCaT cells (immortalized human keratinocytes) was assessed relative to untreated controls using the H2DCFDA (2',7'-dichlorodihydrofluorescein diacetate) assay. Data are presented as mean ± SEM (standard error of the mean); statistically significant differences (*$p < 0.05$) were determined by one-way ANOVA (analysis of variance) followed by Tukey's multiple comparison *post hoc* test.

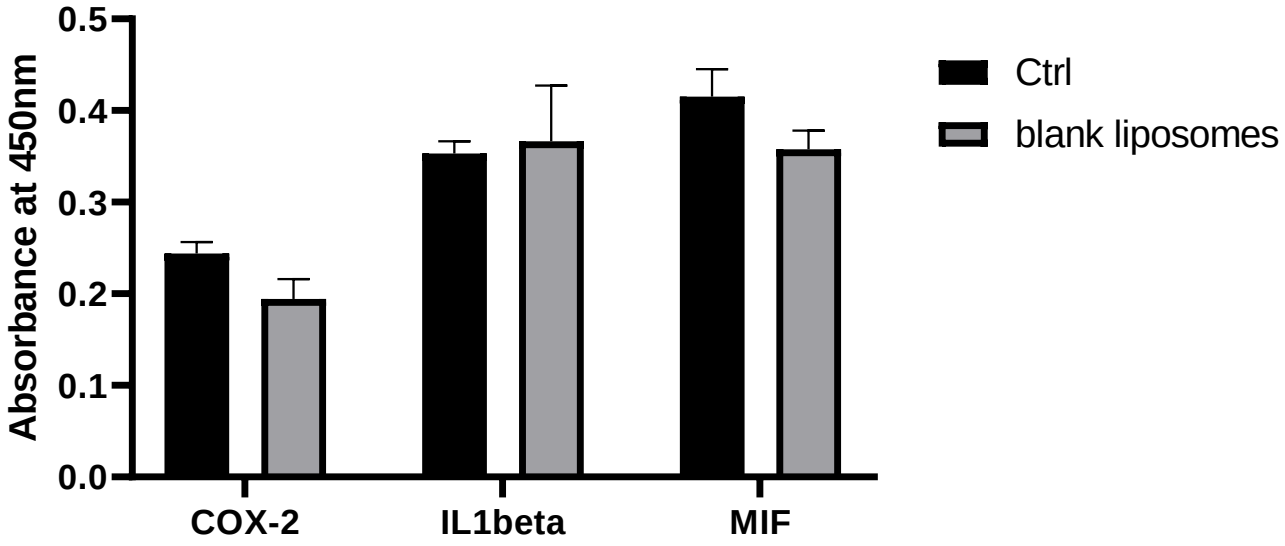

Figure S 10. The influence of 24-h pre-incubation with unloaded liposomal particles at 10 μg/mL on the protein levels of cyclooxygenase-2 (COX-2), interleukin-1 beta (IL-1β), and macrophage migration inhibitory factor (MIF) in HaCaT cells (immortalized human keratinocytes) relative to untreated controls using the cell-based ELISA (enzyme-linked immunosorbent assay) method. Results are presented as mean ± SEM (standard error of the mean).

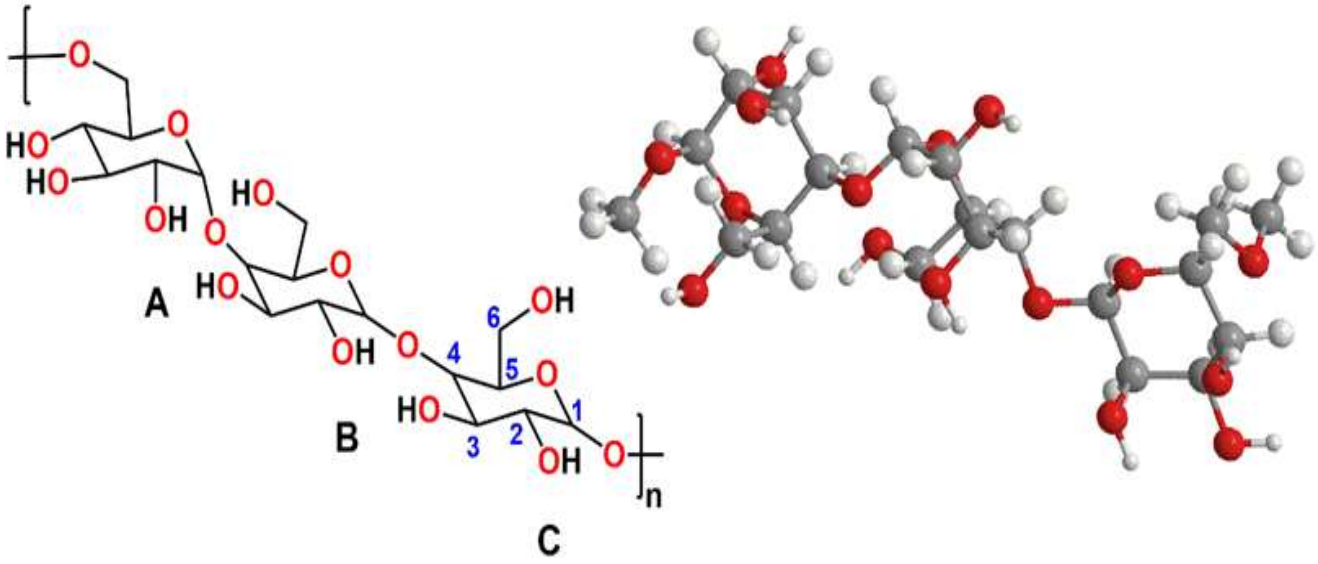

Figure S 11. 2D and 3D structural formulas of the pure compound pullulan

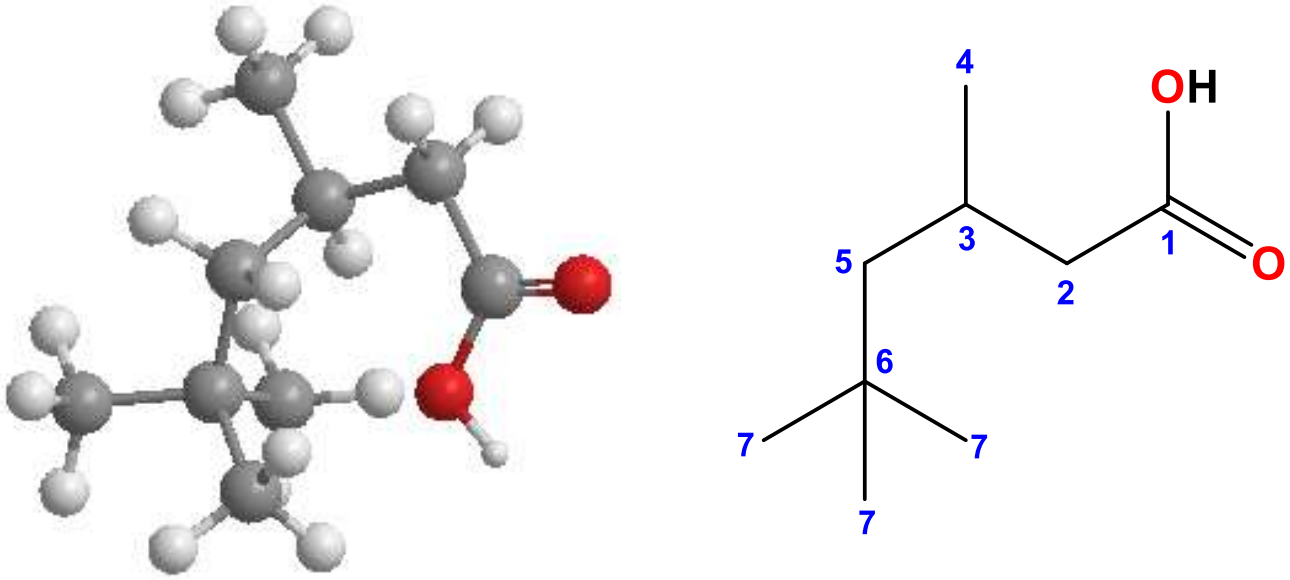

Figure S 12. 2D and 3D structural formulas of isononanoic acid

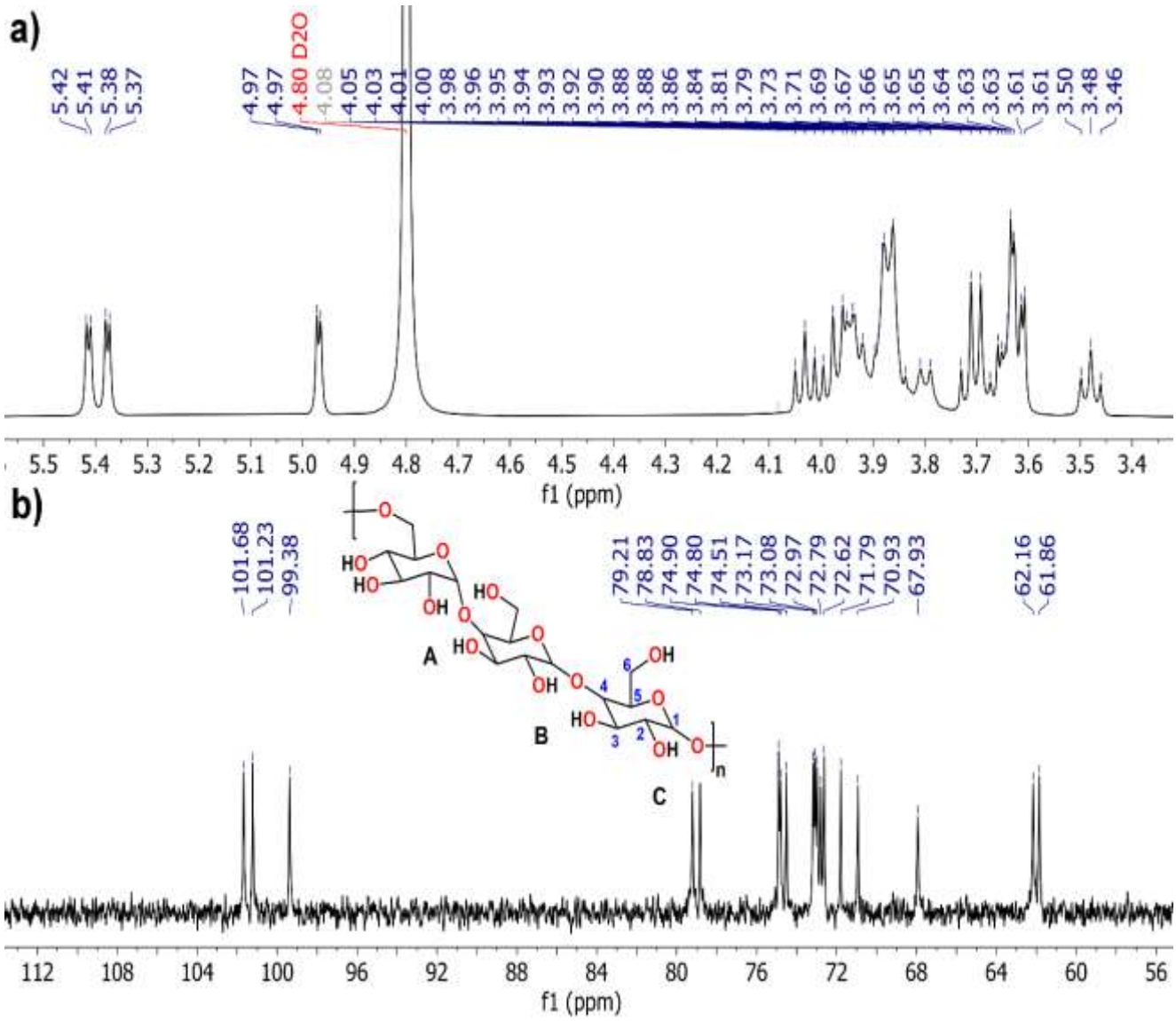

Figure S 13. Nuclear magnetic resonance spectra: a) ^{1}H nuclear magnetic resonance analysis, and b) ^{13}C nuclear magnetic resonance analysis of pure compound pullulan

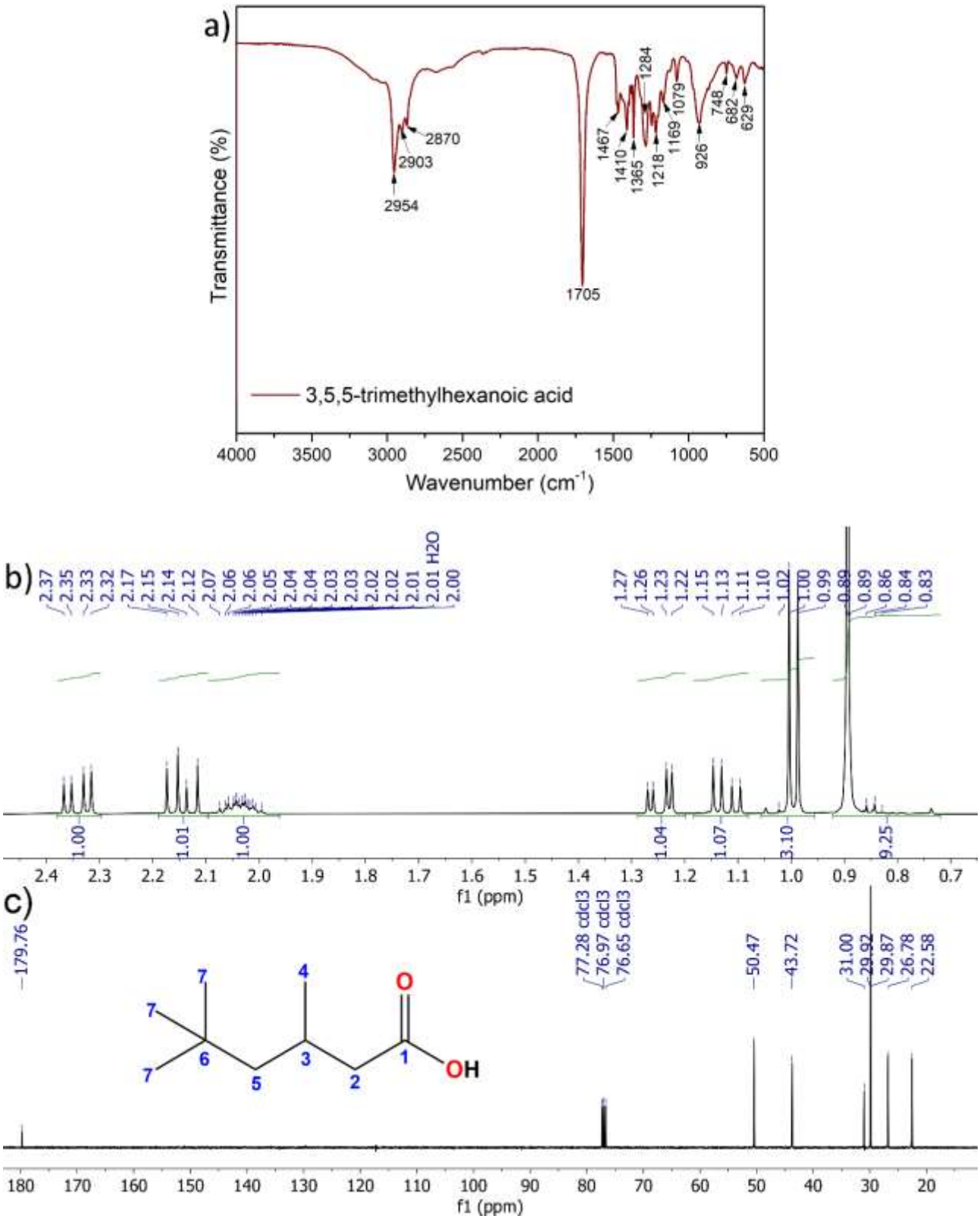

Figure S 14. Visual representation of a) Fourier transform infrared spectroscopy, b) ^{1}H nuclear magnetic resonance analysis, and c) ^{13}C nuclear magnetic resonance analysis of 3,5,5-trimethylhexanoic acid (isononanoic acid)

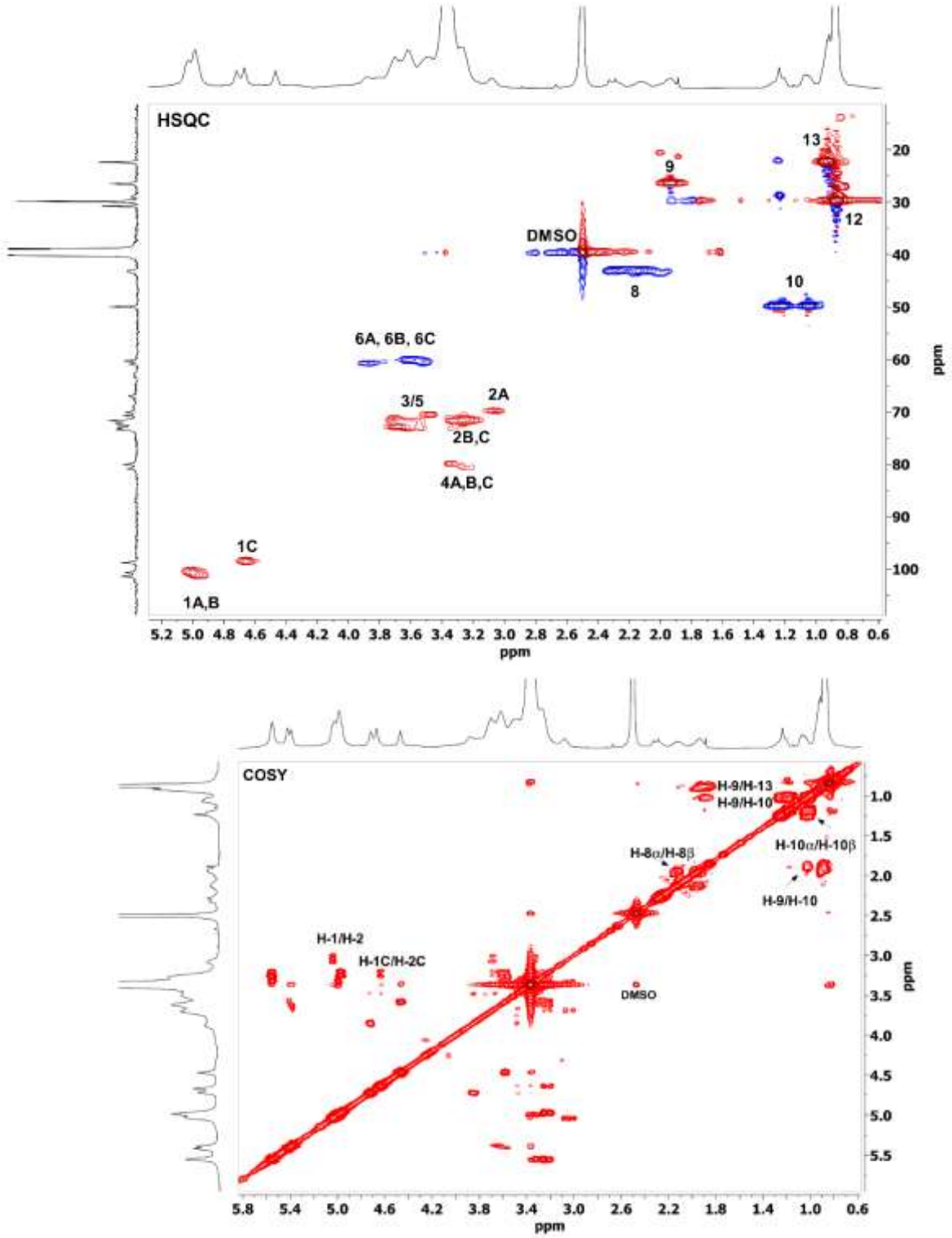

Figure S 15. Two-dimensional HSQC - heteronuclear single quantum coherence (upper panel) and COSY - correlation spectroscopy (lower panel) nuclear magnetic resonance spectra obtained for pullulan isononanoate

FIGURE TITLES

TABLE TITLES

SUPPLEMENTARY FIGURE TITLES

SUPPLEMENTARY TABLE TITLE

BIOGRAFIJA AUTORA

Amjed (Abdullah) Karkad rođen je 10. januara 1985. godine u Tripoliju, Libija. Srednje obrazovanje završio je 2004. godine u gimnaziji Rossol Aldachara Msallatah u Libiji. Osnovne akademske studije završio je 2009. godine na Fakultetu za medicinsku tehnologiju Univerziteta Al-Fatah u Tripoliju, gde je stekao zvanje diplomiranog inženjera medicinske tehnologije. Master akademske studije završio je 2020. godine u Beogradu, na Univerzitetu Metropolitan, u oblasti nauka o životnoj sredini. Školske 2021/2022. godine upisao je doktorske akademske studije na Tehnološko-metalurškom fakultetu Univerziteta u Beogradu, na Katedri za Organsku hemiju. Tokom doktorskih studija položio je sve predviđene ispite, kao i završni ispit.

U periodu od 2013. do 2015. godine radio je kao laboratorijski tehničar u bolnici Msallatah u Libiji, gde je stekao značajno praktično iskustvo u laboratorijskom radu.

Poseduje dobro poznavanje rada na računaru (MS Excel, Word, PowerPoint i korišćenje interneta). Završio je kurs engleskog jezika u Centru za jezike u Tripoliju (Libija) u novembru 2017. godine, kurs srpskog jezika u organizaciji Almorshed za konsalting i edukaciju u Beogradu (početni nivo) u avgustu 2017. godine, kao i kurs engleskog jezika u školi New School English Language u Pančevu, gde je 2018. godine stekao nivo znanja B2.

U novembru 2025. godine prijavio je temu za izradu doktorske disertacije Nastavno-naučnom veću Tehnološko-metalurškog fakulteta. Naučno istraživački rad Amjeda Karkada pripada oblasti Hemijske nauke i usmeren je na inkapsulaciju biološki aktivnih jedinjenja biljnog porekla u lipozome i filmove radi povećanja stabilnosti i bioraspoloživosti, fizičko-hemijsku karakterizaciju dobijenih inkapsulata i ispitivanje biološkog potencijala lipozoma i filmova sa inkapsuliranim bioaktivnim supstancama iz biljnih izvora.

Rezultate svog dosadašnjeg naučno-istraživačkog rada objavio je u ukupno 8 publikacija, od toga 2 rada u časopisima međunarodnog značaja (M21a i M21), 4 saopštenja sa međunarodnih skupova štampanih u celini (M33) i 2 saopštenja sa međunarodnih skupova štampanih u izvodu (M34).

LISTA PUBLIKACIJA

Rad u vrhunskom medjunarodnom časopisu izuzetnih vrednosti (M21a):

1. **Karkad, A.A**., Pirković, A., Milošević, M., Stojadinović, B., Šavikin, K., Marinković, A., Jovanović, A., 2024. Silibinin-loaded liposomes: The influence of modifications on physicochemical characteristics, stability, and bioactivity associated with dermal application. Pharmaceutics, 16(11), p.1476. (IF=5.5) (ISSN: 1999-4923) (https://doi.org/10.3390/pharmaceutics16111476)

Rad u vrhunskom medjunarodnom časopisu (M21):

1. **Karkad, A.A.**, Marinković, A., Jovanović, A., Simić, K., Ivanović, S., Milošević, M., Erceg, T., 2026. Design and optimization of pullulan-isononanoate films with bioactive-loaded liposomes for potential biomedical use. Polymers, 18(2), p.305. (IF=4.9) (ISSN: 2073-4360) (https://doi.org/10.3390/polym18020305)

Saopštenja sa međunarodnih skupova štampana u celini (M33):

1. **Karkad, A.A.**, Milošević, M., Novaković, M., Marinković, A., Jovanović, A., 2024. Multilamellar liposomes as a carrier for *Cotinus coggygria* Scop. extract. Proceedings of the 8th WORKSHOP on Food and Drug Safety and Quality. Belgrade, Serbia, 26th September 2024 (pp.29-32). Belgrade: University of Belgrade, Vinča Institute of Nuclear Sciences - National Institute of the Republic of Serbia (ISBN: 978-86-7306-173-3) (https://doi.org/10.46793/8FDSQ.PA4AK)

2. **Karkad, A.A.**, Milošević, M., Pirković, A., Marinković, A., Jovanović, A., 2025. Radical scavenging activity of silymarin encapsulated in liposomal vesicles: Impact of UV irradiation and lyophilization. Engineering Proceedings, 99(1), p.14. (E-ISSN: 2673-4591) (https://doi.org/10.3390/engproc2025099014)

3. **Karkad, A.A.**, Elferjane, M., Milošević, M., Pirković, A., Lupulović, D., Marinković, A., Jovanović, A., 2025. Storage stability of the liposomal system with encapsulated *Vaccinium myrtillus* extract. Proceedings of IX International Congress "Engineering, Environment and Materials in Process Industry" – EEM2025, Ethno Village Stanišići, Bosnia and Herzegovina, 2–4 April 2025 (pp.58). Zvornik: University of East Sarajevo Faculty of Technology. (ISBN 978-99955-81-52-7)

4. Jovanović, A.A., **Karkad, A.**, Pirković, A., Dekanski, D., Lupulović, D., Novaković, M., Marinković, A., 2025. Stability of *Cotinus coggygria* Scop. extract-loaded liposomes: The impact of storage on physical and antioxidant properties. Proceedings, 119(1), p.4. (E-ISSN: 2504-3900) (https://doi.org/10.3390/proceedings2025119004)

Saopštenja sa međunarodnih skupova štampana u izvodu (M34):

1. **Karkad, A.A.**, Batinić, P., Milošević, M., Pirković, A., Onjia, A., Marinković, A., Jovanović, A., 2024. The influence of lyophilization on liposomal particles with silymarin. Book of Abstracts of the 3rd UNIFood International Conference - UNIFood2024, Belgrade, Serbia, 28–29 June 2024 (p.76). Belgrade: University of Belgrade, Faculty of Agriculture. (ISBN 978-86-7834-438-1)

2. **Karkad, A.A.**, Batinić, P., Milošević, M., Pirković, A., Onjia, A., Marinković, A., Jovanović, A., 2024. Antioxidant capacity of silibinin-loaded liposomes. Book of Abstracts of the 3rd UNIFood International Conference - UNIFood2024, Belgrade, Serbia, 28–29 June 2024 (p.75). Belgrade: University of Belgrade, Faculty of Agriculture. (ISBN 978-86-7834-438-1)

Изјава о ауторству

Име и презиме аутора: **Amjed Abdullah Karkad**

Број индекса: **4044/2021**

Изјављујем

да је докторска дисертација под насловом

„Липозоми и биополимерни филмови за ефикасно контролисано отпуштање силибинина и *Cotinus coggygria* Scop. екстракта“

"Liposomes and Bio-Polymeric Films for Efficient Controlled Release of Silibinin and *Cotinus coggygria* Scop. Extract"

- резултат сопственог истраживачког рада,
- да предложена дисертација у целини ни у деловима није била предложена за добијање било које дипломе према студијским програмима других високошколских установа,
- да су резултати коректно наведени и
- да нисам кршио ауторска права и користио интелектуалну својину других лица.

Потпис докторанда

У Београду, 1. април 2026. године

Изјава о истоветности штампане и електронске верзије докторског рада

Име и презиме аутора: **Amjed Abdullah Karkad**

Број индекса: **4044/2021**

Студијски програм: **Хемија**

Наслов рада: **„Липозоми и биополимерни филмови за ефикасно контролисано отпуштање силибинина и *Cotinus coggygria* Scop. екстракта“**

"Liposomes and Bio-Polymeric Films for Efficient Controlled Release of Silibinin and *Cotinus coggygria* Scop. Extract"

Ментори: **проф. др Александар Маринковић** и **др Тамара Ерцег**

Потписан **Amjed Abdullah Karkad**

Изјављујем да је штампана верзија мог докторског рада истоветна електронској верзији коју сам предао за објављивање на порталу **Дигиталног репозиторијума Универзитета у Београду.**

Дозвољавам да се објаве моји лични подаци везани за добијање академског звања доктора наука, као што су име и презиме, година и место рођења и датум одбране рада.

Ови лични подаци могу се објавити на мрежним страницама дигиталне библиотеке, у електронском каталогу и у публикацијама Универзитета у Београду.

Потпис докторанда

У Београду, 1. април 2026. године

Изјава о коришћењу

Овлашћујем Универзитетску библиотеку „Светозар Марковић“ да у Дигитални репозиторијум Универзитета у Београду унесе моју докторску дисертацију под насловом:

„Липозоми и биополимерни филмови за ефикасно контролисано отпуштање силибинина и *Cotinus coggygria* Scop. екстракта“

"Liposomes and Bio-Polymeric Films for Efficient Controlled Release of Silibinin and *Cotinus coggygria* Scop. Extract"

која је моје ауторско дело.

Дисертацију са свим прилозима предао сам у електронском формату погодном за трајно архивирање.

Моју докторску дисертацију похрањену у Дигитални репозиторијум Универзитета у Београду могу да користе сви који поштују одредбе садржане у одабраном типу лиценце Креативне заједнице (Creative Commons) за коју сам се одлучио.

1. Ауторство (CC BY)
2. Ауторство – некомерцијално (CC BY-NC)
3. **Ауторство – некомерцијално – без прерада (CC BY-NC-ND)**
4. Ауторство – некомерцијално – делити под истим условима (CC BY-NC-SA)
5. Ауторство – без прерада (CC BY-ND)
6. Ауторство – делити под истим условима (CC BY-SA)

(Молимо да заокружите само једну од шест понуђених лиценци.

Кратак опис лиценци је саставни део ове изјаве).

Потпис докторанда

У Београду, 1. април 2026. године

1. **Ауторство.** Дозвољавате умножавање, дистрибуцију и јавно саопштавање дела, и прераде, ако се наведе име аутора на начин одређен од стране аутора или даваоца лиценце, чак и у комерцијалне сврхе. Ово је најслободнија од свих лиценци.

2. **Ауторство – некомерцијално.** Дозвољавате умножавање, дистрибуцију и јавно саопштавање дела, и прераде, ако се наведе име аутора на начин одређен од стране аутора или даваоца лиценце. Ова лиценца не дозвољава комерцијалну употребу дела.

3. **Ауторство – некомерцијално – без прерада.** Дозвољавате умножавање, дистрибуцију и јавно саопштавање дела, без промена, преобликовања или употребе дела у свом делу, ако се наведе име аутора на начин одређен од стране аутора или даваоца лиценце. Ова лиценца не дозвољава комерцијалну употребу дела. У односу на све остале лиценце, овом лиценцом се ограничава највећи обим права коришћења дела.

4. **Ауторство – некомерцијално – делити под истим условима.** Дозвољавате умножавање, дистрибуцију и јавно саопштавање дела, и прераде, ако се наведе име аутора на начин одређен од стране аутора или даваоца лиценце и ако се прерада дистрибуира под истом или сличном лиценцом. Ова лиценца не дозвољава комерцијалну употребу дела и прерада.

5. **Ауторство – без прерада.** Дозвољавате умножавање, дистрибуцију и јавно саопштавање дела, без промена, преобликовања или употребе дела у свом делу, ако се наведе име аутора на начин одређен од стране аутора или даваоца лиценце. Ова лиценца дозвољава комерцијалну употребу дела.

6. **Ауторство – делити под истим условима.** Дозвољавате умножавање, дистрибуцију и јавно саопштавање дела, и прераде, ако се наведе име аутора на начин одређен од стране аутора или даваоца лиценце и ако се прерада дистрибуира под истом или сличном лиценцом. Ова лиценца дозвољава комерцијалну употребу дела и прерада. Слична је софтверским лиценцама, односно лиценцама отвореног кода.

ПРОВЕРА ОРИГИНАЛНОСТИ ДОКТОРСКЕ ДИСЕРТАЦИЈЕ

На основу Правилника о поступку провере оригиналности докторских дисертација које се бране на Универзитету у Београду, коришћењем програма iThenticate извршена је провера оригиналности докторске дисертације кандидата **Amjeda Abdullah Karkada** под називом „Липозоми и биополимерни филмови за ефикасно контролисано отпуштање силибинина и *Cotinus coggygria* Scop. екстракта“ ("Liposomes and Bio-Polymeric Films for Efficient Controlled Release of Silibinin and *Cotinus coggygria* Scop. Extract"). Извештај који садржи резултате провере оригиналности ментори су добили дана 19.03.2026. Утврђени проценат подударности је 6%. Овај проценат је последица општих места, односно употребе стручних термина и података који се тичу обрађене теме, назива коришћених метода и њихових скраћеница, личних имена, инструмената, цитиране литературе и изјава кандидата. Део подударности се односи на претходно публиковане резултате докторандових истраживања, који су проистекли из његове дисертације. На основу свега изнетог, а у складу са чланом 8. став 2. Правилника о поступку провере оригиналности докторских дисертација које се бране на Универзитету у Београду, изјављујемо да извештај указује на оригиналност докторске дисертације, те се прописани поступак припреме за њену одбрану може наставити.

У Београду, 20.03.2026. године

Ментори:

проф. др Александар Маринковић,
редовни професор Универзитета у
Београду, Технолошко–металуршки факултет

др Тамара Ерцег,
виши научни сарадник Универзитета у Новом Саду,
Технолошки факултет Нови Сад